Fibrillin-1 and elastin fragmentation in the pathogenesis of thoracic aortic aneurysm in Marfan syndrome

DISSERTATION

zur Erlangung des akademischen Grades des
Doktors der Naturwissenschaften (Dr. rer. nat.)

eingereicht im Fachbereich Biologie, Chemie, Pharmazie
der Freien Universität Berlin

vorgelegt von
Gao Guo
aus China

Berlin, Juni 2011

Die vorliegende Arbeit wurde von Februar 2006 bis Juni 2011 am Institut für Medizinische Genetik und Humangenetik der Charité Campus Virchow-Klinikum, Universitätsmedizin Berlin unter der Anleitung von Herrn Dr. Peter N. Robinson angefertigt.

1. Gutachter: PD Dr. Peter N. Robinson

2. Gutachter: Prof. Dr. Petra Knaus

Disputation am: 08.11.2011

To my wife and son

Acknowledgment

First and foremost I am indebted to my supervisor PD Dr. Peter N. Robinson for overseeing my project and for his immense guidance, assistance, support, advice, constant encouragement and constructive comments throughout my project.

I would like to thank Prof. Dr. Stefan Mundlos, Director of the Institute of Medical Genetics and Human Genetics, for his kind support.

I am extremely grateful to my adjunct Prof. Dr. Petra Knaus of the Free University of Berlin for reviewing my thesis and granting me admission at her University as external student.

I thank Dr. Patrick Booms, a former outstanding postdoc in our department, whose endless efforts made the establishment of the HEK 293 expression system possible.

I thank Dr. Andreas Ney and Kerstin for introducing me to the fascinating technique of molecular biology .

I gratefully acknowledge the skillful technical assistance of Angelika Pletschacher. I thank Dr. Mousa Shaaban-Abd-El-Wahab for the contribution of the immunohistochemistry. I would also like to thank Bianca and Kora for taking care of the animals.

I sincerely wish to thank my colleagues in our Institute for their support and help. Especially, I benefited from the help kindly from Dr. Uwe Kornak, Dr. Jirko Künisch and Björn Fischer.

Many thanks to Dr. Claus Eric Ott and Johannes Grünhagen who helped me tackling various problems especially regarding to genotyping and qPCR. I want to also thank Dr. Begoña Muñoz-García for her tips and suggestions throughout the whole project.

Thanks to Hardy Chan for the lunch we shared, the conservations we had, and the advice he gave.

I am indebted to the members of our bioinformatic group that especially their help with the computer software problems, including: Sebastian Bauer, Sebastian Köhle, Christian Rödelsperger, Marten Jäger, Dr. Peter Krawitz, Marcel Schütze and Verena Heinrich.

This project would not have been possible without the understanding and support of my wife Yun, who helped me through the ups and downs during our stay in Berlin. Additionally, I wish to express my sincere thanks to my sweet 2 year old son Kai Chen for the enormous amounts of joy and happiness he has brought into our lives.

I want to give my special thanks to my father in law and mother in law for taking care of my son during their stay in Berlin last year.

And last but not least, I owe my deepest thanks to my parents and sister for their moral support during all these years.

Parts of this study have been published in the following journals:

- **Guo G**, Booms P, Halushka M, Dietz HC, Ney A, Stricker S, Hecht J, Mundlos S, Robinson PN. Induction of macrophage chemotaxis by aortic extracts of the mgR Marfan mouse model and a GxxPG-containing fibrillin-1 fragment. *Circulation,* 2006;114(17):1855-62. http://dx.doi.org/10.1161/CIRCULATIONAHA.105.601674

- **Guo G**, Gehle P, Doelken S, Martin-Ventura JL, von Kodolitsch Y, Hetzer R, Robinson PN. Induction of macrophage chemotaxis by aortic extracts from patients with Marfan syndrome is related to elastin binding protein. *PLoS ONE,* 2011;6(5):e20138. http://dx.doi.org/10.1371/journal.pone.0020138

- Booms P, Ney A, Barthel F, Moroy G, Counsell D, Gille C, **Guo G**, Pregla R, Mundlos S, Alix AJ, Robinson PN. A fibrillin-1-fragment containing the elastin-binding-protein GxxPG consensus sequence upregulates matrix metalloproteinase-1: biochemical and computational analysis. *J. Mol. Cell Cardiol.,* 2006;40(2):234-46. http://dx.doi.org/10.1016/j.yjmcc.2005.11.009

- **Guo G**, Bauer S, Hecht J, Schulz MH, Busche A,Robinson PN: A Short Ultraconserved Sequence Drives Transcription from an Alternate *FBN1* Promoter *Int. J. Biochem. Cell Biol.,* 2008;40(4):638-50. http://dx.doi.org/10.1016/j.biocel.2007.09.004

The results described in section 3.5 have been submitted for publication:

- **Guo G**, Muñoz-García B, Ott CE, Grünhagen J, Mousa S, Pletschacher A, von Kodolitsch Y, Knaus P, Robinson PN. Antagonism of GxxPG-Fragments Ameliorates Manifestations of Aortic Disease in Marfan Syndrome Mice.

Contents

1 Introduction

1.1 Marfan syndrome

The Marfan syndrome (MFS; MIM154700), named after Antoine Marfan, the French doctor who discovered it in 1896, is an autosomal dominant heritable connective tissue disorder that principally involves the skeletal, ocular, and cardiovascular systems. In 1991, fibrillin-1 gene (*FBN1*) mutation on chromosome 15 was identified as the cause of MFS (1). The prevalence of MFS and related diseases is estimated at between 1:10,000 to 1:5000 (2, 3). MFS most often affects the connective tissue of the heart, eyes, bones, lungs, and dura. This can cause a number of complications including severe scoliosis, pectus excavatum, and dislocated lenses. The leading cause of premature death of the affected individuals is progressive dilatation of the aortic root and ascending aorta, leading to aortic incompetence and dissection. The average life expectancy of patients with MFS without surgical treatment is approximately 32 years (4).

Diagnosis of MFS

MFS can't be diagnosed by a single molecular test but requires a scoring system that combines various diagnostic items. In 1996 the Ghent nosology was made to serve as an international standard for diagnosis of Marfan syndrome (5). However, the specificity of some diagnostic manifestations (for instance dural ectasia) have not been sufficiently validated. Recently a revised Ghent nosology was prospsed, in which ectopia lentis is treated as cardinal feature and some of the less specific manifestations of MFS were either removed or made less influential in the diagnostic evaluation (6). Following the revised Ghent criteria, the presence of ectopia lentis and aortic root enlargement/dissection is sufficient for the unequivocal diagnosis of MFS in individuals without a family history of MFS (6). In absence of any of these two, the presence of bonafide *FBN1* mutation or a scoring of systemic features more than 7 is required (Table 1.1).

Box 1 Revised Ghent criteria for diagnosis of Marfan syndrome and related conditions
In the absence of family history: (1) Ao (Z≥2) AND EL=MFS (2) Ao (Z≥2) AND *FBN1*=MFS (3) Ao (Z≥2) AND Syst (=7pts)=MFS (4) EL AND *FBN1* with known Ao=MFS **In the presence of family history:** (5) EL AND FH of MFS (as defined above)=MFS (6) Syst (=7 pts) AND FH of MFS (as defined above)=MFS (7) Ao (Z≥2 above 20 years old, =3 below 20 years) +FH of MFS (as defined above)=MFS
Box 2 Scoring of systemic features
Scoreing based on different systemic features. Maximum total: 20 points; score =7 indicates systemic involvement. Details found in (6).
Box 3 Criteria for causal *FBN1* mutation
Presence of different kinds of *FBN1* mutations. Details found in (6).
Abbreviations: Ao, aortic diameter at the sinuses of Valsalva above indicated Z-score or aortic root dissection; EL, ectopia lentis; FH, Family History; Syst, Systemic score; *FBN1*, fibrillin-1 mutation (as defined in box 3); *FBN1* not known with Ao, *FBN1* mutation that has not previously been associated aortic root aneurysm/dissection; *FBN1* with known Ao, *FBN1* mutation that has been identified in an individual with aortic aneurysm

Table 1.1: Revised Ghent criteria for diagnosis of Marfan syndrome. Details found in (6).

1.2 Clinical Characteristics of MFS

1.2.1 Skeletal and muscle system

Most of the readily visible signs of MFS are associated with the skeletal system. Affected patients are characterized by dolichostenomlia and arachnodactyly as a result of excessive linear growth of the long bones (Figure 1.1). The overgrowth of the tubular bones leads to pectus deformities (i.e., pectus excavatum and pectus carinatum). Pectus excavatum occurs in approximately two-thirds of patients with MFS (7). Abnormal curvature of the spine such as scoliosis and kyphosis is also a common feature which may begin at any time before skeletal maturity and progress at any

age. Sponseller et al. (8) evaluated spinal deformity in 113 patients with MFS, 82 of whom were skeletally immature. Scoliosis was found in 52 of the 82 patients, with equal prevalence for the sexes. The thoracic portion of the curve was convex to the right in all but 2 patients. Additionally, bone mineral density appears to be reduced at the spine and hip in MFS (9), but no associated increase in fracture rate has been observed.

Although skeletal muscle myopathy is not classically considered a component of MFS, it has been often reported in many patients with MFS (5, 10, 11). It was hypothesized that unsatisfactory anchoring and an abnormal relation between extracellular matrix and muscle fiber basement membrane may contribute to the poor muscle development (10).

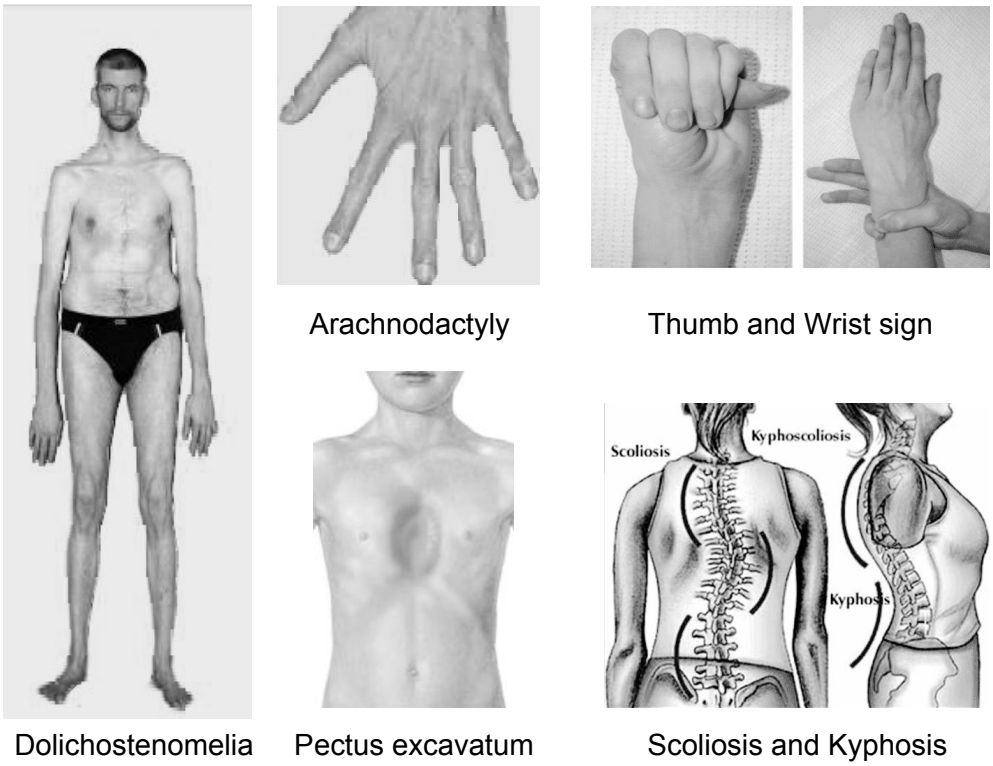

Figure 1.1: Skeletal features of MFS

1.2.2 Cardiovascular system

Aortic aneurysm resulting from progressive dilation of aortic root and leading to acute aortic dissection is the major cause of premature death in Marfan patients (12–14). Dilatation of the aorta is found in 50 percent of children with MFS and usually progresses with time. Echocardiography demonstrates that alomost all adult patients have dilatation of the aortic root (normal <35 mm), often with aortic regurgitation, that may involve other segments of the thoracic aorta, and the abdominal aorta (15). Progressive thoracic aortic dilatation can result in aortic valve incompetence

with left ventricular failure and markedly increases the risk of fatal aortic dissection (16). Clinical management in MFS aims to decrease the rate of aortic root dilatation and reduce the risk of dissection and rupture. Prophylactic resection of ascending aortic aneurysms is recommended when the aortic diameter reaches 5.0 to 6.0 cm, or when the aortic diameter exceeds twice the diameter of the normal aorta (17). Mitral valve prolapse (MVP) is the most common finding in children with MFS and is more common in women than in men (18). MVP can progress to severe mitral regurgitation. Cardiomyopathy appears occasionally and may represent a defect in cardiac muscle function associated with some fibrillin-1 mutations. A retrospective study by Alpendurada et al. (19) showed the existence of a primary cardiomyopathy in a subgroup of Marfan patients. Additionally, aortic regurgitation and tricuspid valve prolapse, seems to occur with higher prevalence in patients with MFS (3, 5).

1.2.3 Eye and other systems

MFS can cause a number of eye problems in a majority of patients. Ectopia lentis is seen in approximately 60% of affected individuals and can occur in one or both eyes. It is thought that the ocular pathologic changes are primarily caused by stretching of the tunica scleralis, and that the zonular fibers may rupture in their area of presumably least density (20). The craniofacial anomalies in MFS include vertical midface hypoplasia, maxillary and mandibular retroposition and increased palatal height (21). MFS is also a risk factor for spontaneous pneumothorax. Hall et al. (22) reported that the frequency of spontaneous pneumothorax was 4.4% in patients with MFS who are more than 12 years old. Dural ectasia is a skeletal manifestion with enlargement of the outer layer of the meningeal sac leading to ballooning or widening of the dural sac, which can be observed in >60% patients with MFS (23). Patients with MFS often exhibit three types of dental anomalies involving dentin formation: root deformities; calcified pulp inclusions; and abnormal pulp shape (24). Manifestations in the skin and integument include hernias and skin stretch marks (striae distensae).

1.2.4 Differential diagnosis

The diagnosis of MFS is complicated by a genotype-phenotype inconsistency that presents with widely variable clinical manifestations. Loeys-Dietz syndrome (LDS) is an autosomal dominant disorder of the connective tissue due to mutations in the transforming growth factor beta-receptor Type 1 or Type 2 genes (*TGFBR1* and *TGFBR2*). The phenotypic features of individuals with

LDS overlap with other genetic connective tissue disorders like MFS (25). However, there are characteristic phenotypic features that point to a clinical diagnosis of LDS, which has been described as being characterized by a triad of arterial tortuosity and aneurysms, hypertelorism and bifid uvula or cleft palate (25). Besides MFS a series of other fibrillinopathies associated with different of *FBN1* mutation have been reported. These diseases have greater or lesser degrees of clinical overlap with MFS. For instance, the neonatal MFS (nMFS) represents the most severe end of the clinical spectrum of the fibrillinopathies and is associated with mutations in exons 24-32 (26, 27). The Sphrintzen-Goldberg syndrome (SGS) shares many clinical features of the MFS, but craniosynostosis and mental retardation are not manifestations of MFS (28). Till now, two alterations in the fibrillin-1 gene have been identified in individuals with SGS (29). Patients with Weill-Marchesani syndrome have ectopia lentis, but unlike patients with MFS, are of short stature. Other *FBN1* mutation associated disorders include isolated ectopia lentis, MASS (Mitral valve, Aorta, Skeleton, Skin) syndrome, isolated skeletal features of MFS, and familial thoracic aortic aneurysms (FTAA).

1.3 Fibrillin-1

1.3.1 Structure of fibrillin-1

The Fibrillin-1 gene (*FBN1*), mapping to chromosome 15q21.1, contains 65 exons and spans about 235 kb of genomic DNA (30–33). Three alternatively spliced exons initially termed exons B, A, and C, are located upstream of the first coding exon (31). We showed that transcription of this gene is driven by a ultraconserved sequence lying in the upstream of exon A in this dissertation (34).

The Fibrillin-1 protein, is a 350 kDa multidomain glycoprotein component of the 10-20 nm extracellular microfibrils, which are ubiquitous in the connective tissue space and organs both in association with elastin within elastic fibers and as elastin-free bundles (35). The fibrillin-1 monomer is a large cyteine-rich flexible molecule, extending approximately 148 nm in length, that assembles into microfibrils in a head-to-tail orientation (36).

The most common domain in fibrillin-1 is the epidermal growth factor (EGF)-like domain, which occurs 47 times in Fibrillin-1, 43 of the EGF domains contain a consensus sequence for calcium binding and are termed calcium-binding EGF modules (cbEGF) (30, 32) (Figure 1.2), calcium binding causes stretches of tandemly repeated cbEGF repeats to take on a rigid, rod-like con-

formation (37, 38). Depending on the adjacent domains, the cbEGF domains bind calcium with different affinities ranging from the low nanomolar to the low micromolar range (39, 40).

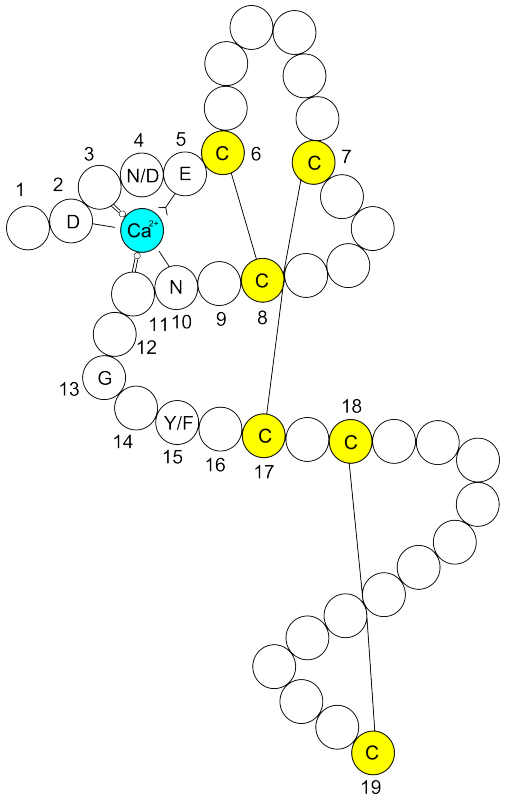

Figure 1.2: Schematic of a calcium binding epidermal growth factor-like motif (cbEGF). The positions marked with the numbers 1 to 19 comprise the six highly conserved cysteine residues as well as the consensus calcium binding sequence. Modified from Robinson et al. (14).

The 8-Cys module (also variously referred to in the literature as the 8-cysteine module, the TB module, or the LTBP module) also occurs in fibrillin-1. The 8-Cys domain is characterized by the presence of eight cysteine residues, three of which are arranged in tandem as an unusual Cys-Cys-Cys motif. An experiment using a recombinant construct of one of the seven 8-Cys modules of fibrillin-1 showed that the structure is stabilised by four intradomain disulfide bonds (41). In addition to these domains, there are a hybrid domain, a proline-rich region and N- and C-terminal regions. The hybrid module termed 8-Cys hybrid module with similarities to both the cbEGF module and the 8-Cys, can mediate intermolecular disulfide bonding between fibrillin-1 monomers, which may be an important step in the assembly of microfibrils (32, 42).

Fibrillin-1 contains 15 sites for N-linked glycosylation and several putative sites for O-glycosylation. The glycosylation is known to be important for correct folding and stability of fibrillin-1 polypeptide. Excessive N-glycosylation was reported to be related to the severe phenotype of nMFS (43). In vitro evidence suggests that fibrillin-1 protein undergoes intracellular N-terminal process-

ing at signal peptide sequences followed by a consensus processing sequence for propeptides RX(K/R)R (44). In addition, carboxyl-terminal processing within the secretory pathway locates after a tribasic processing signal(RX(K/R)R) (44, 45). It has been demonstrated that processing of the C-terminal propeptide is required for deposition into the extracellular matrix (46).

1.3.2 Family members of fibrillins

Other fibrillins include fibrillin-2 (*FBN2*) and fibrillin-3 (*FBN3*) (Figure 1.3). The structures of *FBN1*, *FBN2* and *FBN3* are highly similar, with the most significant difference being the glycine-rich sequence near the N terminus of *FBN2*, where *FBN1* has a proline-rich sequence (47). Like *FBN1*, *FBN2* is also known to be involved in assembly of microfibrils (48). *FBN3* has been described but its role in vascular physiology remains unknown (49).

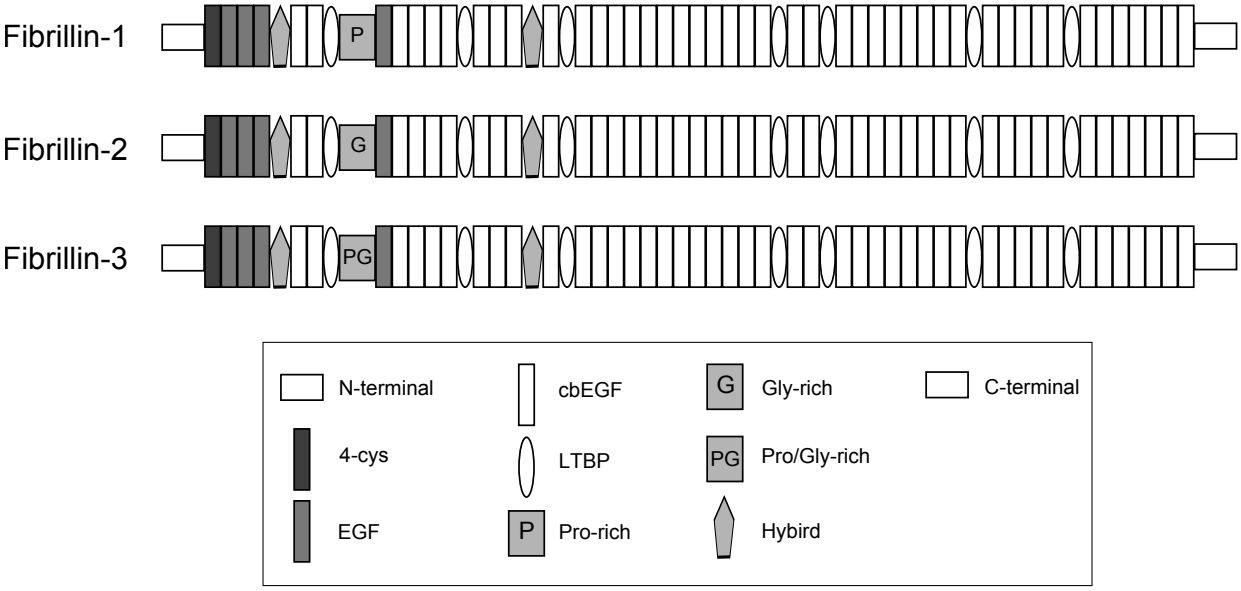

Figure 1.3: Domain structure of proteins of the fibrillin-1,-2 and -3, The dark gray box corresponds to the 4-cys domain, and the light gray boxes to the EGF like domains. The 43 white boxes correspond to EGF domains that additionally have a consensus sequence for calcium binding (cbEGF). The seven ovals correspond to LTBP domains, and the pentangle to the hybrid domain of fibrillin-1. EGF, epidermal growth-factor; cbEGF, calcium binding EGF; LTBP, latent TGF-β-binding protein; Adapted from Robinson et al. (46).

1.4 Mouse models of Marfan syndrome

It has become routine to use transgenic mice or knock-out mice to model human genetic disorders. Different mouse models targeting fibrillin-1 gene have been developed to understand the pathogenic mechanisms of MFS or fibrillin-1 associated disease. Pereira et al. (50) reported a murine model mgΔ, in which exons 19 to 24 of *Fbn1* were deleted. The mgΔ mice express

fibrillin-1 protein at about 10% of wild type level. While heterozygous mgΔ mice were indistinguishable from wild type mice, homozygous mgΔ mice die of severe MFS-like cardiovascular complications approximately 3 weeks after birth. During the generation of mgΔ model another mouse line named mgR was generated unintentionally. In this model, the neomycin-cassete was found to be inserted into the intron region between exon 18 and 19 instead of the deletion of exon 19 to 24 as previously planned. Homozygous mgR mice demonstrate a 5-fold decrease of fibrillin-1 expression compared with wild type. Both heterozygous and homozygous mgR mice showed normal phenotype at birth, but homozygotes developed phenotypic features in the skeletal system, including significant kyphosis and overgrowth of ribs. mgR/mgR mice die at the age of around 4 months from pulmonary and vascular insufficiency.

Recently, a heterozygote for the mutant *Fbn1* allele mgΔ^{loxPneo}, carrying the same internal deletion of exons 19 to 24 as the mgΔ mouse model, but with neoR flanked by lox-P sequences, is reported to present defective microfibrillar deposition, emphysema, deterioration of aortic wall and kyphosis, however, homozygosity of the mutation is lethal during gestation (51). Additionally, the authors demonstrate that heterozygous animals from the 129/Sv strain manifested an earlier onset of a clinical phenotypes than those from the B6 background (51). Mice without fibrillin-1 (mgN/mgN) die within the first two weeks of postnatal life from ruptured aortic aneurysms and impaired pulmonary function, while heterozygous mgN/+ mice live a normal lifespan (52).

Another line of mice heterozygous for an *Fbn1* allele encoding a cysteine substitution, Cys1039 Gly (C1039G), lying in an EGF-like domain of fibrillin-1, has a mutation analogous to mutation causing MFS in humans. Heterozygous C1039G mice (*Fbn1*$^{\text{C1039G/+}}$) demonstrate histological features of aortic disease, but live a normal life span, however, *Fbn1*$^{\text{C1039G/C1039G}}$ mice die during the perinatal period (53).

To investigate the role of mutant fibrillin-1 in microfibril assembly, two lines of mutant mouse were generated by Charbonneau et al. (54). One of them was called GT-8, in which fibrillin-1 is truncated and tagged with enhanced green fluorescent protein (eGFP). In the heterozygous state, these mice develop features of MFS. Homozygotes die early after birth. The second line (H1Δ) was generated by Cre-mediated removal of *Fbn1* exon 7, flanked by loxP sites, in all cells. However both heterzygous and homozygous mice survived normally, and manifested no apparent phenotype.

The tight skin mouse (Tsk) occurred as a spontaneous mutation as the result of a tandem dupli-

cation of fibrillin-1. This mouse is heterozygous for a genomic duplication of some 30 to 40 kb encompassing exons 17 to 40 of *Fbn1*. The Tsk/+ mouse has thickened skin and visceral fibrosis that results from an accumulation of extracellular matrix molecules, and thus was proposed to be a model of scleroderma, hereditary emphysema, and myocardial hypertrophy (55).

Model	**Mutation**	***Fbn1* expression**	**Phenotype**
mgΔ	Deletion of exons 19-24	10% of wild-type *Fbn1*	Homozygous mice exhibit early postnatal death (50)
mgR	Insertion of Neomycin-cassette in intron region between exon 18 and 19	20-25% of wild-type *Fbn1*	Death from aortic dissection in homozygous mice (50)
mgN	Null allele	Extreme hypomorph	Homozygous mice exhibit early postnatal death (52)
mgΔ^{loxPneo}	Deletion of exons 19-24	78%$\pm$10 of wild-type *Fbn1*	Heterozygotes present some aspects of MFS phenotype. Homozygosity of the mutation is lethal during gestation (51)
C1039G	Missense mutation C1039G	Normal expression	Heterozygotes live normal live span. Homozygotes die perinatally due to vascular failure (53)
Tsk/+	Large in-frame duplication	NA	Early embryonic death (55)
GT-8	Truncation, tagged with eGFP	NA	Heterozygous mice develop features of MFS. Homozygous mice show early postnatal death (54)
H1Δ	Deletion of exon 7	NA	Normal life span (54)

Table 1.2: *Fbn1* mutant mouse model, NA, Not available.

1.5 Pathogenesis of Marfan syndrome

Initially, it was suggested that the pathogenesis of MFS is solely accounted for by the loss of connective tissue integrity. Recent genetic studies of human patients and murine models have revealed that multiple factors such as fibrillin-1 halpoinsufficency, increased activation of TGF-β signaling, active MMPs have been considered to contribute to the pathogenesis of MFS.

1.5.1 Perturbation of microfibril assembly in MFS

The 10-12 nm microfibrils are located primarily around the periphery of the amorphous elastin component of the elastic fibers. During development of elastic tissues, microfibrils are the first elastic fiber structure which is formed. Morphologically identical microfibrils have been found in association with elastin in a wide variety of tissues, including skin, lung, kidney, blood vessels, cartilage, and tendon. Microfibrils not associated with elastin may be observed in other tissues, such as the ciliary zonule (35). The classical view of Marfan pathogenesis is that mutant fibrillin-1 molecules alter microfibril assembly in a dominant-negative manner. Although molecular evidence is still lacking, it seems clear that a certain subset of mutations in fibrillin-1 may result in a substandard threshold of microfibrils by interfering with the assembly of microfibrils (56, 57). Therefore, weakness of the aortic wall was believed to result from defects of fibrillin-1 microfibrils that prevented proper assembly of elastic fibers. This hypothesis was supported by the observation of dramatic paucity of extracellular microfibrils in patient-derived tissues (58, 59). A large portion of the fibroblasts studied showed impaired incorporation of the mutant fibrillin-1 into the extracellular matrix, suggesting functional disturbances in early stages of the assembly mechanism (60–62).

Alternatively, mutant fibrillin-1 may assemble, but incorporation of mutant fibrillin-1 may destabilize microfibrils (38, 42). For instance, pulse-chase studies of patient fibroblasts containing G1127S, which showed normal synthesis and secretion of fibrillin-1 but reduced deposition in the extracellular matrix, suggest that this substitution has an extracellular dominant negative effect during or after incorporation of fibrillin-1 into the microfibril (63). Recent in vivo studies of microfibrils demonstrate that mutations in fibrillin-1 that destabilize microfibril structure underlie the pathological features of the MFS, while mutations that do not destabilize microfibril structure are not associated with Marfan phenotypes (54).

Besides their mechanical role, microfibrils and microfibrillar components can also be involved in cell adhesion. In the developing aorta, microfibrils/fibrillin come in direct contact with endothelial cells by passing through the basement membrane and smooth muscle cells, and mediate the anchoring of these cells to the internal elastic lamina (64, 65). Therefore, in MFS, fibrillin-1 impairment may alter physiological fibrillin-1 signaling in endothelial cells, contribute to endothelial dysfunction, and therefore lead to disease (66). It is known that the RGD (Arginine-Glycine-Aspartic acid) motif in the fourth TGF-β-binding protein-like domain of human fibrillin-1 is flexible and accessible, and regulates cell adhesion and migration through binding to integrins

(67, 68). Lorena et al. (69) demonstrated that a recombinant human fibrillin-1 polypeptide rF16 containing the RGD (N-terminal half of fibrillin-1) far from being proadhesive, displayed antiadhesive properties. Detachment of endothelial lining associated with loss of structural connection between the intimal and medial layers was observed in fibrillin-1 null mice (mgN/mgN) (52). Loss of microfibrillar connection between smooth muscle cells and elastic laminae is believed to be an initial factor of aortic aneurysm in MFS (46).

1.5.2 Haploinsufficiency

The findings in the *Fbn1*$^{C1039G/+}$ mice suggest that haploinsufficiency with half-normal production of normal protein, rather than presence of mutant protein, is required to cause the Marfan phenotype (53). The mechanism of haploinsufficiency can be further confirmed in mgΔ model, in which microfibrils containing the mutant fibrillin-1 were still assembled and elastic fibers develops normally. These findings in the series of mouse model of MFS emphasized the predominant role of wild type fibrillin-1 in tissue homeostasis rather than in elastic matrix assembly (50, 70). In humans, it has been suggested that functional haploinsufficiency through nonsense-mediated decay of most of the mutant mRNAs plays a role in the pathogenic mechanism of MFS (46, 56, 71). Matyas et al. (72) report two *FBN1* deletions in two patients with MFS. Interestingly, these two deletions affect the putative regulatory and promoter region of the *FBN1* gene, strongly indicating that they abolish transcription of the deleted allele. This finding extends the molecular etiology of MFS by providing the evidence that true halpoinsufficiency is sufficient to cause MFS (72). In addition, two missense fibrillin-1 mutations, C1117Y and C1129Y, were retained intracellularly in the endoplasmic reticulum, indicating that specific mutant proteins retained as a consequence of misfolding may result in functional halpoinsufficiency, or alternatively, have an intracellular dominant negative effect (63).

1.5.3 Impaired vasomotor function

MFS is associated not only with extensive degeneration of elastic fibers, but also with endothelial dysfunction and reduction of smooth muscle contractility in the vasculature (73). Vasomotor function in mesenteric arteries, including maximal force development, is detrimentally affected in the *Fbn1*$^{C1039G/+}$ mice (74). The vasomotor dysfunction in Marfan thoracic aorta was thought to be associated with accumulation of oxidative stress due to unbalanced protein expression of superoxide-producing and superoxide-eliminating enzymes (75). Upregulation of

cyclooxygenase-2 (COX-2) in the Marfan aorta has been reported to contribute to the compromised aortic vasomotor function by causing an imbalance in the release of endothelial relaxant and constricting prostanoids (73). It was hypothesized that the loss of vessel elasticity and increase in pulse wave velocity in the Marfan aorta (76) could induce COX-2 expression (77). The endothelium releases a variety of vasoactive mediators, including prostaglandins, endothelial nitric oxide (eNO) to regulate smooth muscle contractility and thus vascular smooth muscle tone (78, 79). eNOS/Akt downstream signaling is significantly impaired in the thoracic aorta during the progression of MFS, leading to the impairment of nitric oxide-mediated endothelial-dependent relaxation (73). Chung and his colleagues have shown that doxycycline treatment normalized the endothelium-dependent relaxation and the basal NO level of *Fbn1*$^{C1039G/+}$ mice as a result of the preservation of elastin fibers (80).

1.5.4 Inflammatory infiltrate in thoracic aortic aneurysm

MFS is the most well known genetic disease characterized by thoracic aortic aneurysm (TAA). Studies have found inflammatory and immune cells around focal cystic medial degeneration (CMD) in patients with MFS and isolated TAA (81–83). CMD is the most common pathology associated with TAAs, which is described as noninflammatory lesion characterized by elastin fragmentation, focal fibrosis, haphazardly distributed areas with loss of VSMCs, and accumulation of collagen (82). Immunohistochemistry of aorta from patients with MFS, familial or sporadic TAAs consistently show the presence of T cells (CD3+) and macrophages (CD68+), particularly in the adventitia, along with an increase in the density of the vasa vasorum and local endothelial activation (84). The authors further confirmed that infiltration of inflammatory cells in the adventitia of Marfan patients was more intense compared with those of sporadic TAA (84). In our previous study (Section 2.5), CD68 immunstaining of the surgical aortic specimen in 28 patients with MFS showed significant increase in the number of macrophages in the tunica media (85). In the mgR/mgR mice, as early as 8 weeks, monocytes begin to infiltrate the medial layer, followed by adventitial inflammation with fragmentation of the medial elastic network and fibroblast hyperplasia, these findings suggesting that inflammatory infiltration is relevant to the progression of aortic aneurysm in this Marfan mouse model (50). Contrary to TAA accumulation of inflammatory cells including T and B lymphocytes, mast cells, and macrophages is one of the main characteristics of the abdominal aortic aneurysm (AAA) (86–88). The current hypothesis for AAA is that the recruitment of inflammatory cells into the adventitia and media, with subse-

quent increased expression of proinflammatory cytokines and extracellular matrix turnover may contribute to the rapid growth and rupture of larger AAA (89, 90). The findings in Marfan patients and mouse model support the notion that inflammation could also play an important role in the pathogenesis of MFS, which underscores the need for further research of the inflammatory change in TAA.

1.5.5 Upregulation of matrix metalloproteinases (MMPs)

Matrix metalloproteinases (MMPs) are potent proteinases involved in a broad range of normal and pathological processes, including embryonic development, tissue remodeling, inflammation and wound healing. Various studies have confirmed that MMPs could contribute to the progression of thoracic aortic aneurysm in MFS. For instance, study of aortic specimens of Marfan patients demonstrated upregulated MMPs and tissue inhibitor of MMP (TIMP) activity at the border of areas of cystic medial regeneration (CMD) (73, 82). Cultured vSMCs from Marfan patients demonstrate MMP-2 overexpression and the abnormal apotosis of these vSMCs is thought to be a result of upregulated MMP-2 (81). Moreover, increased concentrations of MMP-1, MMP-3 and MMP-9 have been observed in zonular fibers of dislocated lens in Marfan patients (91). MMP-9 is thought to be produced by infiltrating neutrophils and macrophages and is not present in large amounts in nondiseased aorta (92). Wild type fibrillin-1 and elastin are susceptible to digestion by several MMPs like MMP-2, -9 and -12 (50, 93, 94). Study of the Marfan mouse models C1039G/+ and mgR/mgR demonstrates that the upregulation of MMP-2 and -9 correlated with the extent of loss of elastic content and elastic fiber architecture during TAA formation (50, 73). Moreover, Ikonmidis et al. (95) demonstrated that MMP-9 gene deletion attenuated aortic dilatation in a murine model of TAAs. MMP-12, a macrophage-specific metalloproteinase, is the predominant matrix-degrading proteinase secreted by macrophages (96). Macrophages found in Marfan aortic specimens may therefore reflect the involvement of MMP-12 in TAA. Actually, elevated MMP-12 has been shown to be associated with AAA (97). Furthermore, mice deficient in MMP-12 are reported to be protected from cigarette smoke induced emphysema (98). The involvement of MMP activity in TAA has been further confirmed by the fact that treatment with doxcycline, a nonspecific MMP inhibitor, significantly prolonged the survival of the mutant mice and decreased the development of aortic aneurysm in Marfan mouse model (80, 99). The therapeutic efficacy of doxycycline was replicated in mgR homozygous mice with intraperitoneal injection of neutralizing antibodies against MMP-2 and -9 (80).

1.5.6 Proteolytic degradation of mutant fibrillin-1

To date, more than 600 mutations have been identified in *FBN1* (http://www.umd.be). The mutations are spread throughout almost the entire gene without obvious prediction for any given region. Around 60% of the mutations are missense mutations, and most of these affect one of the conserved cysteine residues or a residue of the cbEGF modules (71, 100). It is known that calcium binding by cbEGF modules is essential for the conformation and stability of fibrillin-1 (101, 102). Such mutations are reported to reduce the calcium affinity of affected modules (103–106), which could be an explanation of the observations that a number of *FBN1* mutations can increase the susceptibility of recombinant fibrillin-1 fragments to in vitro proteolysis by exposing specific cryptic proteolysis sites (Table 1.3). For example, our group has shown that a mutation affecting a residue of the calcium-binding consensus sequence (K1300E) found in a patient with relatively mild clinical manifestations of classic MFS caused a modest increase in susceptibility to in vitro proteolysis by trypsin, whereas a mutation affecting the sixth cysteine residue of the same cbEGF module (C1320S) reported in a severely affected patient caused a dramatic increase in susceptibility to in vitro proteolysis by trypsin (107). It has been reported that authentic human fibrillin-1 and recombinant human fibrillin-1 subdomains, spanning the whole molecule, showed significantly slower proteolytic degradation in the presence of $CaCl_2$ than in the presence of EDTA, demonstrating that calcium stabilizes the structure of fibrillin-1 and protects the molecule against proteolytic degradation (107, 108).

The fact that different mutations within cbEGF modules can have a differential effect on susceptibility to proteolysis, provides a potential explanation for some genotype-phenotype correlations in MFS (46, 107). Assuming that increased susceptibility to proteases does play a role in the pathogenesis of MFS, then there are at least two mechanisms that could be important. Proteolytic degradation of mutant fibrillin-1 monomers could take place following secretion into the extracellular space but before incorporation into the microfibrils, thus reducing the total amount of fibrillin-1 available for assembly of microfibrils. Alternatively, mutant fibrillin-1 monomers could be incorporated into microfibrils and then represent a sort of Achilles' heel causing increased susceptibility of the entire microfibrillar structure to proteolysis and fragmentation (14, 46). It is worth mentioning that the increased proteolysis is not only limited to mutant fibirllin-1 protein, for instance, mutations in the actin-modulating protein gelsolin, which is known to be associated with neurodegenerative disease familial amyloidosis of Finnish type (FAF), is susceptible to aberrant proteolysis by furin in the trans-Golgi network as a result of disruption of the Ca^{2+}-binding

site (109). Collectively, it can be hypothesized that proteolytic degradation of mutant fibrillin-1 monomers leads to fragmentation and progressive loss of microfibrils, which may be an initiating factor in the development aortic dissection.

Mutation	Location	Reference
N548I	cbEGF4	Reinhardt et al (102)
R627C	cbEGF6	Vollbrandt et al (110)
C750G	cbEGF7	Vollbrandt et al (110)
E1073K	cbEGF12	Reinhardt et al (102)
G1127S	cbEGF13	Whiteman et al (106)
K1300E	cbEGF17	Booms et al (107)
C1320S	cbEGF17	Booms et al (107)
D1406G	cbEGF20	Robinson and Booms (14)
C1408F	cbEGF20	Robinson and Booms (14)
C1977R	cbEGF30	Suk et al (103)
C1977Y	cbEGF30	Suk et al (103)
N2183S	cbEGF33	McGettrick et al (111)

Table 1.3: *FBN1* mutations identified in individuals with MFS that have been shown to increase susceptibility to in vitro proteolysis. The predicted amino acid change and the affected cbEGF modules are shown. Note that N2183S is a protein-engineered mutation and has not been found in patients. Adapted from Robinson et al. (46).

1.5.7 Abnormal TGF-β signaling

TGF-β has long been implicated in the pathogenesis of fibrotic diseases like scleroderma, fibrosarcoma, and idiopathic pulmonary fibrosis (112). TGF-β is synthesized as an inactive precursor containing an N-Terminal prodomain termed latency associated peptide (LAP). Mature TGF-β associated with LAP is referred to as the small latent complex (SLC). The SLC is covalently bound to another protein called latent TGF-β binding protein-1 (LTBP-1), forming the large latent complex (LLC) (113). Microfibrils were known to regulate TGF-β activity through the binding of the N-terminus of fibrillin-1 to the C-terminus of LTBP-1, a large molecule that keeps TGF-β in an inactive state in the matrix (114) (Figure 1.4). This was further confirmed by the finding that transgenic mice expressing LTBP-1 lacking the C-terminus binding region demonstrate inappropriately increased TGF-β activation (115). Additionally, in tissues, proteolysis of crosslinked LTBP-1 by enzymes such as bone morphogenetic protein-1 (BMP-1), MT1-MMP and plasmin are initiating events in TGF-β activation (116, 117).

It was proposed that fibrillin-1 gene mutation associated with microfibril deficiency in MFS

leads to dysregulation of TGF-β (118), thus, further reinforcing the proposed vicious cycle in the development of aortic aneurysm (73). Studies on mice lacking or underexpressing fibrillin-1 (mgΔ/mgΔ, mgN/mgN, mgR/mgR) documented increased activity of TGF-β signaling due to to inadequate sequestration (50, 118). Dietz and his colleagues (119) reported that phosphorylation and subsequent nuclear translocation of pSmad2, which are induced by TGF-β signaling, are markedly increased in the aortic media of *Fbn1*$^{C1039G/+}$ mice relative to wild-type mice. Besides Marfan mouse model, increased expression of TGF-β1 and 3 has also been observed in aortic specimens from Marfan patients (120). Moreover, circulating TGF-β1 concentrations were found to be elevated in patients with MFS (121). Additionally, increasing TGF-β independent SMAD2 signaling have been reported in the primary cultures of vSMCs from Marfan patients, indicating a possible epigenetic control in the pathogenesis of TAA in MFS (122). Actually, increased TGF-β activity is not limited to TAA in MFS. For instance, recently, van de Laar et al. (123) found mutations in SMAD3 caused a new syndrome presenting with aortic aneurysm in association with enhanced pSMAD2 activity through the medial vSMCs in affected individuals. The selective angiotensin II receptor 1 blocker (ARB), losartan potassium and TGF-β neutralizing antibodies haven been shown to effectively rescue aortic aneurysm in mouse model of MFS (118, 119). A pilot study in 18 children with severe MFS (median age 6.5 years) showed a significant reduction in the rate of progression of aortic wall dilatation following treatment with ARBs (124). The circulating TGF-β1 concentrations in human patients and *Fbn1*$^{C1039G/+}$ mice decrease significantly after administration of losartan or beta-blocker (121). The striking outcoming of these treatments further confirmed the important role of TGF-β in the development of MFS.

It is of note that TGF-β can initiate multiple downstream signaling cascades, including both canonical (SMAD-dependent) and noncanonical (SMAD-independent) pathways (125). Recently, Carta et al. (126) have shown that elevated pSmad2 activity could be identified in the culture of aortic vSMCs from different Marfan mice (mgN/mgN, mgR/mgR, *Fbn1*$^{C1039G/+}$) and the noncanonical Smad signaling p38 is thought to be responsible for the early accumulation of endogenous pSmad2 in mgN/mgN vSMCs. Additionally, recent studies have shown that noncanonical (Smad-independent) TGF-β signaling is a prominent driver of aortic disease in MFS mice, and selective inhibition of extracellular signal-regulated kinase (ERK1/2) or Jun N-terminal kinase-1 (JNK1) activation ameliorated aortic growth, and Smad4 deficiency exacerbated aortic disease and caused premature death in MFS mice (127). Furthermore, the same research group demonstrated that losartan inhibit TGF-β mediated activation of ERK (127, 128).

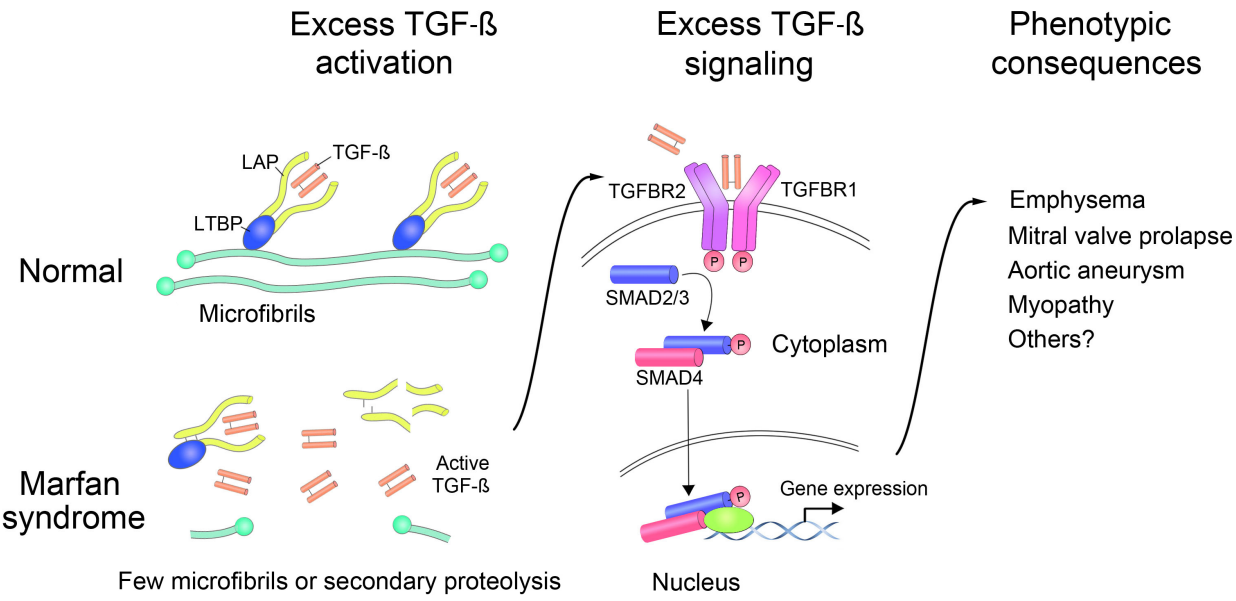

Figure 1.4: Loss or proteolysis of microfibrils leads to multiple phenotypic features that may result in part from activation of TGF-β. Fragmented microfibrils are associated with release of active TGF-β, resulting in excessive TGF-β activation. Excessive TGF-β signaling is responsible for different phenotypic consequences. LAP, latency-associated protein; LTBP, latent TGF-β binding protein. Modified from (132) and (133).

Mutations in the genes for *TGFBR1* and *TGFBR2* have been identified in disorders with varying degrees of overlap with classic MFS (25, 129, 130). The impact of different mutations in *TGFBR2* might be responsible for clinical phenotype variability observed in *TGFBR2* mutations related diseases. For instance, it has been reported that R460C, which has been mainly found in familial TAAD, showed a less-severe dominant-negative effect compared with mutations associated with LDS and MFS2 (131).

1.5.8 Secondary cellular events caused by fragmentation of extracellular matrix

Fibrillin-1 and elastin fragmentation has been documented in the aorta of Marfan patients and the mouse model of MFS (53, 82, 134–136). For instance, abnormalities in fibrillin-1 immunostaining patterns were observed in skin and cutaneous fibroblast culture of patients with MFS (137). Immunohistochemistry of fibrillin-1 in cultured human Marfan vSMCs demonstrates that extracellular fibrillin-1 might be reduced, disrupted, and dysfunctional (81). Fragmentation of fibrillin-1 was also observed by fibrillin immunonstaining of aortic specimens in patients with MFS (134).

Several lines of evidence support the hypothesis that fragmentation of extracellular matrix (ECM) may have signaling activities that the corresponding intact molecules do not have (138), which could be interperated as that the presence of fibrillin-1, elastin other ECM fragments could have

various abnormal secondary cellular activities which in turn could cause further fragmentation in aortic wall. For instance, distinct fragments of fibronectin are able to increase expression of MMP-1 (139), MMP-3 (140), and MMP-13 (141). Our group has shown that recombinant fibrillin-1 fragments containing Arg-Gly-Asp (RGD) site are also known to upregulate expression levels of MMP-1 and MMP-3 in the culture of fibroblasts (142). Another recombinant fibrillin-1 fragments containing exon 44 to 49 can release the active TGF-β by inhibiting the binding of LTBP-1 to N-Terminal of fibrillin-1 (143). Gene Ontology (GO) analysis of the human proteome showed that proteins with multiple pentapeptide Gly-x-x-Pro-Gly (GxxPG) motifs are highly enriched for GO terms related to the extracellular matrix (144). The GxxPG motif is known as the consensus sequence of ligand of elastin binding protein (EBP). EBP is is a peripheral 67-kDa protein, one of three subunits making of the elastin binding receptor. The other two membrane-associated protein include a 55-kDa subunit as the protective protein, also called cathepsin A and a 61-kDa sialidase (neuraminidase) (145, 146). EBP is capable of transmitting physiological signals from the extracellular matrix into the cell interior, the downstream of EBP signaling seems to be very different dependent on stimulating cell type (147). The repeating hexapeptide Val-Gly-Val-Ala-Pro-Gly (VGVAPG) has been identified as a chief ligand for the EBP (148, 149), and VGVAPG was known to be chemotactic for fibroblasts and monocytes (150). Moreover, some peptides other than VGVAPG have also been shown to have chemotactic effects related to EBP binding, including PGAIPG (151) and GVLPG and GVAPG (152). Elastin derived peptides (EDPs) containing the GxxPG motif, in particular, are biologically active, as these are able to interact with the EBP (145, 149, 153, 154). For instance, chemotactic effects of α elastin may result from the stimulation of cGMP and cGMP-dependent protein kinase mediated by binding of GxxPG to EBP present on the surface of mononuclear phagocytes (155). Elastin degradation products were reported to stimulate proliferation of arterial smooth muscle cells as a result of elastin receptor-transduced signaling cascades involving the phosphorylation of ERK1/2 (146). Brassart and colleagues reported that pertussis toxin-sensitive G proteins and tyrosine kinase are involved in the EBP-mediated up-regulation of MMP-1 in cultured fibroblasts (156). Furthermore, EDPs have been noted to stimulate the production of MMP-1 (157) and typical bone proteins in cultured aortic SMCs (158).

1.6 Hypothesis of this study

In this study we hypothesized that GxxPG containing fibrillin-1 or elastin fragments in MFS could deliver secondary cellular effects through their interaction with EBP, therefore contributing to the development of TAA in MFS (Figure 1.5). Since EBP possesses galactolectin properties, when galactosugars bind it, its affinity for EDP dramatically decreases, leading to their release and further dissociation of EBP from the complex. Galactosugars, such as lactose, are therefore commonly used as EBP antagonists (159). It is also well-known that a monoclonal anti-elastin antibody called BA4 especially recognizes the GxxPG motif (160), thus blocking the interaction between GxxPG and EBP.

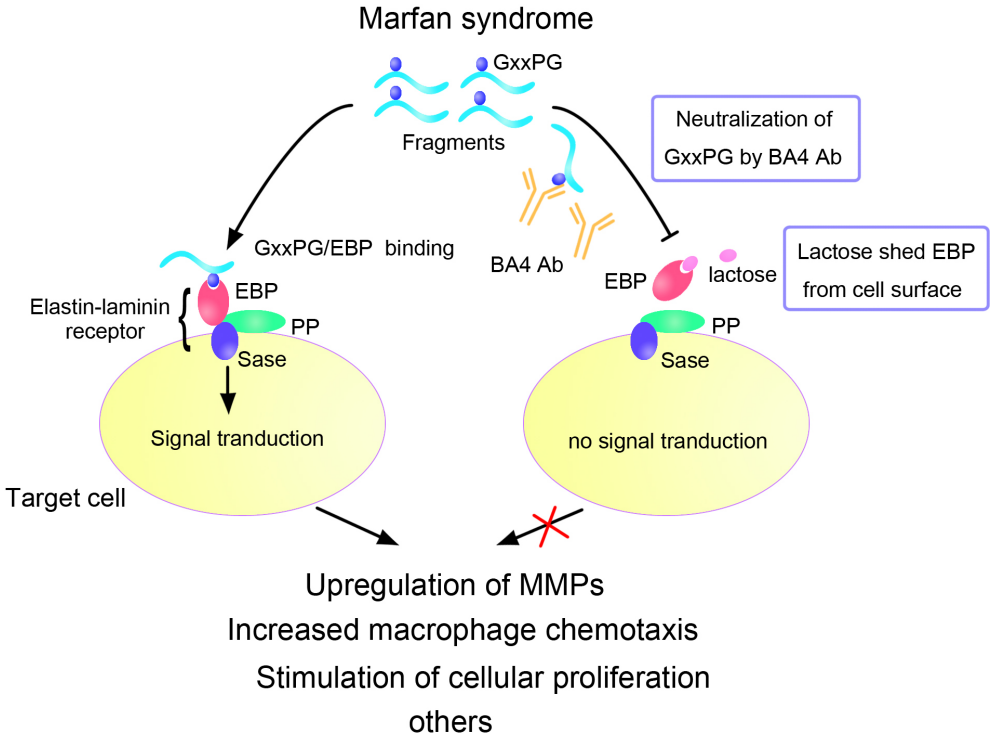

Figure 1.5: Proposed model for secondary cellular events caused by GxxPG containing fragments. GxxPG fragments caused by fibrillin-1 proteolysis or elastolysis binds to EBP, triggering EBP downstream pathway, leading to secondary effects which may be related to the development of TAA in MFS. BA4 especially recognize GxxPG motif. Lactose causes the EBP to be shed from the cell surface. EBP, Elastin-binding-protein; PP, Protective protein; Sase, Silidase.

1.7 Aim of this study

The main aim of this dissertation was the investigation of the role of fibrillin-1 and elastin fragments in the pathogenesis of MFS. To analyze the abnormal activities of fibrillin-1 fragments, recombinant fibrillin-1 polypeptides containing GxxPG motif were generated for chemotaxis as-

say. Additionally, macrophage chemotaxis toward aortic extracts from a Marfan mouse model (mgR/mgR) and Marfan patients was also investigated. Although the role of inflammation in the pathogenesis of TAAs remains unclear, we believe that valuable data from the abdominal aneurysm literature should be considered in the study of TAAs. For instance, anti-inflammatory therapy in AAA mouse model or patients have been confirmed to be successful (161, 162). Studies with animal models have helped us understand some of the pathophysiologic mechanisms of MFS and created new therapeutic opportunities. Losartan, a blocking agent of TGF-β or doxycycline, an unspecific MMPs inhibitor, have been reported to successfully decrease the development of TAA in Marfan mouse model (80, 99, 119). These striking findings motivated us to to investigate whether neutralization of GxxPG-fragments by BA4 or anti-inflammatory treatment in homozygous mgR mice can prevent the progress of aortic aneurysm. The results of this study can not only further clarify the role of fibrillin-1 and elastin fragments or inflammatory infiltration in the development of TAA but may also provide us another possible therapeutic strategy.

2 Material and Methods

2.1 Material

2.1.1 Chemicals and Reagents

Name	Manufacturer
30% Acrylamid/0.8% Bisacrylamid	Roth
Agarose	Invitrogen
Ampicillin sodium salt	Sigma
Ammonium persulfate (APS)	Sigma
Bovine Serum Albumin (BSA)	Sigma
Bromphenol blue	Sigma
Chloroform	Merk
Protease Inhibitor Cocktail Tablets	Roche
Coomassie G250	Pierce
Dimethyl sulfoxide (DMSO)	Merk
Dithiothreitol (DTT)	Serva
Doxycycline hyclate	Sigma
Fluoromount-G	Science Services
Entellan	Merk
Ethylenediaminetetraacetic acid (EDTA)	Sigma
Ethidiumbromide	Roth
Formaldehyde	Merk
Glycine	Roth
Glycerol	Sigma
30% H_2O_2	Merk
Indomethacin	Sigma
Imidazole	Sigma
Lipofectamine® 2000	Invitrogen
Mayert's Hematoxylin	Invitrogen
β-Mercaptoethanol	Sigma
Methanol	Merk
Ni-NTA-agarose	Qiagen
Phosphate buffered saline (PBS)	Biochrom
Phosphatase Inhibitor Cocktail	Roche
Prestained Protein Standard	Fermentas
Sodium dodecylsulfate (SDS)	Sigma
N,N,N,N-Tetramethylethylenediamine (TEMED)	Sigma

TRIzol®	Invitrogen
Triton X-100	Serva
Tween 20	Sigma
Zeocin	Invitrogen

Table 2.1: Chemicals and reagents

Anorganic salts, acids and bases and alcohols were purchased in analytical grade from Sigma-Aldrich, Roth or Merck Bioscience.

2.1.2 Composition of prepared buffers

Buffer	**Composition**
Aorta extraction buffer	2 M NaCl in PBS pH 7.4
Blocking buffer for Western blot	5% nonfat dry milk in 1xPBS-T
Blocking buffer for immunofluorescence	3% BSA in PBS
Chemotaxis buffer	1% BSA in RPMI 1640
Elution buffer for Ni-NTA-Agarose	50 mM NaH_2PO_4, 300 mM NaCl, 250 mM Imidazole, pH 8.0
Protein loading buffer	200 mM Tris-HCl pH 6.8, 0.8% SDS, 0.4% Bromophenol blue, 40% Glycerol
LB Medium	1% bacto-trypton, 0.5% yeast extract, 0.5% NaCl
LB-Agar	LB medium, 1.5% agar
PBST	PBS, 0.05% Tween-20
4% paraformaldehyde (PFA)	4% paraformaldehyde in PBS pH 7.4
5xSDS Sample buffer	2% SDS, 60 mM Tris/HCl pH 6.8, 50% glycerin, 14.4 mM β-mercaptoethanol, 0.1% bromphenol blue
RIPA buffer	0.05% SDS, 50 mM Tris-HCl pH 7.4, 150 mM NaCl, 0.5% sodium deoxycholate, 1% NP40, 1 mM EDTA
SDS-PAGE running buffer	25 mM Tris-HCl pH 8.8, 250mM glycine, 0.05% SDS
TBE	20 mM Tris-HCl pH 8.0, 445 mM boric acid, 10 mM EDTA
TBS	150 mM NaCl,10 mM Tris-HCl,pH 7.5
TBST	TBS, 0.05% Tween-20
Western blot transferring buffer	192 mM glycine, 25 mM Tris-HCl, 20% methanol
Wash buffer for Ni-NTA agarose	50 mM NaH_2PO_4, 300 mM NaCl, 20 mM Imidazole, pH 8.0

Table 2.2: Composition of prepared buffers

2.1.3 Enzymes and Peptides

Name	Concentration	Manufacturer
Alkaline phosphatase	1 U/μl	Promega
Collagenase type II	125 U/mg	Worthington Biochemical
T4 DNA ligase	400 U/μl	NEB
Restriction enzymes	10 U-20 U	NEB
PNGase F	500 U/μl	NEB
Proteinase K	10 mg/ml	Roche
Pfu DNA Polymerase	2.5 U/μl	Fermentas
Taq DNA polymerase	5 U/μl	Promega
Shrimp alkaline phosphatase (SAP)	20 U/μl	Fermentas
SYBR Green PCR Master Mix	2x	Applied Biosystems
Val-Gly-Val-Ala-Pro-Gly (VGVAPG)	–	Sigma
Pro-Gly-Phe-Pro-Pro-Gly (PGFPPG)	–	Peptide Company
Cys-Gly-Cys-Pro-Pro-Gly (CGCPPG)	–	Peptide Company
Glu-Gly-Phe-Glu-Pro-Gly (EGFEPG)	–	Peptide Company
Glu-Gly-Phe-Glu-Ser-Gly (EGFESG)	–	Peptide Company
Elastin peptides	–	Elastin Products

Table 2.3: Enzymes and Peptides

2.1.4 Antibodies

Name	Dilution	Manufacturer
Anti-α smooth muscle actin FITC-conjugated antibody	1:200	Abcam
Anti-mouse IgG, HRP (horseraddish peroxidase) coupled	1:2000	Abcam
Anti-rabbit IgG, HRP (horseraddish peroxidase) coupled	1:2000	Abcam
Alexa Fluor® 555 goat anti-rabbit IgG	1:1000	Invitrogen
Mouse monoclonal anti-β actin	1:2000	Abcam
Mouse monoclonal anti-elastin (BA4)	1:1000	Sigma
Monoclonal mouse anti-F4/80	1:150	Abcam

Rabbit polyclonal anti-COX-2	1:100	Abcam
Rabbit polyclonal anti-phospho-ERK1/2	1:1500	Cell Signaling
Rabbit polyclonal anti-ERK1/2	1:1500	Cell Signaling
Rabbit polyclonal anti-MMP-2	1:2000	Abcam
Rabbit polyclonal anti-MMP-9	1:2000	Abcam
Rabbit monoclonal anti-MMP-12	1:2000	Abcam
Rabbit polyclonal anti-pSMAD2	1:3000/1:150	Cell Signaling
Mouse monoclonal 6xHis-tag	1:1000	Abcam
Mouse monoclonal anti-Myc	1:2000	Santa Cruz

Table 2.4: Antibodies

2.1.5 Media, antibiotics for cell culture

Name	**Manufacturer**
Dulbecco's Modified Eagle's Medium (DMEM)	Gibco
RPMI 1640	Biochrom
100xPenicillin/streptomycin mix	Gibco
Trypsin-EDTA	Gibco
Cell dissociation solution	Sigma

Table 2.5: Media, antibiotics for cell culture

2.1.6 Solutions for Modified Verhoeff Elastic-Van Gieson Stain and Immunohistochemistry

Name	**Manufacturer**
Alcoholic Hematoxylin, 3%	Electron Microscopy Sciences
Ferric Chloride, 2% aqueous	Electron Microscopy Sciences
Lugolt's Iodine	Electron Microscopy Sciences
Ferric Chloride, 0.4% aqueous	Electron Microscopy Sciences
van Gieson's Solution	Electron Microscopy Sciences
Trypsin enzymatic antigen retrieval solution	Abcam

Table 2.6: Solutions for Modified Verhoeff Elastic-Van Gieson Stain and Immunohistochemistry

2.1.7 Kits, Consumables

Kits, Consumables	**Manufacturer**

BCA Protein Assay	Thermo Fisher Scientific
BigDye terminator cycle sequencing ready reaction kit	PE Biosystems
Diaminobenzidine tetrahydrochloride (DAB)	Thermo Fisher Scientific
Dialysis cassette	Thermo Fisher Scientific
ECL Western Blotting Reagent	Amersham
QIAquick Gel Extraction Kit	Qiagen
QIAquick PCR Purification Kit	Qiagen
MagAttract® DNA M48 Kit	Qiagen
Vecatastain® ABC Kit	Vector Labs
MaxiSorp flat-bottom 96 well plate	Nunc
Perioxidase Supperssor	Thermo Fisher Scientific
Plasmid mini Kit	Promega
Polyvinylpyrrolidone-free polycarbonate membrane	Neuro Probe
SuperScript II First-Strand Synthesis system for RT-PCR	Invitrogen
PVDF membrane	Thermo Fisher Scientific
Parafilm	Pechiney
Slides and coverslips	Roth
Syringes	Braun

Table 2.7: Kits, Consumables

2.1.8 Plasmids and Bacterial strains

Name	**Manufacturer**
Top 10 *E.coli*	Invitrogen
DH5 alpha	Invitrogen
pSec Tag A	Invitrogen

Table 2.8: Plasmids and Bacterial strains

2.1.9 Laboratory Equipment

Equipment	**Manufacturer**
Agarose gel electrophoresis apparatus	Biometra
Cell culture incubator	Heraeus
Centrifuges	Heraeus, Eppendorf
BioRobort M48 workstation	Qiagen
Boyden Chemotaxis Chamber AP48	Neuro Probe

Film processor	AGFA Curix 60
Gel electrophoresis equipment	Bio-Rad
GeneAmp5700 Sequence Detection system	Applied Biosystems
Microplate Reader	Berthold
Microscope	Carl Zeiss
Microwave	Ordinary type
pH Meter	Mettler-Toledo GmbH
Pipettes, adjustable	Eppendorf
Power supply	Bio-Rad
Semi-dry western blotting apparatus	Bio-Rad
Spectrophotometer	Beckman
Thermocycler	Biometra, Eppendorf
Tissue processor TP1020	Lecia Microsystems
Transilluminator, UV	UV, INC
Vortexer	Stuart Scientific
Whatman 3 MM paper	Whatman

Table 2.9: Laboratory Equipment

2.1.10 Synthetic oligonucleotides

All synthetic oligonucleotides used in this study were synthesized by MWG Biotech or by Metabion, Germany.

2.1.11 Animals

Healthy wild-type C57BL6 or homozygous mgR mice were housed in room with controlled photoperiod and temperature. Animals were given free access to water and pelleted diet and were maintained under pathogen-free, controlled conditions. The mice were sacrificed by CO_2 suffocation or cervical dislocation. All procedures were in accordance with ethical guidelines laid down by the local governing body and approved by Landesamt für Gesundheit und Soziales in Berlin (LaGeSo, Reg 0137/07).

2.2 Methods: Molecular Biology

2.2.1 Agarose gel electrophoresis

Conventional agarose gel electrophoresis was used to separate double stranded DNA molecules with sizes between 100 bp and 10,000 bp. Agarose was typically used at a concentration between 1% and 2% in 0.5xTBE buffer, ethidium bromide was added from a 0.5 mg/ml stock solution to a final concentration of 0.1 μg/ml. Samples were mixed with 2 volumes of loading buffer (Fermentas) and loaded onto the gel. After electrophoresis DNA fragments were visualized using an ultraviolet transilluminator.

2.2.2 RNA isolation and reverse transcription

5×10^4 HEK 293 cells were lysed for 5 min at room temperature in 1 ml Trizol Reagent (Invitrogen). After addition of 0.3 ml chloroform, the samples were mixed vigorously, following centrifugation at 12000xg for 15 min at 4°C, RNA in the aqueous phase was precipitated with 0.5 ml isopropanol, incubated for 10 min at room temperature and centrifuged at 12,000 x g at 4°C, RNA pellet was washed with 75% ethanol with subsequent centrifugation at 7500xg for 5 minutes, air-dried and dissolved in 50 μl RNase-free water and stored at -80°C. cDNA synthesis was performed by using SuperScriptTM II First-Strand Synthesis System (Invitrogen) according to the manufacturer's instructions.

2.2.3 Polymerase chain reaction (PCR) amplification for cloning

PCR was used to amplify specific DNA sequences by simultaneous primer extension of complementary strands of DNA (163). A template fragment flanked by the primer sequences is produced in large quantities by using the PCR. Gene-specific PCR primers were designed to add recognition sites for restriction nuclease to the 5' and 3' end of the amplified DNA sequence. PCR reactions for cloning containing 10xPCR buffer, 0.4 μM of each primer, 0.2 mM dNTP, and 1 unit Pfu polymerase (Fermentas) in a total volume of 50 μl and approximately 2 μl cDNA as template. Cycling conditions included an initial denaturation step at 95°C for 5 min, followed by 35 cycles of 30 seconds at 95°C 30 seconds at the specific annealing temperature, 1 min at 72°C, and a final extension step at 72 °C for 7 min.

2.2.4 Gel extraction and PCR purification

After PCR or enzymatic modification, DNA was separated by agarose gel electrophoresis and purified by using the QIAquick gel extraction kit according to the manufacturer's instructions.

2.2.5 Restriction digest and ligation

200 ng - 1 μg of DNA was digested using 10 U of the restriction enzyme (NEB) and 5 μl of restriction buffer in 50 μl volume, BSA was added to the digest depending on the enzyme used. The reactions were incubated for 3 h or overnight for digestions at the temperature required for the respective restriction enzyme. All ligations were carried out as sticky end ligations with 4 fold molar ratios of inserts to vectors. Ligations were performed in a total volume of 10 μl containing 2 μl of T4 DNA ligase (NEB) and 1xligation buffer at 16°C overnight. Alternatively a quick ligation using 2xligation buffer was preformed at RT for half an hour up to 2 hours.

2.2.6 Transformation

Aliquots of chemically competent TOP 10 *E. coli* cells (Invitrogen) were thawed on ice and mixed with 2 μl of the ligation product. The mixtures were kept on ice for 30 min and then incubated at 42°C for 30 sec. Then 250 μl SOC medium were added and the culture incubated at 37°C with shaking for 60 min. The cells were then plated on LB selection plates with 50 μg/ml Ampicillin and the plates incubated at 37°C overnight. 5 to 10 colonies were selected and used to inoculate LB cultures with 50 μg/ml Ampicillin for mini (5 ml) preparations.

2.2.7 Isolation of plasmid DNA from bacterial cultures

The isolation of plasmid DNA from 5 ml of overnight culture medium with bacteria was done using Promega Plasmid Purification Mini Kit 2.0 following the manufacturer's instructions.

2.2.8 Cell culture

The murine macrophage cell line RAW 264.7 (ATCC TIB-71) and HEK 293 cells were grown in RPMI 1640 and DMEM, both media were supplemented with 10% FBS and penicillin/streptomycin mix (final concentration: penicillin, 100 IU/ml; streptomycin, 100 μg/ml) and were grown at 37°C in a cell incubator in a 5% carbon dioxide / 100% humidity. RAW 264.7 cells have properties

similar to those of mouse resident macrophages and exhibit responsiveness to chemotactic stimuli (164). Cells were split twice a week after reaching 90% confluency. In order to distinguish live and dead cells, dead cells were stained by Trypan blue in a 1:10 dilution. 20 μl of the diluted cell suspensions was transferred to the chamber for counting under the microscope. At least 4 large squares were counted. The number of cells per ml was calculated with the following formula: Cells/ml = mean cell count * dilution factor ($1x10^5$).

2.3 Method: Protein chemistry

2.3.1 SDS-Polyacrylamide Gel Electrophoresis (SDS-PAGE)

The polyacrylamide gel were prepared according to standard protocols. Protein samples for SDS-PAGE were prepared by mixing them with loading buffer and denaturing for five minutes at 95°C. The proteins are loaded onto a 10% or 15% polyacrylamide gel and separated by denaturing SDS-PAGE according to their molecular weight. The prestained molecular weight marker (Fermentas) was used as a size reference. After electrophoresis the proteins are visualised by coomassie staining or detected by Western blot with corresponding antibodies.

2.3.2 Coomassie-G stain of proteins

Staining of proteins with Coomassie-G is based on the nonspecific adsorption of this triphenylmethane dye to basic or aromatic residues of proteins. Coomassie-G stain is normally performed after SDS-PAGE and recognizes as little as 0.5 μg. Briefly, after gel electrophoresis, SDS-PAGE gel was washed in dH_2O for 10 min. Afterwards, the gel was stained in Coomassie-G staining solution (Bio-Rad) for 1 hour. Destaining was accomplished by the addition of dH_2O until the background is clear.

2.3.3 Western blot analysis

For western blot analysis, protein samples were first separated via SDS-PAGE and subsequently transferred to microporous polyvinylidene difluoride (PVDF) membrane (Millipore) using a semi-dry apparatus (Bio-Rad). The membrane and blot paper were soaked in western transfer buffer. The transfer was carried out for 1 hour at 10 V. After transfer, membrane was incubated with blocking buffer for 1 hour at room temperature (RT), and then incubated overnight at 4°C or 2 hours at RT with primary antibodies diluted in blocking buffer. Membrane was washed three

times in TBST, and incubated for 1 hour at RT with peroxidase-conjugated anti-rabbit IgG or anti-mouse IgG. Following 3 times washes in TBST, the immunreactive bands were detected with ECL kit (Amersham Bioscience) according to the manufacturer's instructions.

2.3.4 BCA protein assay

The BCA protein assay is a common colorimetric method for protein quantification of a sample. Its detergent-compatible formulation is based on bicinchoninic acid (BCA). This method combines the well-known reduction of Cu^{+2} to Cu^{+1} by protein in an alkaline medium (the biuret reaction), which causes a purple-colored reaction product formed by chelation of 2 molecules of BCA with 1 cuprous ion (Cu^{+1}). The chelate complex exhibits a strong extinction at 562 nm and is linear over a range from 20 to 2000 μg/ml protein. In this study the Thermo Scientific Pierce BCA Protein Assay Kit was used following the manufacture's instructions. Briefly, BSA standard or appropriately diluted samples were transferred onto a 96-well microtiter plate in duplicate. After adding the 200 μl mixed reagent A and B (50:1), the plate was incubated at 37°C for 30 min, absorbance was measured at the Berthold microplate reader. The standard curve was used for interpolation of sample protein.

2.3.5 Enzyme Linked Immunoabsorbent Assay (ELISA)

GxxPG containing fragments concentration was measured by using a competitive ELISA method as described previously by Wei et al.(165), with some modifications. Maxisorb 96-well microtiter plates (Nunc) were coated with 50 μl of elastin peptide (0.5 μg/ml, CB573, Elastin Products Company) in PBS, pH 7.4 and incubated overnight at 4°C. The wells were blocked with 100 μl of 0.5% BSA in PBS containing 0.05% Tween 20 (PBST). Spike-and-recovery experiment detects a discrepancy between standard diluent (PBS) and 2 fold diluted extraction buffer. Therefore, in oder to generate a standard curve, a variable concentration of elastin peptides from 10 ng/ml-10 μg/ml diluted in 1:2 extraction buffer is mixed with a 1:1000 dilution of the mouse monoclonal antibody derived from immunization against bovine α-elastin (mAb BA4, Sigma-Aldrich) and incubated in a 0.5% BSA precoated plate. The standard curves were fitted using a four-parameter logistic model. Simultaneously, 25 μl of each sample was diluted 2 times with PBS and were mixed with 50 μl of 1:1000 diluted BA4 antibody. After overnight incubation with mild shaking at 4°C, 100 μl mixtures were then added to each well in the elastin peptide coated plate and incubated for 30 min at 37°C, the plates were washed three times with PBST, followed by the

addition 50 μl of secondary antibody (1:2000 anti-mouse IgG peroxidase conjugate). After 1 hour incubation at 37°C, the plates were washed three times, 50 μl of tetramethylbenzidine substrate solution (Thermo Fisher Scientific) was added, and after 10 min incubation at RT the reaction was quenched by adding 50 μl 1 M H_2SO_4 to each well. The absorbance was measured at 450 nm using a micro-plate reader. The concentration of GxxPG containing fragments was normalized against the total protein concentration of the aortic extracts. The level of BA4 antibody in mouse serum was measured in a similar manner. Except that the samples added to the elastin peptides coated plates were changed to mouse serum diluted 1:100 in PBS. And the standard curve was generated by serially diluted BA4 antibody in PBS. The accuracy and precision of the quantitative range of the ELISA was determined by replicate analyses.

To measure the cross-reactivity of BA4 antibody against fibrillin-1 fragments, BA4 antibody diluted 1:1000 in PBST with 0.5% BSA was added to the microtiter plate precoated with the 500 ng/well rFib47^{wt}, rFib47^{mt}, rFib11 and a control His-Tag protein previously used in another study (166). After 1 hour incubation at 37 °C, the plates were washed and then incubated with 50 μl of secondary antibody (1:2000 dilution), finally, the signal was developed as described above. The quantification of reactivity of recombinant protein was calculated as the percentage of the OD values displayed by wells precoated with elastin peptides.

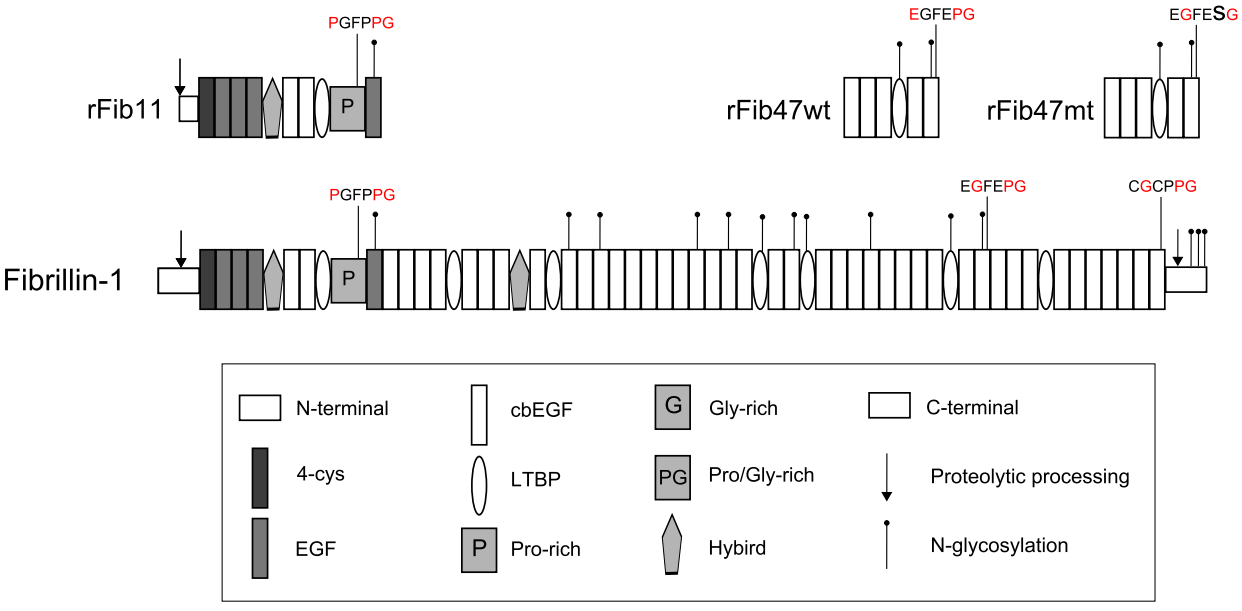

Figure 2.1: Recombinant constructs and synthetic hexapeptides used in this study. Three recombinant constructs were generated by HEK 293 expression system as described in method. N-glycosylation sites in fibrillin-1 are shown as vertical lines with dots above the protein, and the N and C-terminal processing sites are shown with arrows. The amino acid sequences and locations of the three synthetic peptides with GxxPG sequences investigated this study are shown. Synthetic hexapeptides were purchased from Peptide Company or Sigma.

2.4 Generation of recombinant fibrillin-1 fragment

2.4.1 Fibrillin-1 constructs

The recombinant fibrillin-1 fragment (rFib11) includes the region from exons 1 to 11, which contains the PGFPPG motif at amino acids 2194-2199 (Figure 2.1). The primers for generating rFib11 were 5'-gtatggcccagccggccAGAGGCGGTGGAGGACAC-3' and 5'-gtatgggcccAATACA CTCCCCACGGAG-3', which contained a unique 5' *Sfi*I site and a unique 3' *Apa*I site (the *FBN1*-specific sequence is capitalized). Following restriction digestion with *Sfi*I and *Apa*I enzymes, the PCR product was ligated with the pSec Tag A vector, giving rise to the rFib11-hexahistidine tag construct. The PCR conditions was described in the previous section. rFib47^{wt} and rFib47^{mt} constructs were generated by our colleague Booms (144). rFib47^{wt} contains a putative EBP recognition motif EGFEPG at amino acids 2194 to 2199. In rFib47^{mt}, the conserved proline residue at position 2198 is mutated to a serine residue (EGFEPG–EGFESG), thereby abolishing the EBP consensus sequence.

2.4.2 Stable transfection HEK293 Cells

Typically, 4x10^4 HEK 293 cells per well were seeded 24 hours before the experiment, and transfected with 0.6 μg plasmid DNA and 4 μl Lipofectamine® 2000 Transfection Reagent (Invitrogen). Stable selection started 48 h post transfection of cells. Growth medium (DMEM, 10% FBS, penicillin/streptomycin mix) was replaced by growth medium containing the previously determined concentration of Zeocin (100 μg/ml). Clonal colonies were tested for expression by standard western blotting using an anti-myc antibody (1:2000, Santa Cruz).

2.4.3 Expression of recombinant fragments

For production of recombinant polypeptides, cell clones with strongest expression were expanded in selected medium to 90% confluency, after washing twice with PBS harvest medium (DMEM, 100 μg/ml Zeocin) was added for 48 hour, conditioned medium was then collected and phenylmethylsulfonylfluoride (PMFS) was added as a concentraton of 0.5 mM to inhibit protease activity. Second harvest was performed for another 48 hour, altogether around 800 ml serum-free conditioned medium containing secreted recombinant polypeptide was collected.

2.4.4 Purificaiton of recombinant fragments

Conditioned medium was filtered through 0.2 μm filter units (Nalgene) to remove cell debris, following concentration with Centricon Plus-80 filter devices (Millipore), and concentrates (ca. 10 ml) were dialyzed against PBS by using a dialysis cassette (Thermo Fisher Scientific). The dialyzed medium was then passed over a 1-ml nickel-loaded Ni-NTA agarose chelating column. The column was washed and eluted by an increasing gradient of imidazole, whereby the recombinant polypeptides typically eluted at an imidazole concentration between 100 and 150 mM. Eluted fractions were checked for purity and molecular weight by coomassie blue staining after SDS-PAGE. Polypeptide-containing fractions of greater than 95% estimated purity were pooled and dialyzed against PBS.

2.4.5 Characterization of recombinant fragments

Fragments rFib11, rFib47^{wt} and rFib47^{mt} contain 1 or 2 putative N-glycosylation sites. For the analysis of N-glycosylation, the recombinant polypeptides were treated with N-glycosidase F (PNGase F). Recombinant fragments (10 μg) were digested in 50 mM Tris/HCl, pH 7.4, with 2 μl of PNGase F at 37°C for 2 hours. A control sample was treated the same way without adding enzyme. The apparent molecular masses of the enzyme-treated and untreated products were estimated by SDS-PAGE followed coomassie blue staining. Reduction with 50 mM dithiothreitol (DTT) or incubation of recombinant protein in 5 mM EDTA followed by non-denaturing electrophoresis was performed to investigate the influence of disulfide bonding and calcium binding, respectively, on electrophoretic mobility.

2.5 Study of chemotactic effects

2.5.1 Preparation of murine and human aortic extracts

At 2 and 4 months after birth, the mgR/mgR mice were killed and the ascending aortas were prepared. Aortic tissue extracts were prepared using a modification of a previously described protocol (167). Briefly, adventitia was dissected from aorta, tissue specimens were washed 2 times in PBS and weighed. Specimens were then incubated in PBS with 2 mol/L NaCl overnight at 4°C with gentle shaking (20 ml per 1 g tissue). At the end of incubation, aortic tissue was removed, and the incubation solution was centrifuged at 10,000 rpm for 30 min to remove particulate debris. Aortic extract solution was stored at 4°C for experiments on the following day

(or at 20°C for future repeats). Total protein concentration was measured by a BCA assay kit as described in previous section.

Fresh full-thickness aorta specimens were obtained of 25 patients at the time of aortic replacement or cardiac transplantation at the German Heart Institute Berlin between the years 2008 and 2010. Inclusion criteria were Marfan syndrome (n=6), isolated thoracic aortic aneurysm (TAA)(n=8). Additionally, aortic samples from eleven heart donors with no known cardiovascular disease served as control group. The cooled ischemic time was never longer than 3 hours, and therefore, the aortic specimens had been on ice for maximally 3 hours at the time the specimens were taken. The diagnosis of MFS was based on Ghent criteria (5) (The study was completed prior to the publication of the recently revised version of the Ghent nosology (6)). In 5 of the Marfan patients, the diagnosis was additionally confirmed by genetic mutation analysis.

Human tissue samples (about 0.5 x 2 cm) were taken during surgery after the initialization of cardiopulmonary bypass during cross-clamp time and immediately following the aortotomy. Samples were excised from the ascending aorta just above the sino-tubular junction. Tissue samples of donor hearts were cut off during ischemic time just before the implantation of the donor heart at transplantation. The specimens were immediately placed into PBS solution. Then they were stored at 4°C until they were sent to the laboratory on the same day. Aortic tissue extracts were prepared by using the same protocol for the mice.

The study was approved by the ethics commission of the Charité Campus Virchow-Klinikum (EA2/096/07).

2.5.2 Chemotaxis analysis

For harvesting the cells, monolayers of RAW 264.7 cells were washed 2 times with PBS with a nonenzymatic cell dissociation solution (Sigma). After 25 minutes of incubation at room temperature, cells were suspended in PBS, counted, centrifuged, and finally suspended in the chemotaxis buffer consisting of RPMI 1640 supplemented with 1% BSA at 1×10^6 cells/ml.

Chemotaxis assays are experimental tools for evaluation of chemotactic ability of prokaryotic or eukaryotic cells. Chemotaxis was assayed in a 48-well chemotaxis chamber (NeuroProbe) (Figure 2.2). The bottom wells were filled with 25 μl of attractant solution. An 8-μm-pore-diameter polyvinylpyrrolidone-free polycarbonate filter (NeuroProbe, Gaithersburg, Md) was placed on the bottom plate. A silicon gasket and the top plate with 48 holes were then mounted, forming

the top wells. The cells were added in a volume of 50 μl. In parallel experiments, extraction buffer (PBS plus 2 mol/L NaCl) or chemotaxis buffer was loaded into the bottom wells as a negative control. After 2 hours of incubation at 37°C and 5% CO_2, the filter sheet was removed, and nonmigrated cells were wiped off the top side. The filter was then fixed in 70% methanol for 30 seconds and stained in Wright-Giemsa (Sigma).

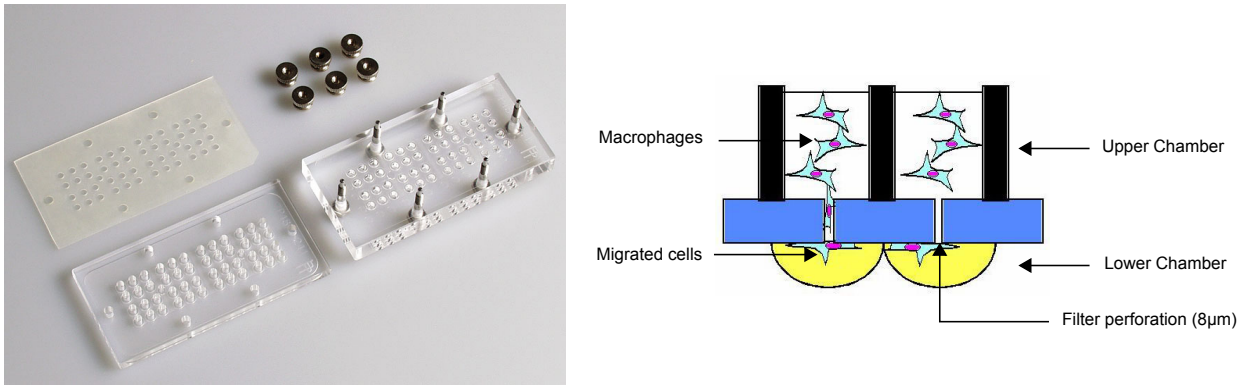

Figure 2.2: AP48 Boyden chamber. Chambers consist of two precision-machined acrylic plates, a silicone gasket, and hardware for assembly. The 48-well chemotaxis chamber has a lower well volume of 25 μl. Corresponding holes in the top plate form the upper wells, with volumes of 50 μl. The membrane is placed over the filled lower wells, then the gasket and top plate are added and fastened down to create a seal between the two plates. These chambers may be used with polycarbonate or cellulose nitrate filters. They use one piece of membrane, 25x80 mm, to cover all the wells. Chemoattractants added to the lower wells act on cells in a suspension added to the upper wells. Modified graphic from Neuro Probe Company.

2.5.3 Synthetic peptides

Synthetic hexapeptides corresponding to the three putative EBP interaction motifs in fibrillin-1 were obtained from Peptide Company (Heidelberg, Germany). They are Pro-Gly-Phe-Pro-Pro-Gly (PGFPPG, positions 422–427, p11), Cys-Gly-Cys-Pro-Pro-Gly (CGCPPG, positions 2672–2677, p63), Glu-Gly-Phe-Glu-Pro-Gly (EGFEPG, positions 2194–2199, p47) and its mutant form Glu-Gly-Phe-Glu-Ser-Gly (EGFESG, $p47^{mt}$). Val-Gly-Val-Ala-Pro-Gly (VGVAPG) hexapeptide was obtained from Sigma-Aldrich.

2.5.4 Experimental design

Chemotaxis was performed duplicates and repeated at least three times. Recombinant fibrillin-1 fragments were used at a concentration of 100 μg/ml. Synthetic peptides were analyzed for two different concentrations (10^{-7}, 10^{-8}mM). For each time interval, 3 or 4 wild type and mutant mice were killed, and all aortic extracts were investigated at least 3 times. Aortic extracts from

patients with MFS and isolated thoracic aortic aneurysm (TAA) were compared against control aortic extracts derived from heart donors with no known cardiovascular disease. Human aortic extracts used for chemotaxis assay were diluted in PBS to make a final concentration of 20 μg/ml of total protein.

To determine whether EBP was involved in mediating macrophage chemotaxis, we performed several experiments to investigate whether the chemotactic activity is mediated by the EBP. The monoclonal antibody (mAb) BA4 can block the chemotactic activity of VGVAPG, a repeated amino acid sequence motif in elastin that is know to bind to the EBP (167). Preincubation of monocytes with VGVAPG peptides can also block the chemotactic response (150). The EBP is known to dissociate in the presence of high levels of lactose, but not glucose (148). Therefore, to investigate a potential role with EBP in the chemotaxis experiments described in this manuscript, cells were exposed to 1 mmol/L lactose or glucose, or 0.1 mmol/L VGVAPG for 1 hour incubation at 37°C before the chemotaxis assays were started. As a further control, samples were preincubated for 30 minutes at room temperature with the mouse mAb BA4 derived from immunization against bovine α-elastin (Sigma) or with murine IgG (Sigma), both at a dilution of 1:1000.

All assays were done in triplicate during the same experiment. In each well, 4 random fields were chosen with the microscope set at x200 magnification. The fields were observed and recorded photographically with the Leica DC viewer program. Fields were scored by 2 observers blinded to the chemotactic stimulus (or control) using an in-house Java program. PBS or chemotaxis buffer was loaded into the bottom wells as a negative control. The results were expressed as the number of migrated macrophage or chemotactic index (CI) that is the number of cells having migrated in the presence of the chemotactic agent divided by the number of cells having migrated in the presence of PBS buffer alone.

2.6 Therapeutic application of mgR Mouse model

2.6.1 Design of therapeutic application

Two treatment scenarios with 6 mg/L indomethacin in drinkwater or intraperitoneal injection (i.p. injection) of BA4 antibody were evaluated in the homozygous mgR mice (Figure 2.3). Both treatments started at 3 week of age and continued for 8 weeks. Using an insulin syringe, the mice were given an intraperitoneal application of three different dosages of BA4 antibody diluted

in PBS (10 mg/kg, 5 mg/kg, 1 mg/kg). In the eleventh week, mice were sacrificed by CO_2 suffocation or cervical dislocation, aortic root, ascending aorta and arch were collected and either flash frozen in liquid nitrogen and stored at -80°C or placed in 1x PBS with 4% paraformaldehyde (PFA) overnight at 4° C for preparing sections. Details of ex vivo analytical methods are given below.

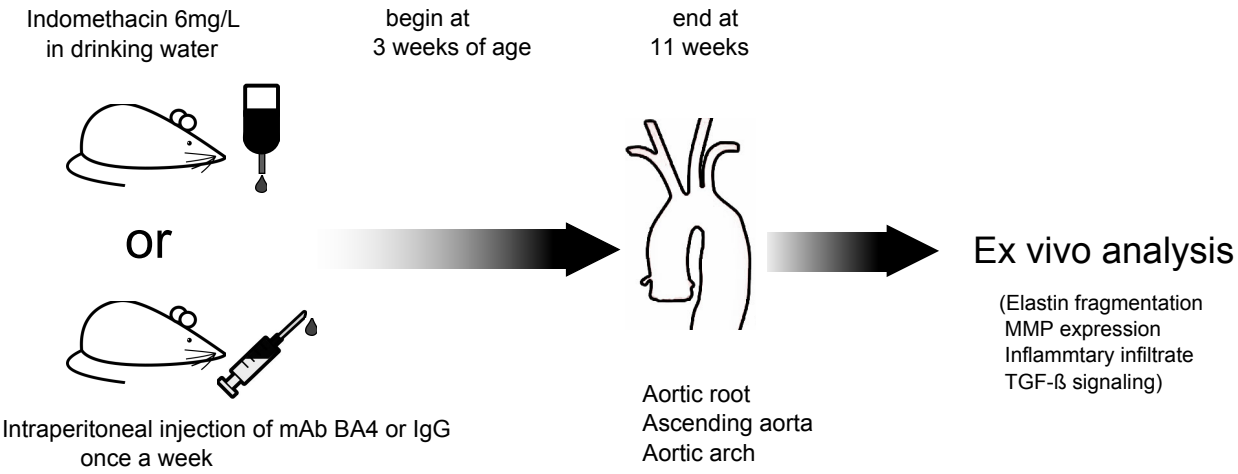

Figure 2.3: Therapy scheme. Idomethacin is diluted as 6 mg/L in drinkwater, or intraperitoneal injection of BA4 antibody with three different dosis (10, 5 and 1 mg/kg). IgG antibody was given as a control. The therapy was began at around 3 weeks of age and continued 8 weeks. In the eleventh week, the mice were sacrified, aortic root, ascending aorta and arch were prepared for ex vivo analysis.

2.6.2 Mouse Genotyping

Mice are genotyped by PCR or qPCR of tail genomic DNA. The procedure used for the extraction of genomic DNA from tail was done by using the automated BioRobortM48, which provides fully automated nucleic acid purification for up to 48 samples. The tail of a mouse was cut between 8-14 days of age and was then digested in 200 μl lysis buffer in the presence of proteinase K, after incubation at 56°C for 30 min with agitation (250 rpm on a heated shaker). DNA was extracted from the lysis buffer by using the MagAttract DNA M48 kit protocol as described by the Qiagen manual. DNA concentration is measured by spectrometry.

PCR was performed by using corresponding primers to detect the native fibrillin-1 gene or the introduced neomycin cassette, respectively (Table 2.10). Further qPCR was performed to distinguish homozygotes and heterzygotes. qPCR reaction volume used was 20 μl containing 0.25 μm of each primer, 15 ng genomoic DNA, 10 μl 2xSYBR-Green (Applied Biosystems). The reaction and measurements were performed in real time with the GeneAmp5700 Sequence Detection sys-

tem (Applied Biosystems). The qPCR thermoprofile is 50 °C for 2 min, 95°C for 10 min, then 40 cycles of 95°C for 15 s followed by 1 min at 60 °C. The specificity of the reaction was evaluated by performing a melting reaction. The target gene expression was normalized to the expression of Albumin using the standard-curve method. Primers for qPCR are listed as in the following Table.

Name	Forward	Reverse
Fbn-wt	5'-CTCCGTGGGACCTACAAATG-3'	5'-CCAGGTGTGTTTCGACATTG-3'
Neo-PCR	5'-GTGTTCCGGCTGTCAGCGCA-3'	5'-GTCCTGATAGCGGTCCGCCA-3'
Neo-qPCR	5'-TGAATGAACTGCAGGACGAG-3'	5'-AGTGACAACGTCGAGCACAG-3'
Albumin	5'-CTGCAATCCTGAACCGTGT-3'	5'-TTCCACCAGGGATCCACTAC-3'

Table 2.10: Primers for genotyping

2.7 Ex vivo analytical methods

2.7.1 Aorta protein extraction

Whole mouse aorta tissues were grinded in 200 μl RIPA buffer with protease and phosphatase inhibitors (Roche Applied Science, Mannheim, Germany) and homogenized in a homogenizer. Samples were then mixed thoroughly by vortexing 4 times for 20s and cooling on ice for 10-15 min. Afterwards samples were centrifuged with 10,000g at 4° C for 15 min. The supernatant was then transferred to a fresh tube and stored at -20°C. Protein concentration was determined with BCA assay kit as described in previous section. 15 μg protein samples were electrophoresed in 10% SDS-PAGE, followed by immunoblotting with specific antibodies against MMP-2 (Abcam), MMP-9 (Abcam), MMP-12 (Abcam), phospho-SMAD2 (Cell Signaling), phospho-ERK1/2 and ERK1/2 (Cell Signaling). Membranes were stripped and reblotted with anti β-actin antibody (Abcam) to ensure equal protein loading.

2.7.2 Histological Methods

2.7.2.1 Section preparation

Freshly prepared mouse ascending aorta and arch were fixed in 1x PBS with 4% PFA overnight at 4 °C. Tissues were then washed 2 times for 10 min in 1x PBS at RT. The tissue was deposited in 70% ethanol and stored at 4 °C until the embedding procedure. Tissues were embedded in

paraffin using the semi-enclosed tissue processor TP1020. The final embedding in paraffin was performed using the EC 350 paraffin embedding center. The solidified paraffin-embedded tissues were then stored at 4°C. These blocks were then sectioned into 5 μm microsections and used for further histological analysis after drying for at least one night.

2.7.2.2 Modified Verhoeff Elastic-Van Giesen stain

The sections were deparaffinized in xylene x2 for 10 min and then rehydrated in a graded alcohol series (100%, 100%, 95%, 80% and 70% ethanol followed by water for 2 min each). The slides were stained in modified Verhoeff at room temperature for 7 min. Slides were then washed in running warm tap water for 1 min and were differentiated in 0.4% Ferric Chloride for 75 seconds followed with washing for 5 min. Afterwards slides were counterstained in Van Gieson solution for 60 seconds. Finally the slides were covered with 3-4 drops permanent mounting medium Entellan (Merck) with a coverslip, air-dried and stored at RT. Free ends of elastic lamellae per millimeter aorta length were counted by two independent observers.

2.7.3 Immunohistochemistry

Immunohistochemical examinations were carried out using a ABC streptavidin-biotin method with Vectastain ABC kit (Vector Laboratories, Burlingame, CA, USA) according to the manufacturer's protocol. Briefly, after deparaffinization and rehydration, endogenous peroxidase activity was quenched by a 5-min incubation in 3% H_2O_2, after antigen retrieval with trypsin enzymatic antigen retrieval solution (Abcam) at 37°C for 30 min, tissue sections were then pre-incubated in prediluted blocking horse serum for 10 min to block nonospecific binding. Binding of primary antibody rabbit anti-pSMAD2 (1:150, Cell Signaling), rat anti-F4/80 antibody (1:150, Santa Cruz) and rabbit anti-COX-2 (1:100, Abcam) was carried out overnight at 4 °C. The sections were then washed and subsequently incubated with biotinylated panspecific universal secondary antibody for 10 min. After washing streptavidin peroxidase complex was added for 5 min. Antigen detection was performed by a 3 min incubation with 0.1% diaminobenzidine tetrahydrochloride (DAB) and 0.01% H_2O_2. The sections were then counterstained with hematoxylin, mounted in entellan (Merk) and analyzed on a Leica MZ 12.5 stereomicroscope (Leica) coupled to the AxioCam HRc camera and the AxioVision 4.2 image analysis software. Infiltrated macrophage counts were cacculated in four contiguous 200x fields by two independent observers. Morphometric analysis of histologic sections was used to determine the COX-2 positive area in the aortic wall.

2.7.4 Isolation of mouse aortic vSMCs

Ascending thoracic aortas were removed and placed in PBS. For mouse aortic vSMC culture the tunica adventitia was separated from the tunica media under aseptic conditions in the cell culture hood. Afterwards, pieces of tunica media were incubated in DMEM containing collagenase type II (Worthington Biochemical Corporation, NJ; 1mg/ml) at at 37°C with 5% CO_2 for 1 hour. Subsequently, the cell suspension was centrifuged at 1000 rpm for 5 minutes. The pellet was then incubated in a six-well plate in DMEM containing 10% FCS and antibiotics at 37°C with 5% CO_2. Cells from passage 3 to 5 were used. vSMCs were identified by immunostaining with anti-α SMA FITC-conjugated antibody (1:200, Abcam).

2.7.5 Immunofluorescene

vSMC cells were rinsed in PBS and fixed in 4% paraformaldehyde in PBS for 10 min at 4°C. After rinsing with PBS, cells were permeabilized in 0.25% Triton X-100 in PBS for 5 min, followed by blocking the nonspecific binding sites with 3% BSA in PBS for 30 min. Cells were incubated with anti-pSMAD2 antibody (1:150 dilution) overnight at 4°C followed 30 min incubation of secondary Alexa Fluor®-conjugated antirabbit IgG antibody.

2.8 Statistics

The results are reported as mean±standard error (s. e. m.) or mean±standard derivation (SD), as stated when presenting the data. Tests of significance were conducted by Student's *t* test. Additionally, Fisher's exact test was performed to compare the gender distribution in the two patient groups, and the Mann-Whitney test was performed to compare age, CI and BA4 reactivity between two patient groups. $P < 0.05$ was considered as statistically significant.

3 Results

3.1 Characterization of recombinant fibrillin-1 polypeptides

In order to investigate whether the GxxPG motifs in fibrillin-1 protein could induce macrophage chemotaxis, three recombinant fibrillin-1 fragments were generated by using the HEK 293 expression system. The glycosylation status of the recombinant fibrillin-1 fragments was determined with amidase PNGase F, which removes N-linked carbohydrate. There was a reduction in molecular weight of all three recombinant fragments (rFib47^{wt}, rFib47^{mt}, rFib11). The molecular mass observed for rFib47^{wt} and rFib47^{mt} without N-linked carbohydrate (ca. 40 kDa) was higher than the calculated molecular mass of the amino acid sequence (35 kDa)(Figure 3.1A). Electrophoretic mobility of the three polypeptides under non-reducing conditions was also altered following incubation in EDTA or reduction with DTT, suggesting that the recombinant peptides bound calcium and were disulfide-bonded (Figure 3.1B). The construct rFib47^{mt} contains the mutation EGFESG and the position on the gel corresponding to rFib47^{mt} is similar to rFib47^{wt} after different treatment (Figure 3.1B), indicating that posttranslation modification has not been influenced by the mutation EGFESG.

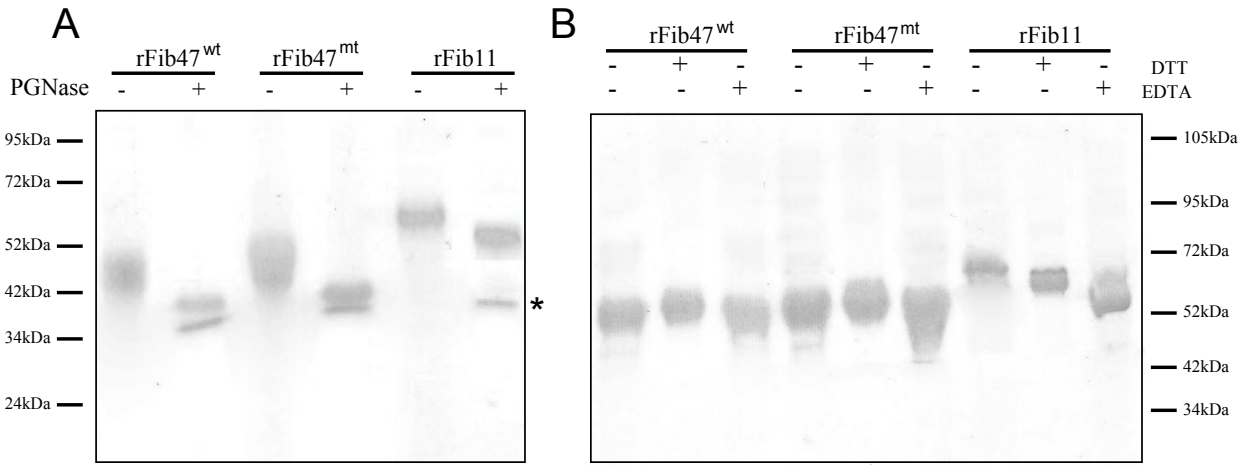

Figure 3.1: Characterization of recombinant fibrillin-1 polypeptides. **(A)** PGNase digestion of rFib47^{wt}, rFib47^{mt} and rFib11. The recombinant fragments were denatured prior to deglycosylation and incubated in PGNase at 37°C. As a control, the peptide was treated identically but PGNase was omitted (-). PGNase-treated peptide (+) migrates more rapidly than untreated peptide, because of the removal of N-linked carbohydrate. **(B)** Recombinant fibrillin-1 protein fragments demonstrate different electric mobility under DTT or EDTA pretreatment. PNGase F is indicated with an asterisk.

3.2 Effects of GxxPG motif in *FBN1* on migration of RAW 264.7 cells

Owing their ability to induce MMP expression as observed previously (144), GxxPG containing fibrillin-1 fragments could contribute to the development and progression of TAA in MFS. The goal of the present study was to investigate whether the three GxxPG motifs in fibrillin-1 might be able to induce increased macrophage chemotaxis. The migratory potency of recombinant polypeptides was further characterized using a modified Boyden chamber system. The results showed that both rFib11 and rFib47^{wt} constructs can stimulate macrophage chemotaxis, and this effect was not observed in rFib47^{mt} construct (Figure 3.2A), in which EGFEPG is mutated to EGFESG to remove the GxxPG motif. In addition, all three synthetic hexapeptides corresponding to GxxPG motif in fibrillin-1 can stimulate the macrophage migration with two different dosages. As a control, no effects could be found in the mutant peptide (p47^{mt}) (Figure 3.2B). It is of note that all three peptides induce macrophage migration to the same extent, as no significant difference in chemotactic index was observed between the peptides. We point out here that similar to the VGVAGP sequence other three synthetic hexapeptide concentrations as low as 10^{-8} mM proved sufficient to stimulate RAW 264.7 migration.

3.2.1 GxxPG motif in *FBN1* induced chemotaxis is mediated by EBP

Incubation of macrophages in lactose causes them to shed the EBP, and this can be used to demonstrate specificity of a chemotactic stimulus on ligand-receptor interactions involving the EBP (150). To further investigate whether the migratory stimulus of GxxPG motif is mediated by EBP, RAW 264.7 cells were pretreated by lactose before performing chemotaxis assay. As presented in Figure 3.3, pretreatment with lactose significantly reduced migratory response of RAW 264.7 to rFib11, rFib47^{wt}, all three synthetic peptides (10^{-7}mM) and VGVAPG (10^{-7}mM). However, no inhibitory effect was observed in fMLP, a well-known chemotactic reagent (Figure 3.3A). Additionally, the incubation of rFib11, rFib47^{wt}, synthetic peptides with BA4 antibody caused a significant decrease of macrophage chemotaxis. The chemotactic index of p63 decreased nearly to base line (Figure 3.3B). These findings indicate that macrophage chemotaxis toward GxxPG motif containing recombinant fibrillin-1 fragments or hexapeptides is mediated by EBP.

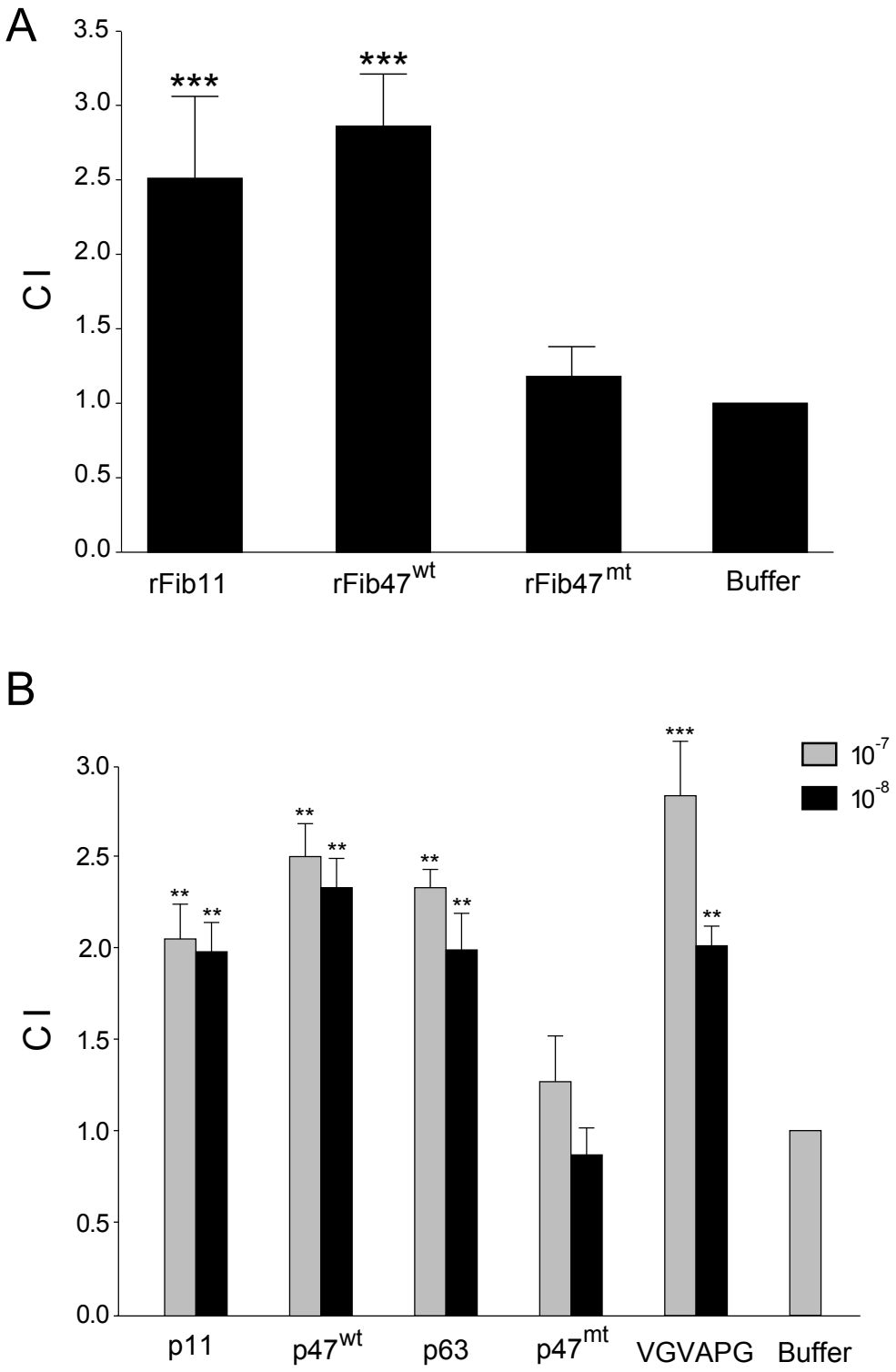

Figure 3.2: Migration of RAW 264.7 cells in response to different recombinant fibrillin-1 fragments and different concentrations of synthetic peptides. Cell migration was measured in a transwell assay system as described in method. **(A)** The fibrilin-1 recombinant polypeptides rFib11 and rFib47^{wt} both induce macrophage chemotaxis. The recombinant polypeptide rFib47^{mt}, in which the GxxPG motif has been mutation to GxxSG, served as a negative control. **(B)** All three GxxPG peptides of fibrillin-1 can induce macrophage chemotaxis. In our experiments, all three fibrillin-1 peptides induced an approximately three fold increase in macrophage chemotaxis, which was comparable to the effect observed for the VGVAPG chemotactic peptide (150) of elastin. Data are representative of three independent experiments. The error bars indicate s.e.m. $^{**}P < 0.01$; $^{***}P < 0.001$ against buffer. CI, chemotactic index.

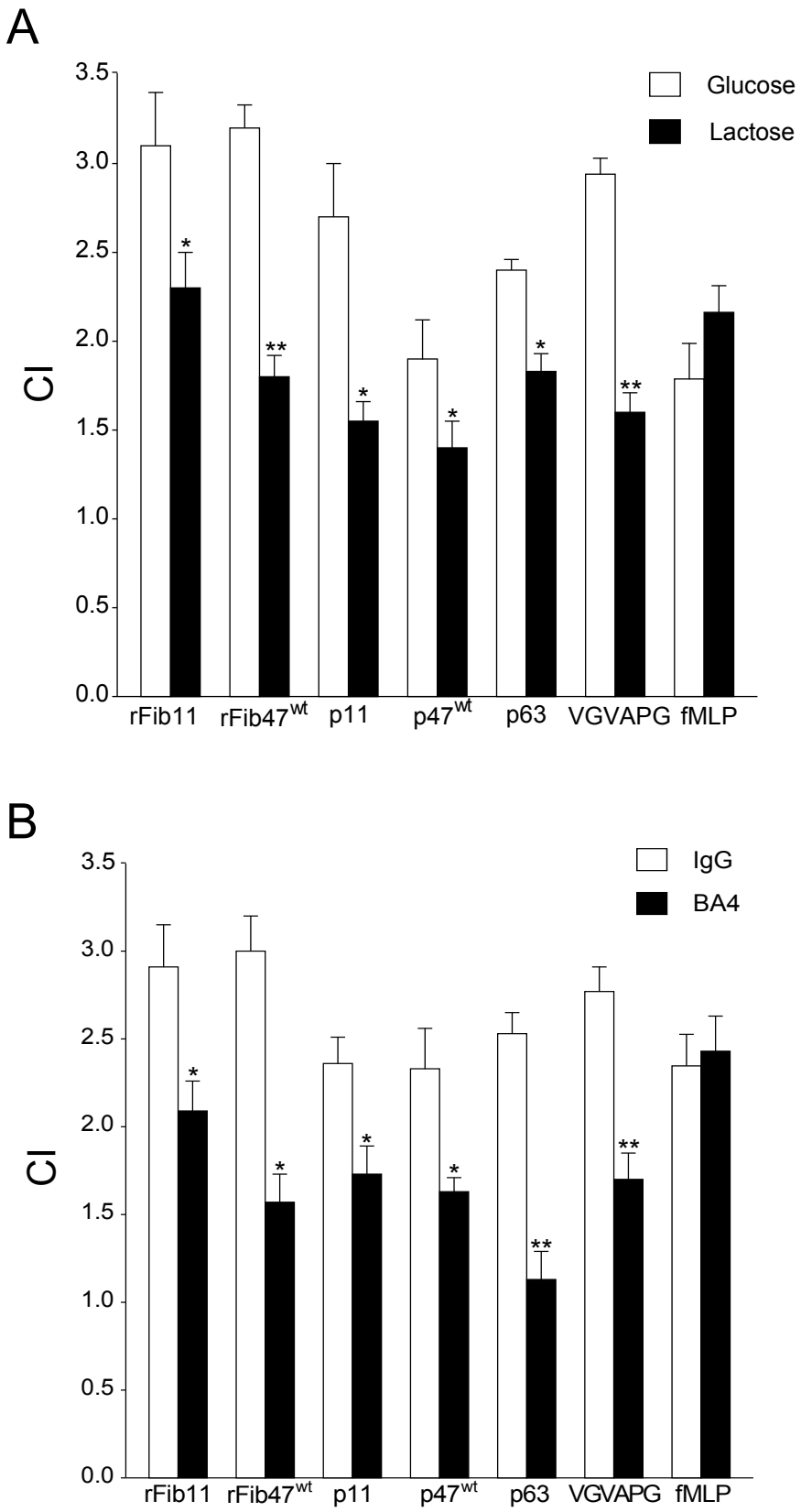

Figure 3.3: Inhibition of chemotaxis by lactose or BA4 antibody. **(A)** RAW 264.7 macrophages were pretreated with 1 mmol lactose for 1 hour. **(B)** Polypeptides or synthetic peptides were incubated with BA4 antibody (1:1000) for one hour before performing chemotaxis analysis. Data are representative of three independent experiments. The error bars indicate s.e.m. $*P < 0.05$; $**P < 0.01$ against glucose or IgG antibody. CI, chemotactic index.

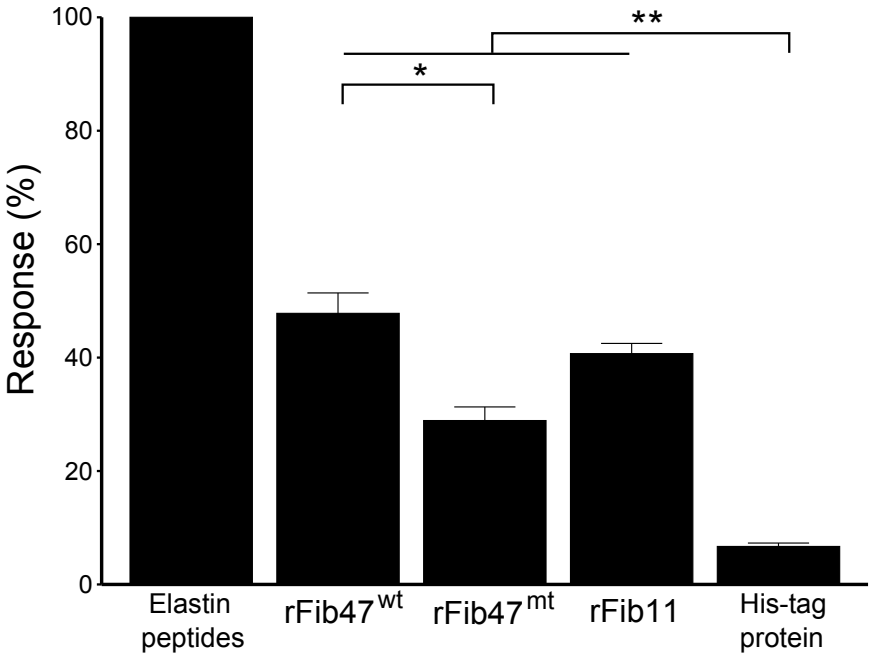

Figure 3.4: Specificity and cross-reactivity of BA4 antibody against different recombinant fibrillin-1 fragments. Cross-reactivity was examined by precoating microtiter plate with the 500 ng/well elastin peptides, rFib47^{wt}, rFib47^{mt}, rFib11 and a control His-tag protein (166). Data are expressed as the percentage of maximum reactivity, which was considered to be 100% for elastin peptides. $*P < 0.05$; $**P < 0.01$.

3.2.2 Cross-reactivity of BA4 to recombinant fibrillin-1 fragments

It has been reported that peptide sequences selected by BA4 antibody are ligands for the elastin binding protein (EBP) (160). The previous section has shown that the chemotactic activity of rFib47^{wt} and rFib11 decreased after incubating with BA4, however the binding of the BA4 to non-elastin fragments such as fibrillin-1 fragments has not been directly confirmed. Cross-reactivities of BA4 antibody were observed in the two recombinant fibrillin-1 fragments. rFib11 and rFib47^{wt} demonstrate 40.7% und 47.8% of BA4 cross-reactivity respectively, as expected, rFib47^{mt} showed decreased reactivity (Figure 3.4).

3.3 Murine aortic extracts induce macrophage migration by interaction with EBP

Aortic extracts from 2- and 4-month-old mgR/mgR mice were tested for their ability to induce chemotaxis using a chemotaxis chamber system. The results showed that mgR/mgR aortic samples from 2 month old mice stimulated monocyte chemotaxis 3 to 4 times more than extracts from wild type mice or controls. The difference was statistically significant (Figure 3.5A). 4-month-old mice also showed a similar degree of increased chemotaxis, but the difference between both age

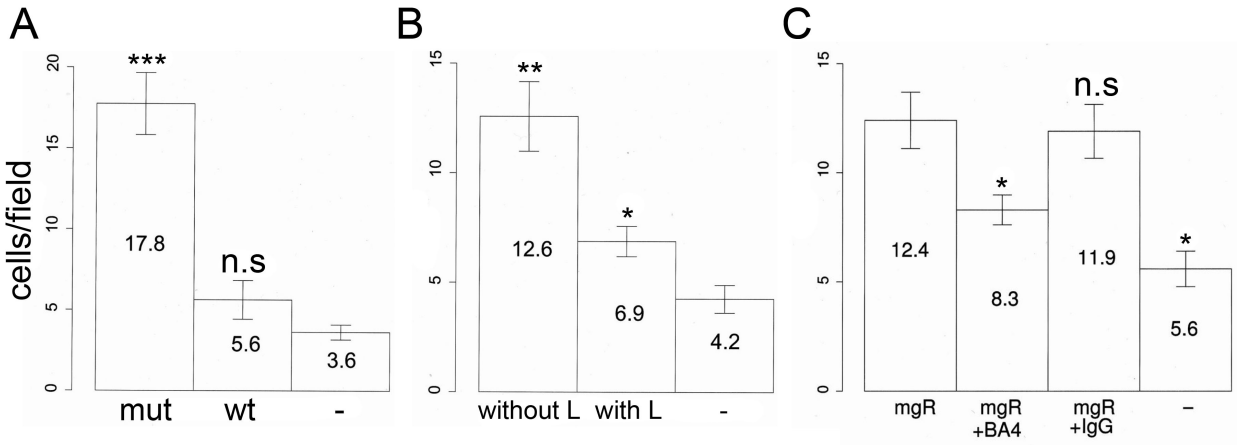

Figure 3.5: mgR/mgR aortic extracts induce chemotaxis. **(A)** Aortic extracts of 2-month-old mutant (mut) and wild-type (wt) mice were added to the lower wells of chemotaxis chamber separately. Chemotaxis is expressed as the number of migrated RAW 264.7 macrophages. **(B)** Reduction of chemotactic effect by lactose. Macrophages were exposed to 1 mmol/L lactose for 1 hour, and aortic extracts of 2-month-old mutant mice were added to the lower wells of the chemotaxis chamber. Without L indicates no lactose preincubation; with L, lactose preincubation. **(C)** Chemotactic response of RAW 264.7 macrophages is inhibited by pretreatment with monoclonal antibody BA4. The 4-month-old mgR/mgR aortic extract was analyzed in isolation, with mAb BA4, or with IgG. Extraction buffer was used as negative control (-). Results are mean $\pm$ s.e.m. n=12 per group (4 fields each for 3 wells during the same experiment. $*P < 0.05$; $**P < 0.01$; $***P < 0.001$.

Upper wells		
Lower wells	Aortic Extracts (Mutant)	Chemotaxis Buffer
Aortic extracts (Mutant)	4$\pm$2.7	18$\pm$5.4
Extraction buffer	4$\pm$1	3.5$\pm$1.2

Table 3.1: Checkerboard Analysis of RAW 264.7 Macrophage Migration Stimulated by Aortic Extracts. Lower wells contained aortic extracts or extraction buffer. Upper wells contained aortic extracts or chemotaxis buffer with RAW 264.7 macrophages. Results are mean $\pm$ s.e.m. n=12 (4 fields each for 3 wells during the same experiment).

groups was not statistically significant.

We repeated the experiments with preincubation of macrophages in lactose for 1 hour. This treatment significantly reduced chemotaxis in 2-month-old mutant mice (Figure 3.5B). Additionally, pretreatment of mgR/mgR aortic extracts from 4-month-old mice with BA4 significantly reduced the chemotactic response of RAW 264.7 (Figure 3.5C). We then performed checkerboard analysis to determine whether the macrophage migration was related to directed chemotaxis or undirected chemokinesis (Table 3.1). Macrophages showed migration only in the presence of mutant aortic extracts in the lower well, and adding mutant aortic extracts to the upper well greatly reduced the observed cell counts. This result indicates that the observed cell migration is caused by chemotaxis rather than by (undirected) chemokinesis.

3.4 Analysis of human aortic extracts

Since we have shown that aortic extracts from mgR/mgR exhibit migratory properties in RAW 264.7, it seemed interesting to investigate whether this migration could be also observed in aortic extracts from Marfan patients.

3.4.1 Patient Data

Fresh aortic specimens were collected between the years 2008 and 2010. Six specimens were obtained from individuals with MFS and eight specimens were obtained from individuals with isolated thoracic aorta aneurysms (TAA). 4 of the Marfan patients were receiving prophylactic treatment with beta blockers at the time of the operation. Additionally, samples from 11 heart donors with no known cardiovascular disease were used as controls. The average age of the patients with MFS was 38.5$\pm$16.1 years, and five of the six patients were male. The average age of the patients with isolated TAA was 58.6$\pm$12.1 years, and all eight patients were male. Details of patient characteristics are shown in Table 3.2. There is a significant difference regarding age between the MFS and TAA groups (Table 3.3).

3.4.2 Analytical performance of ELISA.

BA4 reactivity was determined from calibration curve derived from standards of known elastin peptide concentration (from 10 ng/ml to 10 μg/ml). The quantitative range of the assay was 75 ng/ml to 2 μg/ml (80 - 20% inhibition values), with 50% inhibitory concentration at 390 ng/ml. The precision of the assay was acceptable with intra- and inter-assay coefficients of variation (CV) ranged from 2.5% to 6.3% and 2.6% to 8.7%, respectively. These results indicated that the values obtained with competitive ELISA in this study were highly reproducible and reliable.

3.4.3 Higher BA4 reactivity observed in aortic extracts

We first asked whether the concentration of GxxPG fragments (defined operationally as reactivity against the BA4 antibody) was increased in specimens from individuals with Marfan syndrome. As described in the Methods section, we developed an ELISA assay based on the BA4 antibody to measure GxxPG containing fragments. The BA4 reactivity was significantly higher in Marfan patients ($P < 0.05$) and also in patients with isolated TAA ($P < 0.05$) compared with control specimens (Figure 3.6A).

Patient	Diagnosis	Age	Sex	Description
1	MFS	23	m	Dilatation and dissection of the ascending aorta and abdominal aorta, maximum diameter of ascending aorta 4 cm. Atenolol.
2	MFS	45	m	Aneurysm of ascendending and descending aorta, status post previous surgical repair of ascending aorta with leakage of anastomosis.
3	MFS	21	f	Sinus valsalvae aortic aneurysm, status post previous surgical repair of ascending aorta. Metoprolol.
4	MFS	65	m	Infrarenal aortic aneurysm, maximum diameter 6.1 cm. status post previous surgical repair of ascending aorta. Nebivolol.
5	MFS	37	m	Thoracoabdominal aneurysm, status post previous surgical repair of ascending aorta. Nebivolol.
6	MFS	40	m	Dilatation of ascending aorta
7	TAA	62	m	Aneurysm of ascending aorta, III° aortic insufficiency. Metastatic colon cancer
8	TAA	40	m	Subacute dissection of the ascending aorta, status post previous surgical repair of ascending aorta, Erdheim-Gsell media degeneration, maximal diameter of sinus valsavae 4.1 cm. *FBN1* mutation excluded.
9	TAA	65	m	Aneurysm of ascending aorta, maximal diameter 6.3 cm, three-vessel coronary artery disease, arterial hypertension, hyperlipoproteinemia, sleep apnea syndrome.
10	TAA	71	m	Acute type A dissection, maximal diameter 4.2 cm. Arterial hypertension, hyperlipoproteinemia
11	TAA	73	m	Aneurysms of ascending and abdominal aorta. Maximal diameter of ascending aorta 5.3 cm. Arterial hypertension, hyperlipoproteinemia, osteoporosis
12	TAA	60	m	Dilatation of the ascending aorta, status post surgical replacement of the aortic valve. III°atrioventricular block
13	TAA	43	m	Type A dissection, septic multiorgan failure related to fuliminat pneumonia, status post surgical supracoronary aorta replacement.
14	TAA	55	m	Aneurysm of the ascending aorta. Combined vitium of the aortic valve. Arterial hypertension.

Table 3.2: Characteristics of the patients included in this study. MFS: Marfan syndrome; TAA: isolated thoracic aortic aneurysm; m: male, f: female; The column description provides details of the indications for aortic surgery and information about other relevant medical conditions, and treatment with beta blockers.

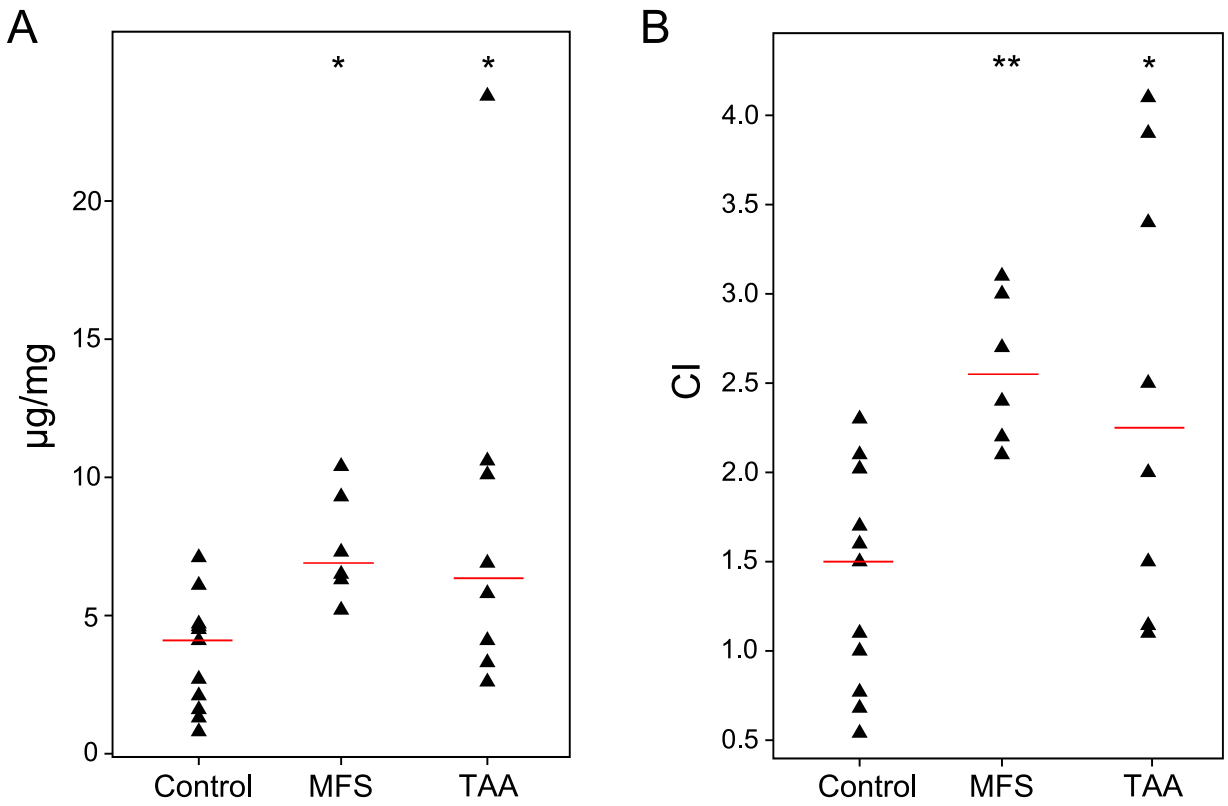

Figure 3.6: EDP concentration and chemotactic activity of human aortic extracts. **(A)** EDP concentration was measured by competitive ELISA in aortic extracts from patients with MFS (n=6), isolated TAA (n=8), and controls (n=11). A statistically significant increase in BA4 activity as compared to control samples was observed for the samples from individuals with Marfan syndrome and isolated TAA. **(B)** Chemotactic activity of the same extracts were measured by a Boyden chamber. Red lines indicate the median levels of EDP concentration or chemotactic index (CI). A statistically significant increase in chemotactic activity as compared to control samples was observed for the samples from individuals with Marfan syndrome and isolated TAA. $*P < 0.05$; $**P < 0.01$.

3.4.4 Aortic extracts from Marfan patients demonstrate chemotactic activity

We then used aortic extracts from the same samples to investigate a potential induction of macrophage chemotaxis. Extracts from Marfan patients showed significantly higher chemotactic activity (CI=2.58±0.42, $P < 0.01$) than that of 11 control samples (CI=1.42±0.61)(Figure 3.6B). The maximal RAW264.7 migration upon stimulation by aortic extracts from individuals with Marfan syndrome was 110% of that observed upon stimulation with 10^{-7} mmol/L VGVAPG. The CI of RAW264.7 cells toward extracts from patients with TAA was significant higher (CI=2.45±1.42, $P < 0.05$) compared with control samples and maximal RAW264.7 migration upon stimulation by extracts from both groups was around 135% of that with 10^{-7} mmol/L VGVAPG. There was a non-significant tendency for an increase in the CI for the TAA samples ($P < 0.05$). There was a statistically significant positive correlation (r=0.6, $P < 0.01$) between BA4 reactivity and CI (Figure 3.7).

	MFS	TAA	P*
Male	5	8	.429
Age (years)	39±16	59±12	.020
CI	2.58±0.42	2.45±1.42	.804
BA4 reactivity (μg/mg)	7.495±1.93	8.409±6.884	.670

Table 3.3: Comparison of different paraments between two patient groups *Fisher's exact test and quantitative data by the Mann-Whitney test.

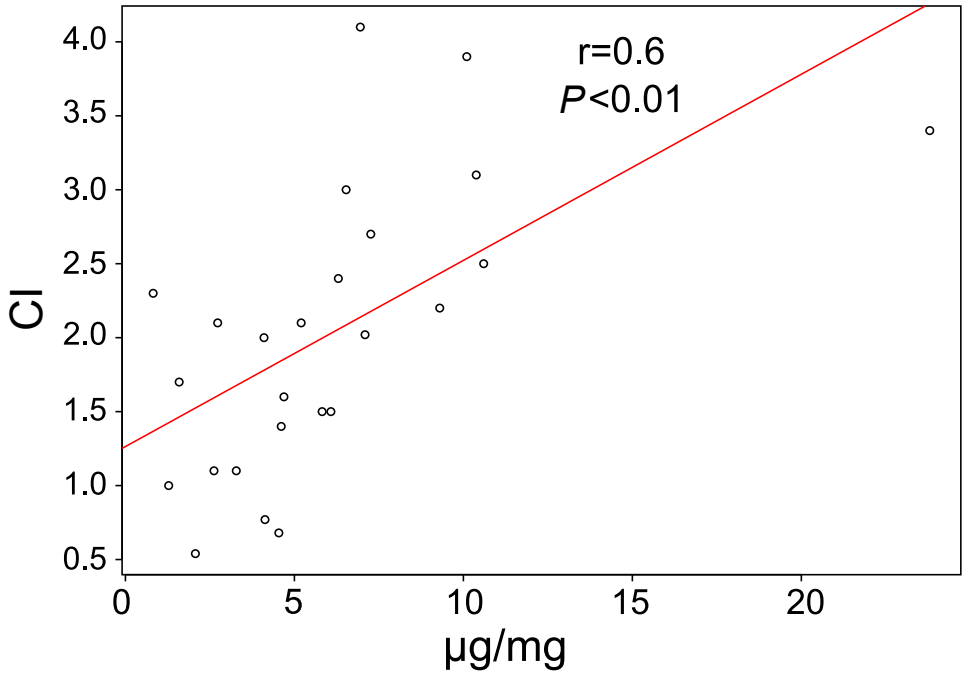

Figure 3.7: BA4 reactivity (μg/mg) versus chemotactic index (CI) of human aortic extracts, with calculated Pearson correlation coefficient (r) and P value

3.4.5 EBP contribute to chemotactic effects of aortic extracts from Marfan patients

To investigate if chemotactic inductive activity of aortic extracts from patients with MFS is related to EBP, chemotaxis analysis was performed as described in the methods section. Chemotactic response of aortic extracts was reduced significantly after lactose and VGVAPG pretreatment, whereas no effects were observed in cells exposed to glucose (Figure 3.8A, B). Additionally, preincubation of extracts with BA4 resulted in a significant reduction of the CI of RAW 264.7 cells in Marfan aorta (Figure 3.8C). These results indicate that the chemoattractive ability of extracts from patients with MFS is at least partially dependent on EBP.

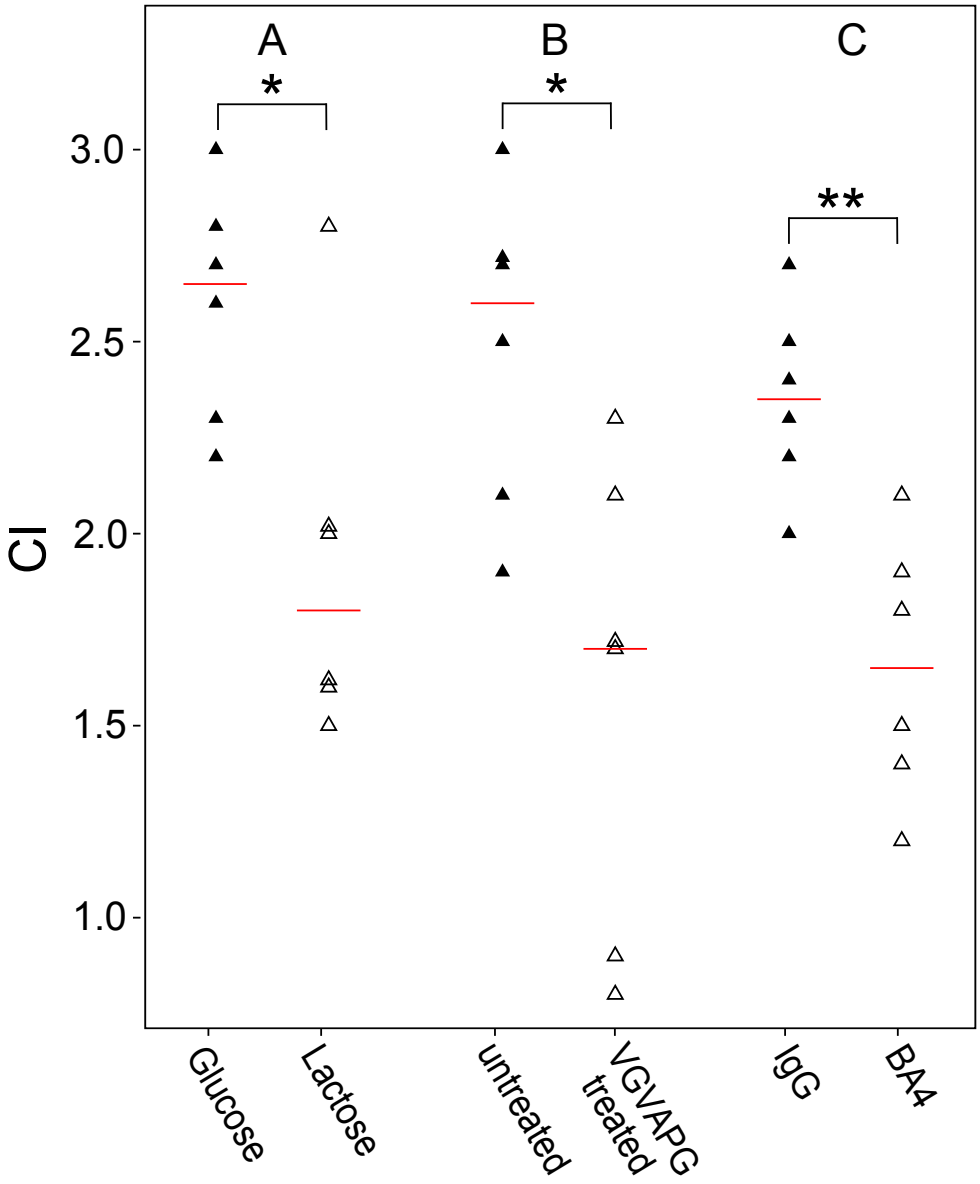

Figure 3.8: Chemotactic index (CI) of RAW 264.7 cells upon stimulation with aortic extracts from individuals with MFS (n=6). **(A)** RAW 264.7 cells were preincubated with 1 mmol/L lactose or glucose for one hour at 37°C prior to exposure to aortic extracts. Pretreatment with lactose led to a statistically significant inhibition of chemotaxis. **(B)** RAW 264.7 cells were preincubated with 0.1 mmol/L VGVAPG hexapeptide for 1 hour incubation at 37°C before the chemotaxis assays were started. There was a statistically significant inhibition of the chemotactic response after VGVAPG pretreatment. **(C)** Aortic extracts were preincubated with BA4 or non-specific IgG for 30 minutes at room temperature prior to chemotaxis assays. There was a statistically significant inhibition of the chemotactic response by BA4 pretreatment. Data are representative of three independent experiments. $*P < 0.05$; $**P < 0.01$.

3.5 Treatment of mgR/mgR mice with BA4 antibody and indomethacin

The in vitro experiments described above showed that recombinant fibrillin-1 fragments and aortic extracts from both mgR/mgR mice and Marfan patients could induce macrophage migration via EBP. Moreover, aortic extracts from Marfan patients demonstrate higher BA4 reactivity. These results led to the question of whether antagonizing these fragments by BA4 antibody can decrease the development of aortic aneurysm in mgR/mgR mice. As macrophage infiltrate could be observed as early as 8 weeks in mgR/mgR mice, a separate anti-inflammatory treatment by using indomethacin was also performed.

3.5.1 Circulating BA4 concentration

To measure levels of circulating antibody, samples of serum was taken from different time points (1, 4, 24 hours and one week) after the last dose of i.p. injection of BA4 antibody (n=3) respectively. Figure 3.9 shown, the concentration in all treated groups reached peak concentration after one hour and decreased gradually with time. The antibody concentration in the 1 mg/kg group fall below the baseline, which was determined just before the start of therapy after 1 week, however the BA4 level in other two groups was still measurable. These data confirm that dosing with 5 and 10 mg/kg at weekly intervals is sufficient for maintenance of circulating levels of BA4 antibody.

3.5.2 Attenuation of thoracic aortic wall degeneration

The elastic lamellae in the aorta of mgR/mgR mice appeared fragmented and disorganized in van Giesen staining as compared to the aorta of wild type mice. Treatment with BA4 at dosages as low as 1mg/kg could already rescue elastin degeneration in mgR/mgR mice. However, no effects could be observed in IgG treated group (Figure 3.10 A). Treatment with indomethacin also resulted in a significant reduction of elastin degradation to a degree that was comparable to that of BA4 treated mice. Quantification of the number of breaks in the elastic lamellae showed significantly fewer breaks in the elastin among the BA4 and indomethacin treated mgR/mgR mice (Figure 3.10 B). Thus, both BA4 and indomethacin prevent progressive deterioration of aortic wall architecture.

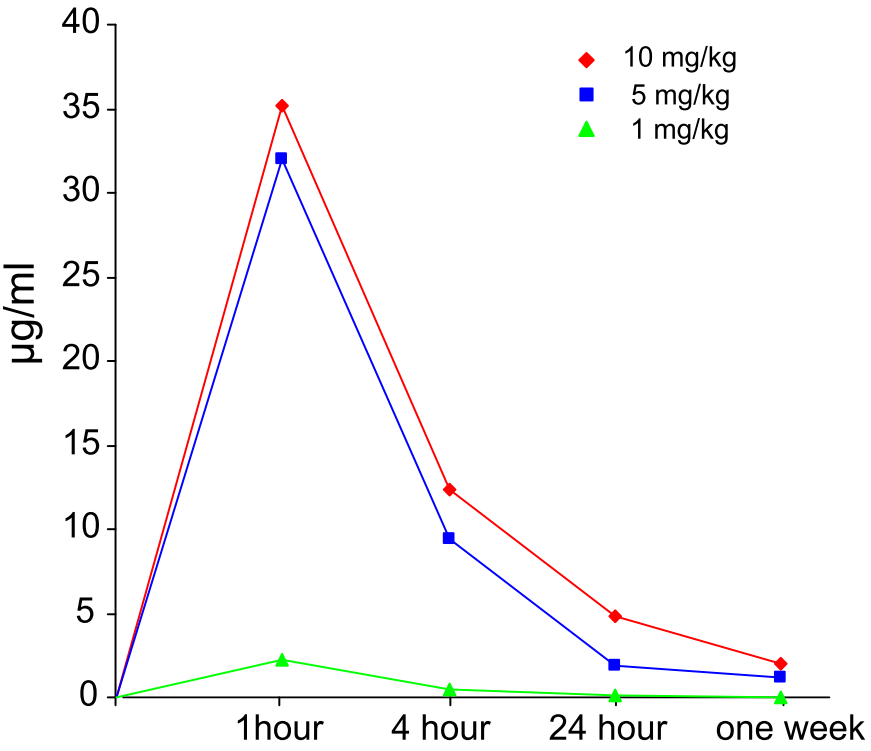

Figure 3.9: Serum levels of BA4 antibody in different time after i.p. injection of three different doses. (Each points represent the mean of 3 animals)

3.5.3 Prevention of upregulation of MMP expression

Upregulation of the gelatinases MMP-2 and MMP-9 may be involved in the pathogenesis of aortic elastic fiber degeneration in Marfan syndrome and their antagonism by oral doxycycline has been shown to be an effective treatment in mouse models of MFS (80, 168). MMP-12, the predominant macrophage MMP, has also been shown to be increased in MFS (169). We therefore assessed the expression of MMP-2, MMP-9, and MMP-12 by western blotting of whole aorta protein. MMP-2, MMP-9 and MMP-12 expression were strongly increased in aorta of mgR/mgR mice compared with wildtype mice. It is of note that two isoforms of MMP 12 (54 kDa and 45 kDa) were detected in the aorta of mice. In concordance with the results observed for elastin fragmentation, treatment with either BA4 or indomethacin resulted in a statistically significant reduction of the signal of the MMP-2, MMP-9, and the 54 kDa isoform of MMP-12 compared with those from IgG treated group or age-related untreated mgR/mgR mice. BA4 at a concentration of 10 mg/kg decreased the level of MMP-2 and 54 kDa isoform of MMP-12 nearly to that of age-related wild-type mice, and the prevention of up-regulation of MMP expression was dose dependent for MMP-2 and MMP-9 expression (Fig. 3.11).

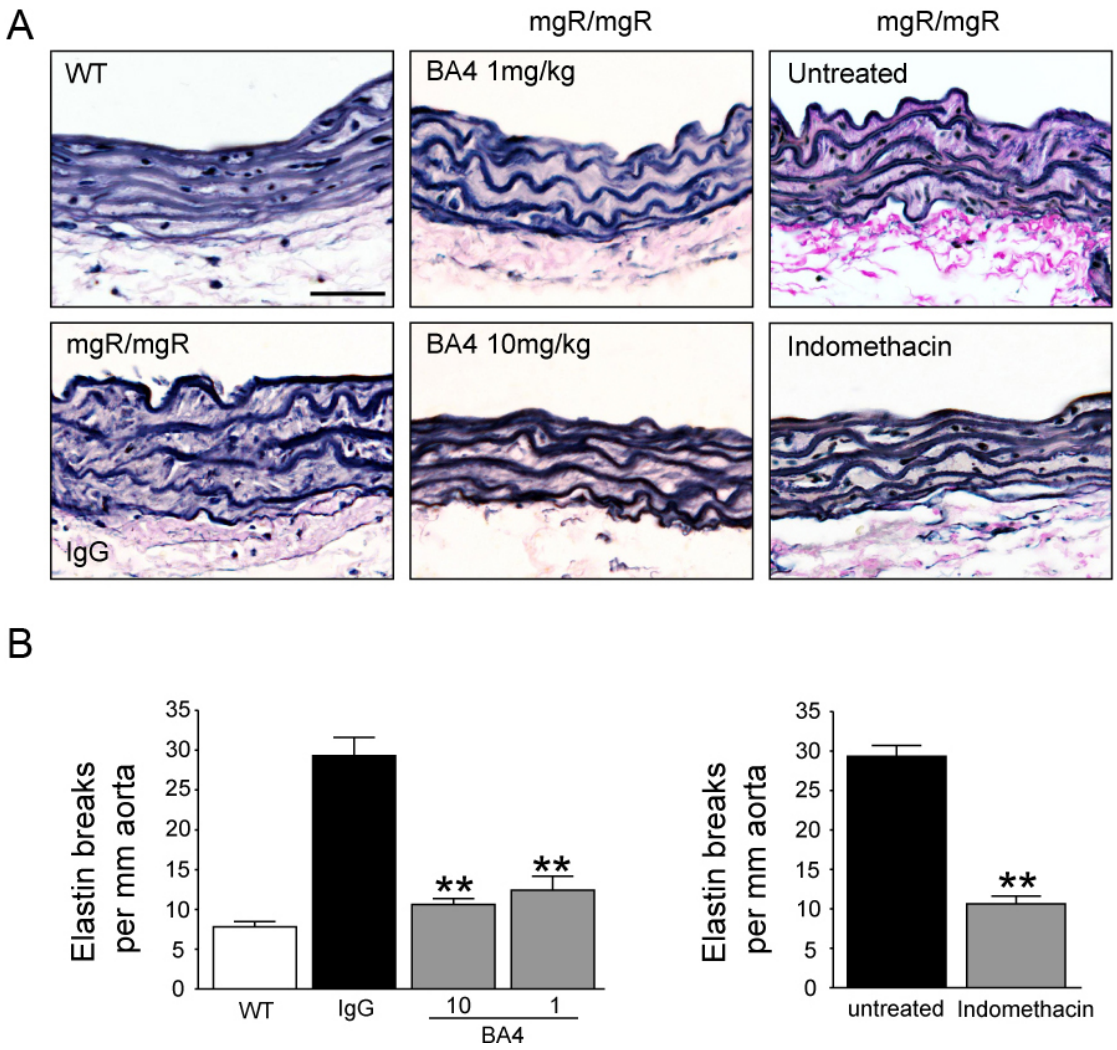

Figure 3.10: BA4 and indomethacin treatment rescue elastin fragmentation in the aorta of mgR/mgR mice. **(A)** Representative van Giesen stained aorta sections from wildtype and mgR/mgR mice in each treated group. IP injection of BA4 and indomethacin treatment resulted in significant preservation of elastin fibers. Scale bar indicates 50 μm. **(B)** Quantification of breaks of elastic lamellae in the aorta. Mice treated with BA4 and indomethacin had significantly lower elastin breaks compared with IgG treated or untreated littermates. All values represent means $\pm$ s.e.m. Number of animals per group were 5-6. Statistically significant differences between BA4 and IgG treated or indomethacin and untreated groups are indicated. **P$<$0.01.

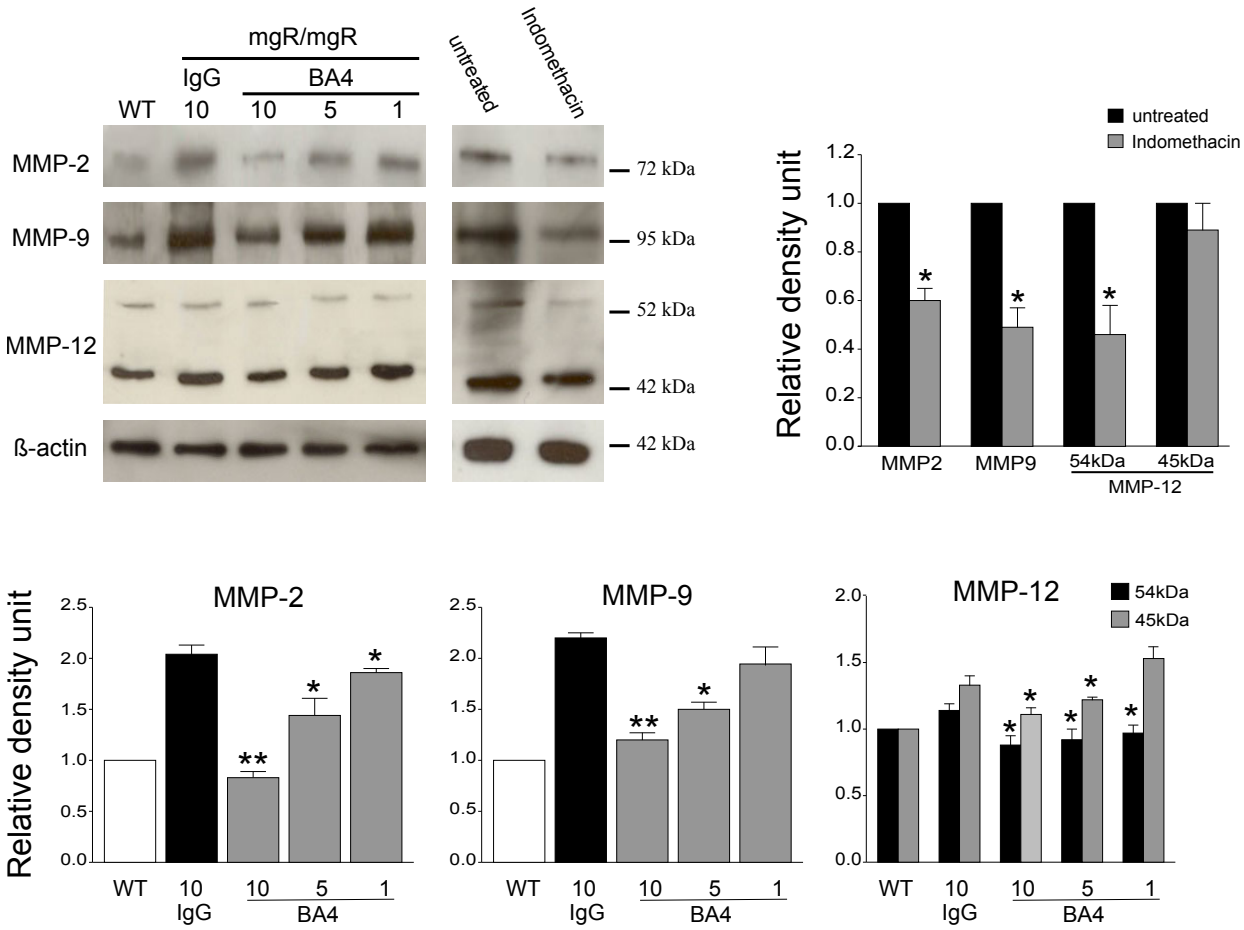

Figure 3.11: MMP expression in the aorta of mgR/mgR mice treated with BA4 and indomethacin. Aortic tissue homogenates were analyzed by western blot for the expression of MMP-2, MMP-9 and MMP-12. The lower panels represent quantification of the specific western blot signals. Relative abundance of MMP-2 and MMP-9 was normalized to β-actin content on each blot. The bands are representative of findings in five to six subjects. All values represent mean $\pm$ s.e.m., in which the value of wild type (WT) or untreated mgR/mgR mice was defined as 1. $^{*}P < 0.05$; $^{**}P < 0.01$ vs. IgG treated or untreated groups.

3.5.4 Reduced macrophage infiltration

We have shown previously that extracts of the mgR/mgR aorta can induce macrophage chemotaxis (see Figure 3.5B). Therefore, we hypothesized that treatment with BA4 would alleviate macrophage infiltration in this mouse. The initial hypothesis is that BA4 may inhibit macrophage migration by neutralizing GxxPG containing fibrillin-1 and elastin fragments and reducing the induction of macrophage chemotaxis into the aortic wall. To characterize the macrophage recruitment into aortic wall in response to both treatments, we performed immunostaining with a macrophage marker F4/80, which is widely used as a marker for mouse macrophages (170). Macrophages are preferentially found within aortic adventitia in mgR/mgR mice (Figure 3.12A). Treatment with BA4 at a dosage as low as 1 mg/kg led to a reduction of macrophage counts in the aortic adventitia, whereas control IgG treatment did not. Even less macrophages were observed in the group treated with 10 mg/kg BA4. Treatment with indomethacin reduced recruitment of macrophages into the aortic adventitia in a similar way (Figure 3.12A). Quantification of these observations showed that BA4 at a dose of 10 and 1 mg/kg is associated with a 60% and 50% reduction in macrophage counts. Indomethacin treatment also significantly reduced macrophage counts to 40% of the count observed in the untreated group (Figure 3.12B).

3.5.5 Decreased TGF-β signaling

TGF-β is a potent inducer of SMAD2 phosphorylation and nuclear translocation (171), and alterations in TGF-β signaling are an important aspect of the pathogenesis of Marfan syndrome (118, 119, 172). Phosphorylation of Smad2 is mediated by the TGF-β signaling. We investigated whether BA4 or indomethacin affected the TGF-β pathway by measuring the pSmad2 expression. Immunstaining of pSmad2 in aorta from mgR/mgR mice showed increased number of pSmad2 positive cells throughout aortic media, no pSmad2 immunopositivity was observed in healthy age-matched controls, indicating the enhancement of TGF-β signaling via pSmad2 is activated in the progress of TAA (Figure 3.13A). Treatment of mice with BA4 antibody significantly reduced the number of pSmad2 positive cells in both aortic adventitia and media, whereas control IgG treatment did not (Figure 3.13A). These results could be further confirmed by western blot, which demonstrate that the BA4 can reduce pSmad2 activity at concentrations as low as 1 mg/kg, and normalized pSmad2 to the control level at 2 months of age at 10 mg/kg. Decreased pSmad2 immunoreactivity was also observed in the indomethacin treated group (Figure 3.13B). These results indicate that both BA4 Ab and indomethacin could antagonize excessive TGF-β activity.

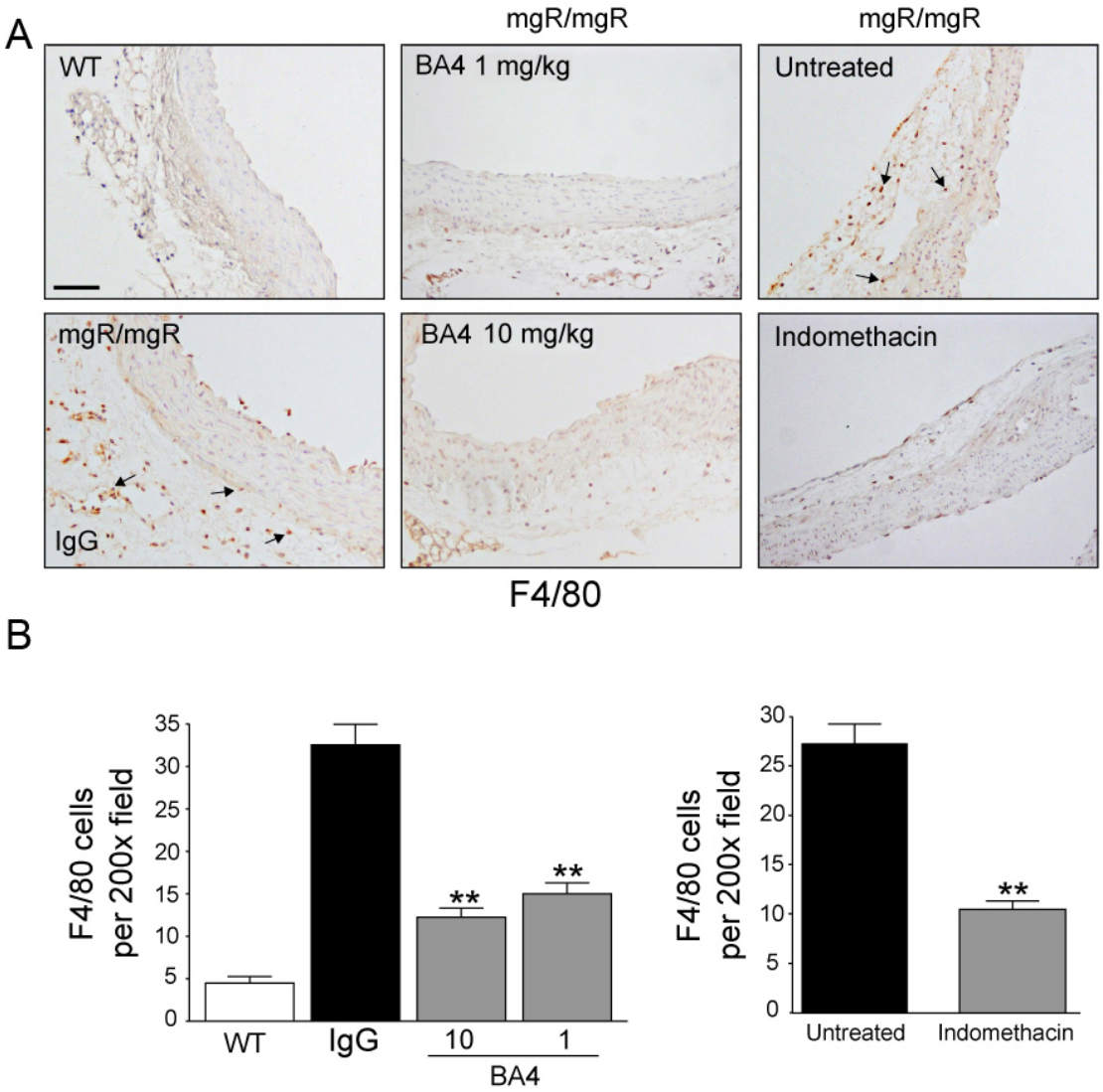

Figure 3.12: Treatment with BA4 or indomethacin decreases adventitial macrophage infiltration in aorta from mgR/mgR mice. **(A)** Representative immunostaining with the F4/80 antibody in the aorta from wild type and mice in each treated group. Arrowheads indicate F4/80 positive cells. Both BA4 and indomethacin treatment led to a marked decrease in macrophage cell numbers. Scale bar indicates 50 μm. **(B)** Quantification of F4/80 macrophage number and per 200x field following treatments. The cell count was obtained from 4 different fields taken from 3 different sections. All values represent mean $\pm$ s.e.m. Number of animals per group were 5-6. $^{*}P < 0.05$; $^{**}P < 0.01$ vs. IgG treated or untreated groups.

3.5.6 Decreased nuclear accumulation of pSmad2 in cultured aortic vSMCs

SMAD2/3 signaling was shown to be constitutively active in *Fbn1* mutant vascular smooth muscle cell (vSMC) cultures and is maintained *in vitro* by vSMC explanted from the aortas of three different murine models of MFS including mgR/mgR (126). To investigate whether the BA4 treatment could also decrease the constitutive pSmad2 expression in cultured aortic vSMCs of mgR mice. We isolated the aortic vSMCs cells from mgR/mgR mice after BA4 treatment. Similar to other findings, immunofluorescene demonstrated increased nuclear pSmad2 expression in

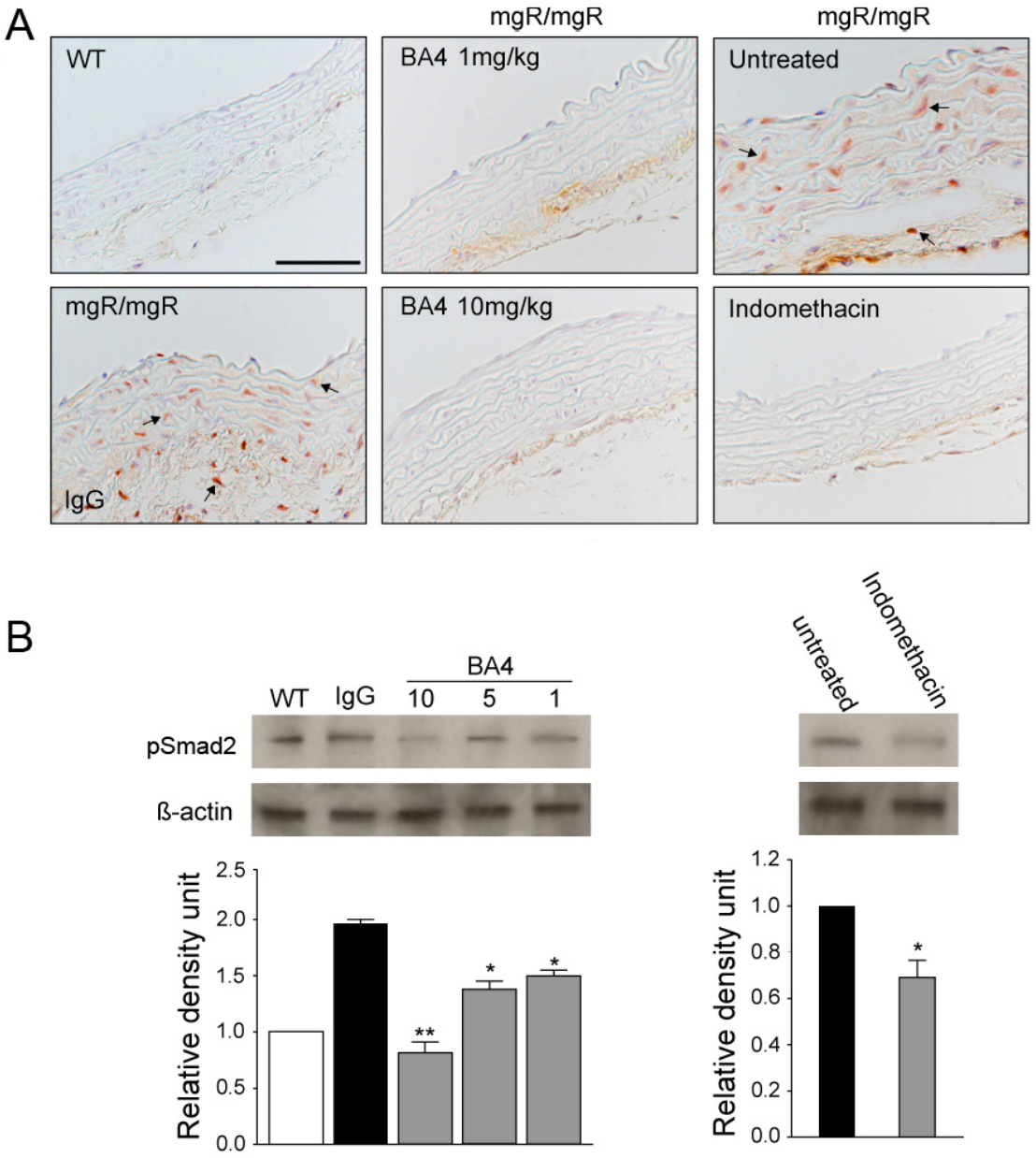

Figure 3.13: Treatment with BA4 or indomethacin decreases upregulation of pSmad2 activity in aorta from mgR/mgR mice. **(A)** Representative immunostaining with pSmad2 antibody in the aorta from wild-type and mice in each treated group. Arrowheads indicate pSmad2-positive cells. Both BA4 and indomethacin treatment led to a marked decrease in pSmad2 positive staining cell numbers. Scale bar indicates 50 μm. **(B)** Levels of pSmad2 activity from BA4 and indomethacin treatment group with different doses were analyzed by western blotting. Relative abundance of pSmad2 was normalized to β-actin content on each blot, in which the value of wild type (WT) or untreated mgR mice was defined as 1. All values represent mean $\pm$ s.e.m. Number of animals per group were 5-6. $^{*}P < 0.05$; $^{**}P < 0.01$ vs. IgG treated or untreated groups.

aortic vSMCs from mgR/mgR mice. BA4 at a dose of 10 mg/kg greatly decreased the nuclear accumulation of pSmad2 (Figure 3.13A). Western blot of the whole cell lysate demonstrates the same finding (Figure 3.13B).

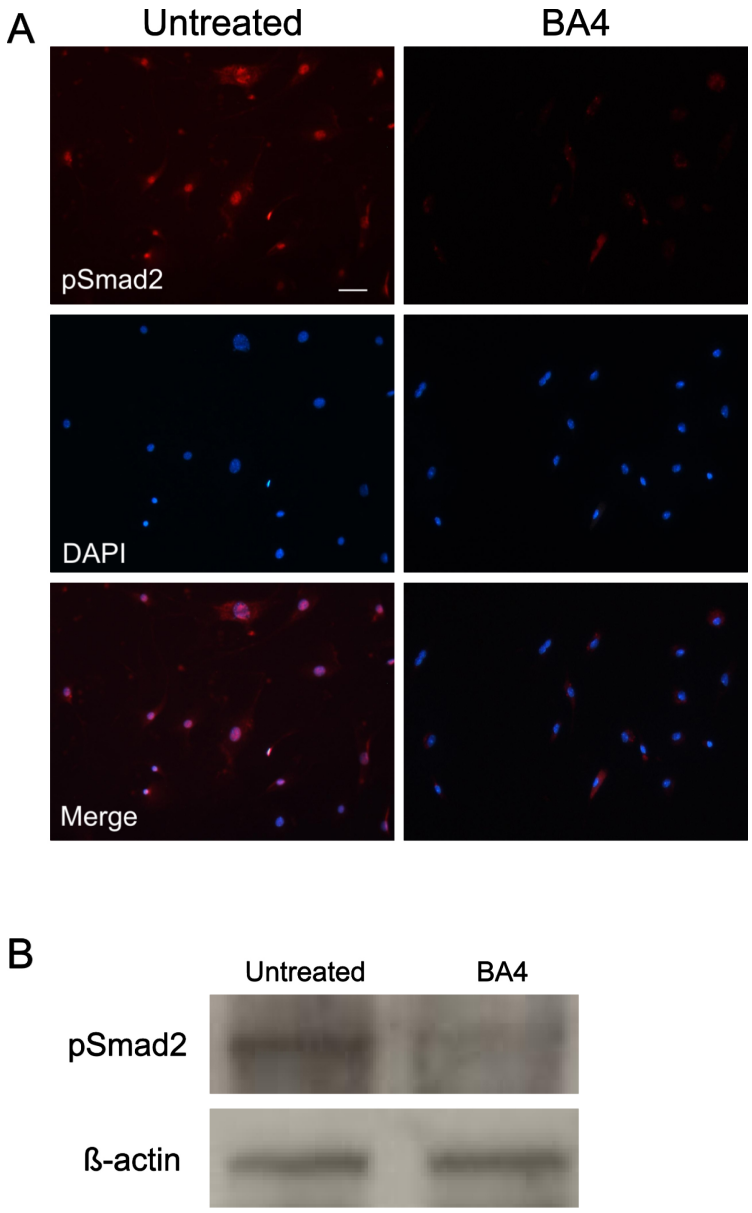

Figure 3.14: BA4 (10 mg/kg) decreases constitutive expression of pSmad2 in cultured aortic vSMCs from mgR/mgR mice. **(A)** Nuclear accumulation of pSmad2 activity was observed in primary cultured aortic vSMCs from mgR/mgR mice. However, no nuclear pSmad2 activity was found in aortic vSMCs after BA4 treatment. Scale bar indicates 50 μm. **(B)** Western blot of protein extract from primary cultured aortic vSMCs showed reduction of pSmad2 activity in cells from animals treated with BA4. Similar results were obtained for three repeated experiments.

3.5.7 BA4 treatment showed no effects on ERK1/2 activation

Recent studies have shown that noncanonical TGF-β signaling like pERK1/2 was upregulated in Marfan mouse model (127, 128). Consistent with this finding, our western blot results showed

a significantly increase of pERK1/2 expression in the aorta of mgR/mgR mice compared with that of age-related wild type mice. However, compared with IgG treated group there was no significant reduction of pERK1/2 expression in the BA4 treated group (Figure 3.15).

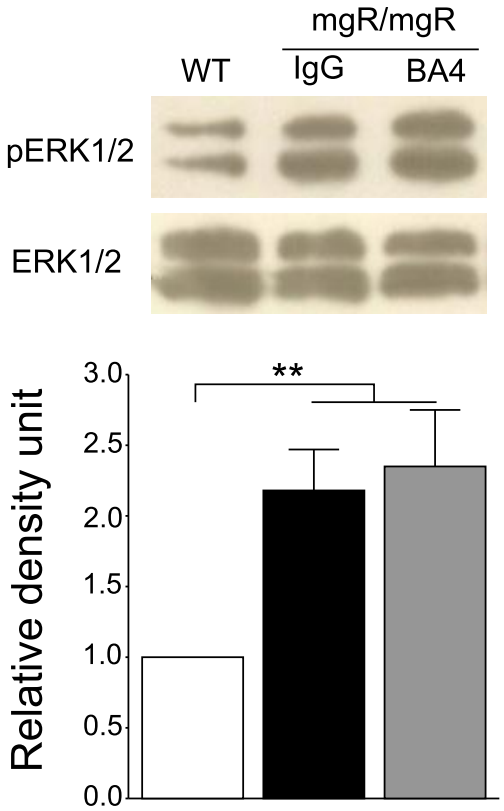

Figure 3.15: pERK1/2 expression in the aorta of mgR/mgR mice after BA4 treatment (10 mg/kg). Relative abundance of pERK1/2 was normalized to ERK1/2 content on each blot. IgG and BA4 treated mgR/mgR mice have a significantly higher pERK1/2 expression than wild type mice (WT). No difference in pERK1/2 expression was observed between IgG and BA4 treated group. The bands are representative of findings in 3 subjects. All values represent mean $\pm$ s.e.m., in which the value of WT mice was defined as 1. $^{**}P < 0.01$.

3.5.8 Indomethacin reduced COX-2 expression

COX-2 has been known to be upregulated in aorta of the *Fbn1*$^{C1039G/+}$ mice (73). In the current study, results of immunohistochemistry showed nearly 4 fold increase of COX-2 positive staining area in aortic media and adventitia in mgR/mgR mice compared with age-matched wild type mice (Figure 3.16). No significant decrease of COX-2 expression was observed in BA4 treated group with both doses. However, compared with untreated group indomethacin reduced positive COX-2 staining significantly (Figure 3.16B).

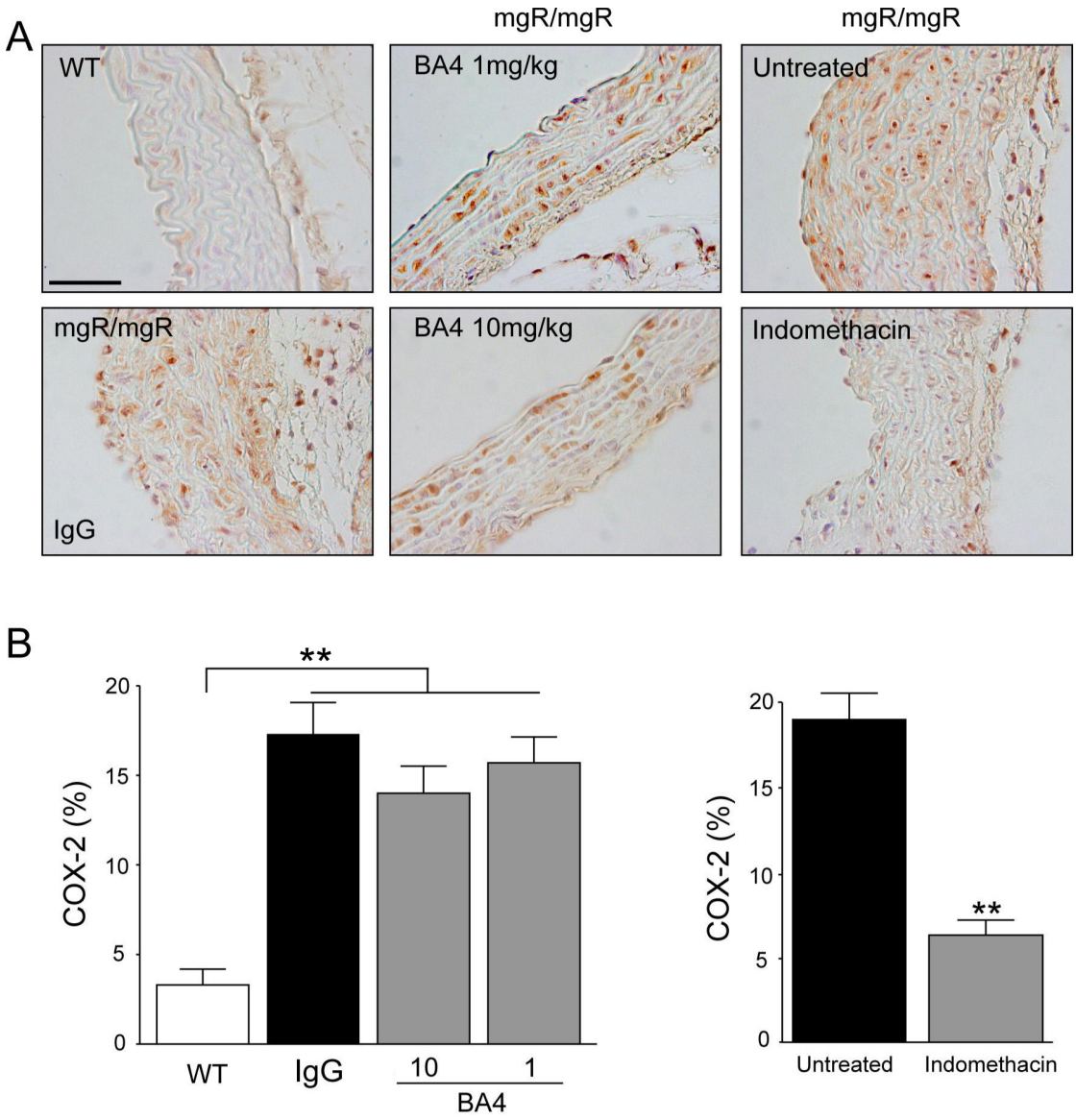

Figure 3.16: Indomethacin decreased COX-2 expression in mgR/mgR mice. **(A)** Representative immunostaining with the COX-2 antibody in the aorta from six groups of mice (Wild type, IgG, BA4 with doses of 1mg/kg and 10 mg/kg, indomethacin treated mgR/mgR mice). COX-2 expression is increased in IgG and untreated mgR/mgR mice. Scale bar indicates 50 μm. **(B)** Quantification of COX-2 positive staining area in aorta. There are no significant differences in COX-2 positive area between BA4 and IgG treated group. However, indomethacin treatment led to a marked decrease in COX-2 positive area. Number of animals per group were 5-6. All values represent means $\pm$ s.e.m. $^{**}P < 0.01$.

4 Discussion

In the aorta, microfibrils act to stabilize the vessel wall by connecting lamellar rings to one another, to smooth muscle cells, and to the subendothelial basement membrane (44). Fibrillin-1 is the major scaffolding component of microfibrils and thus plays a key role in maintaining vessel wall stability. Degradation of microfibrils as a result of fibrillin-1 mutations is thought to be the initial mechanisum in the pathogenesis of MFS. Recently, more and more evidence has shown that ECM fragments such as fibrillin-1 and elastin fragments can have other secondary effects above and beyond structural instability. A number of ECM proteins are known to have multiple biological active binding motifs, which remain masked in the intact ECM. However, once ECM disrupted or injured, these motifs are exposed and can trigger a variety of transduction pathways, resulting in many cellular responses, which lead to further destruction of elastin and other structural elements of the extracellular matrix of the aorta (46). In this and previous work we showed macrophages in aortic specimen from Marfan patients and a Marfan murine model (85). However, the biochemical mechanisms of macrophage migration in Marfan aorta has received little attention. This study provides evidence that GxxPG containing fragments can induce macrophage migration mediated by EBP, suggesting a plausible molecular explanation for the macrophage migration observed in clinical studies and animal models. In addition, we found that inhibiting the GxxPG containing fragments or anti-inflammatory treatment has a beneficial therapeutic effect in a Marfan Mouse model, verifying the secondary deleterious effects caused by GxxPG containing fragments in MFS. These results have considerable importance for understanding the role of ECM fragments in the pathogenesis of TAA in MFS.

4.1 GxxPG motif in fibrillin-1 and chemotacitic activity

In the present study, recombinant fibrillin-1 fragments were generated by an established HEK 293 culture system, which ensures correct folding and posttranslational modifications (Figure 3.1). This system has been demonstrated to produce a number of other correctly folded fibrillin-1 fragments (42, 107, 144, 173). Fibrillin-1 contains three sequences conforming to the GxxPG that thus represent candidates for EBP interaction motifs. We used a Boyden chamber system to investigate whether the GxxPG motifs in fibrillin-1 showed chemotactic activity. Our results demonstrated that two recombinant fibrillin-1 fragments containing GxxPG motif (rFib11 and rFib47^{wt}) are able to induce chemotaxis. However, in vitro mutation of the EBP consensus site in rFib47^{wt}

from EGFEPG to EGFESG severely inhibited the chemotactic effect. Additionally, our studies with the EBP blocking agent lactose and BA4 pretreatment clearly demonstrate that EBP mediates at least a portion of this chemotactic activity. Furthermore, macrophage response to synthetic hexapeptides corresponding to the three GxxPG motifs in fibrillin-1 is also mediated by EBP. Our results support the notion that EBP can mediate GxxPG stimulated macrohage chemotaxis, as reported for several components of the extracellular matrix, including EDPs (150, 174, 175), laminin (149) and collagen (176). Indeed, biological effects of fibrillin-1 fragments are not limited to chemotacic effects. Our previous studies have shown that distinct motifs in fibrillin-1 such as GxxPG and RGD are capable of triggering increases in MMP production (144). ECM proteins with multiple GxxPG sites include fibrillin-1, -2, and -3, elastin, fibronectin, laminin, and several tenascins and collagens (144), indicating that numbers of ECM fragments may deliver various biological activities as a result of the GxxPG and EBP interaction. Studies have documented that GxxP tetrapeptides tend to form a type VIII β-turn (144, 154, 177). Any residue located before the GxxP motif (xGxxP) increases the β-turn stabilization, whereas the residue located after GxxP (GxxPx) has no significant structural effect (154). Results of biophysical studies suggest that the consensus sequence GxxPG protein stabilizes a type VIII β-turn, therefore, maintaining a sufficient conformation to be recognized by the elastin receptor (144, 154). As reviewed in introduction, mutations in any region of *FBN1* that disrupt domain and molecular conformations can increase the susceptibility of fibrillin-1 proteolysis (14, 102, 103, 107, 110, 111, 178), leading to the production of fibrillin-1 fragments which may play a critical pathogenic role in the formation of TAA in MFS. In summary, our results illustrate that chemotactic effects together with other biological processes triggered by GxxPG sequences in fibrillin-1 protein may involve in the further destruction of aorta in MFS. A mouse model of continuously and exclusively expressing fibrillin-1 polypeptides such as rFib47^{wt} in aorta may better elucidate the in vivo role of fibrillin-1 fragments in the pathogenesis of the TAA in MFS.

4.2 Marfan aortic extracts and macrophage migration

The chemotactic stimulatory properties associated with GxxPG motifs led us to hypothesize that GxxPG containing fragments generated upon ECM degradation can contribute to the macrophage migration into aortic wall in MFS. To analyze the soluble ECM derived peptides in aorta, we used a mild extraction method to extract the peptides from aorta, this method was selected to avoid the extraction of insoluble matrix components and to prevent the release of intracellular proteins that

might occur with extensive tissue homogenization (167). Aortic extracts from 2- and 4- month old mgR/mgR mouse demonstrate chemotactic activity, which can be abolished or decreased by pretreating macrophages with lactose, VGVAPG, or preincubating extracts with BA4 before chemotaxis analysis. These findings provide a plausible molecular mechanism for the inflammatory infiltrates observed in the mgR/mgR mice (Figure 3.12). It is worth mentioning that the murine tropoelastin sequence does not contain the VGVAPG sequence; however, it does contain significant quantities of both GxxPG and xGxPG. In fact, these commonly repeated sequences represent 21% of the entire mouse tropoelastin sequence (179). We detected higher BA4 reactivity in aortic extracts from Marfan patients compared to those from healthy controls, in other words, abundant GxxPG containing elastin, fibrillin-1 fragments are present in Marfan aortic tissue. This result may reflect our previous observation that proteins with multiple GxxPG motifs are highly enriched for GO (Gene Ontology) terms related to the extracellular matrix (144). In addition, our observations are in line with the findings of Heinz et al. (180) who reported that there are various peptide fragments containing GxxPG motifs in different bioactive peptides released after the degradation of the natural substrate tropoelastin by the elastinolytic matrix metalloproteinases MMP-7, MMP-9, and MMP-12. Similar to the results of the mgR/mgR mice, aortic extracts from patients with MFS showed a statistically significant ability to induce macrophage chemotaxis compared to samples from controls. Because of the fact that the chemotaxis inductive effect could be inhibited by pretreatment of the cells with lactose, VGVAPG or pretreatment of the samples with BA4, we infer that the induction of chemotaxis is at least partially due to increased concentrations of elastin and perhaps fibrillin-1 degradation products containing an GxxPG epitope. This interpretation is further supported by the statistically significant correlation between the chemotactic index and BA4 reactivity of aortic samples (Figure 3.7).

Elastin is the dominant ECM protein in the tunica media of the arterial and aortic wall, which is composed of a dense population of concentrically organized vascular smooth muscle cells (vSMCs) that synthesize elastin molecules and secrete them as soluble, hydrophobic monomers termed tropoelastin. Elastin is a major synthetic product of aortic tissues in early stages of postnatal development, but synthesis of the protein generally peaks early during arterial growth, decreases rapidly with further development, and essentially ceases in the aortic tissue of adults (181). In humans, mature elastic fibers are extraordinarily stable, showing negligible turnover rates in many adult tissues including lung and aorta (182–184). As a part of the aging process, the aortic wall undergoes a number of alterations including fibrosis and elastin fragmentation, character-

ized by disruption of elastin lamellae (185). Correspondingly, the concentration of soluble elastin fragments in serum gradually increases in healthy subjects with aging (186).

Elastin fragmentation is known to be a component of the complex pathogenesis of pulmonary emphysema, which results in part from elastic tissue digestion by unrestrained elastase activity in the lung in turn leading to the release of soluble elastin fragments, which may be measured in plasma by ELISA (187). It has been reported that serum EDPs was significantly higher in patients with AAA compared to control, indicating increased concentrations of serum EDPs were associated with aneurysm (188). To our knowledge we are the first to demonstrate that high concentrations of GxxPG motifs in aortic extracts in Marfan patients by using a competitive ELISA method with BA4 antibody. By contrast, immunostaining of aortic specimens from AAA patients with BA4 antibody revealed a negative correlation between BA4 immunoreactivity and elastin degradation, the latter was shown to be associated with inflammatory infiltrates in AAA (189). One possibility of this observation is that BA4 could recognize both intact and protease degraded elastin. The aortic extracts in present study contains however mainly soluble ECM derived peptides instead of mature elastin. We choose BA4 reactivity instead of elastin-derived peptides (EDPs) concentration as the definition of ELISA results. The reason of it is that fragmentation of aortic tissue could potentially affect both elastin, fibrillin-1 and other ECM proteins, and BA4 antibody recognize especially GxxPG motif which is enriched in several ECM protein besides elastin. This issue was further supported by our findings that recombinant fibrillin-1 fragments containing GxxPG motifs showed cross-reactivity with BA4 antibody (Figure 3.7).

As reviewed in introduction, tropoelastin and various EDPs are chemotactic for fibroblasts and monocytes, chemotactic sites on the elastin molecule have been identified in the hexapeptide VG-VAPG (Val-Gly-Val-Ala-Pro-Gly) (150, 174, 175) and EDPs have been shown to drive disease progression in a mouse model of emphysema (179). There is some suggestive evidence that EDPs may contribute to progression of vascular diseases. Soluble EDPs released within human abdominal aortic aneurysm tissue can attract mononuclear phagocytes by interacting with the 67-kDa EBP, providing a plausible explanation for the intense inflammatory response seen in that disorder (167). EDPs can induce free radical and protease production and induce oxidation of low density lipoproteins by phagocytic cells (190, 191). However, the relation of elastin and human arterial disease is complex and incompletely understood. Macrophages are not only able to be attracted by elastin fragments, but can themselves produce the elastin precursor elastin, and may contribute to the increase in tropoelastin content that is characteristic of human abdominal aortic

aneurysms and atheromas (192). This is the first study of measuring the chemotactic activity in Marfan aortic extracts, together with findings of inflammatory cell infiltratews in the media and adventitia of Marfan aortic specimens (85); it is therefore possible that early alternations in the ECM of the mgR mouse or human patients themselves have secondary deleterious effects. For instance, fragmentation of the aortic media could release soluble elastin degradation products or fibrillin-1 fragments that recruit macrophages into the aorta, which leads to a vicious cycle of further proteolysis caused by subsequent release of additional proteolytic enzymes by mononuclear cells. Macrophage-released proteases, including MMP-12, could be responsible for further destruction of elastin-rich tissues in the aorta. A similar model has been proposed for cigarette smoke-induced emphysema in a mouse model; cigarette smoke could induce macrophages to produce macrophage elastase, which cleaves elastic tissue, producing elastin-derived peptides that are chemoattractant to monocytes. Thus a positive feedback loop could perpetuate macrophage accumulation and lung destruction (179, 193). Indeed, the paradigm of limited elastic fiber degradation progressing to intense elastolysis in association with inflammatory infiltration of the vessel wall and increased expression of MMPs is emerging as a common theme in the pathogenesis of abdominal aortic aneurysms (89, 194, 195). Taken together, the results of previous and this experiment, highlight the importance of fragmentation in the pathogenesis of MFS.

We additionally investigated another clinical group. Eight patients underwent prophylactic aortic operations because of isolated (idiopathic) thoracic aortic aneurysm (TAA). Several genes and genetic loci have been identified for familial TAA (196), although the etiology of most cases of isolated TAA still remains unknown. Genetic testing was not performed on the eight patients with TAA, but there were no clinical signs suggestive of known monogenic forms of TAA such as Loeys-Dietz syndrome. BA4 reactivity and the chemotactic index for the TAA group was statistically significantly increased, although the individual values showed a larger dispersal than did the samples from the Marfan patients (Figure 3.6B).

Collectively this work has shown that aortic extracts from individuals with MFS and isolated TAA can induce macrophage chemotaxis modulated by the 67-kDa EBP. This suggests that elastin fragmentation may be a common response of the damaged aorta. It remains to be determined whether secondary effects of these fragments that are modulated by the 67-kDa EBP drive progression of some or all of these diseases.

4.3 The blocking effects of BA4 in TAA in MFS

The findings of in vitro experiments suggested that GxxPG containing fragments might be related to the progression of TAA in MFS, these findings motivated us to investigate whether antagonism of GxxPG containing fragments can improve the phenotype of mgR/mgR mice. To test this hypothesis, we used the mouse monoclonal anti-elastin antibody BA4 directed against the GxxPG motif, as our in vitro study has shown that BA4 could effectively inhibit macrophage chemotaxis toward GxxPG containing fragments and Marfan aortic extracts. We chose the mgR/mgR mouse model which bears the Marfan like cardiovascular phenotype and shows that fibrillin-1 deficiency promotes a series of secondary cellular events that exacerbate the progression of aneurysm disease leading to dissection (50). Marque et al. (197) have shown that reduced expression of fibrillin-1 in mgR/mgR mice leads to severe elastic network fragmentation but no change in cross-linking suggesting that fragmentation of the medial elastic network was not related to a defect in early elastogenesis, therefore, we began the treatment at three weeks of age, in an effort to neutralize the GxxPG containing fragments in the initial phase of the ECM proteolysis in TAA of mgR/mgR mice.

In the current study, BA4 treatment greatly improved elastin integrity in the aortic wall of mgR homozygous mice (Figure 3.10). Our findings of elevated MMP-2 and MMP-9 in aorta of mgR/mgR mice are consistent with those from previous reports (99). Expression of MMP-2, MMP-9 and MMP-12 decreased significantly after BA4 treatment, however, no effects could be observed after treatment with control antibody (mouse IgG). As reviewed in the introduction, MMPs such as MMP-2, -9 and -12 are able to cause elastin and fibrillin-1 degradation (50, 93, 94). It has been reported that MMP-12 is expressed in layers of disrupted vSMCs within remodeling arteries (198), suggesting that the presence of elastin fragments in vivo may stimulate elastase production in the arterial wall. Based on our and others' observations that elastin peptides and recombinant fibrillin-1 fragments can induce MMPs expression in cultured fibroblast or aortic vascular smooth muscle cells (144, 157), we suggest that the inhibitory effects on MMP-2 and MMP-9 by BA4 is, at least in part, attributable to its blocking of GxxPG containing ECM fragments, leading to the similar effects as observed in inhibition of MMPs by doxycycline, which has been shown to efficiently reduce the development of aortic aneurysm in *Fbn1*$^{C1039G/+}$ and mgR/mgR mice (80, 99). The blocking effect of BA4 on elastin fragments has also been reported in a previous study, in which intratracheal administration of BA4 antibody could eliminate the cigarette smoke-induced monocyte recruitment to the lung in a murine model of emphysema (179). The elastin binding se-

quence from the EBP demonstrates sequence homology to the NH2-terminal sequence of several serine elastases indicated that these proteins might share a common ligand-binding motif (199). Hinek et al. (199) reported that blocking of EBP-binding domain on elastin by BA4 prevent the elastolytic activity of porcine pancreatic elastase. Taddese et al. (200) has shown that MMP-12 degrades tropoelastin extensively and has the potential to generate small peptides that contain the GxxPG motif. These findings provide another possible mechanism of BA4 treatment efficacy. It can be hypothesized that BA4 binds to the GxxPG motif enriched elastic fibers, fibrillin-1 or other ECM protein, therefore protecting them from proteolysis by serine elastase or MMP-12. However, further experiments need to be performed to confirm this hypothesis.

In our experiment, macrophages could be found in the aortic adventitia from 2 month old mgR mice, which is consistent with the previous report that macrophage infiltration is an important feature in the initial phase of TAA in mgR/mgR mice (50). We showed in this study that BA4 at a dosage as low as 1 mg/kg could already decrease migrated macrophages in the aortic adventitia of mgR/mgR mice, whereas IgG control antibody had no effect. This finding further confirmed our hypothesis that GxxPG containing fragments are responsible for the macrophage infiltration observed in the aorta from mgR/mgR mice. Indeed, macrophages are also sources for MMP-2, -9 and -12 expression, suggesting that the inhibition of macrophage recruitment to the aorta by BA4 may result in the reduction of MMP expression.

Excessive pSmad2 immunostaining could be found throughout the aortic adventitia and media in mgR/mgR mouse, which is similar to the observation in the *Fbn1*$^{C1039G/+}$ mice. Studies have shown that TGF-β blockade by neutralizing antibodies or a selective angiotensin II type 1 (AT1) receptor blockers rescue the phenotype of a Marfan mouse model (118, 119). Consistent with these findings, analysis of pSmad2 nuclear staining and western blot showed that BA4 can also antagonize TGF-β signaling in the aortic wall of mgR/mgR mice. The mechanism of this effect still remains to be elucidated. It seems reasonable that decreased TGF-β activity is a result of the preservation of elastin integrity, which maintains the ability of fibrillin-1 protein to control active TGF-β. Actually, microfibril proteolysis has been thought as a common mechanism for the release of active TGF-β 1 from ECM in heritable fibrillinopathies (143). Furthermore, the impact of BA4 by decreasing MMP expression could also be as a result of the sequestration of TGF-β. This idea was supported by the observation that TGF-β can modulate MMP-2 and MMP-9 production (201). For instance, it has been shown that TGF-β itself can increase MMP activity in some circumstances (202). Another important finding of this study is that BA4 treatment

decreased the constitutive pSmad2 activation in cultured aortic vSMCs from mgR/mgR mice (Figure 3.14). The specific pSMAD2 overexpression in human aortic aneurysm vSMCs is thought to be associated with modifications of the histone H3 marker pattern in the vicinity of the 1a transcription start site (TSS) on the SMAD2 promoter (122). We infer that BA4 treatment may decrease pSmad2 expression by preventing the epigenetic reprogramming of aortic vSMCs in the initial phase of the disease. Taken together, the above data indicate that interrupting the interaction between GxxPG fragments and EBP by BA4 blocks the initial and secondary deleterious effects caused by GxxPG fragments, emphasizing the critical role of GxxPG containing fragments during TAA formation in MFS and providing a potential therapeutic strategy for treatment in the TAA of MFS.

In this study upregulated pERK1/2 expression could be observed in the aorta of mgR/mgR mice, suggesting that similar to *Fbn1*$^{C1039G/+}$ mice noncanonical TGF-β signaling also contriubtes to the development of TAA in mgR/mgR mice. However, BA4 treatment showed no effects on ERK1/2 activity in spite of its efficient impact on pSmad2 activity. It was very recently shown that treatment with the angiotensin II type 1 receptor (AT1) inhibitor losartan attenuates aortic aneurysm development in the *Fbn1*$^{C1039G/+}$ mouse model of MFS by antagonism of extracellular signal-regulated kinase (ERK) signaling (127). The same research group reported that enalapril, an angiotensin converting enzyme inhibitor (ACEi), decreased Smad2 activation in *Fbn1*$^{C1039G/+}$ mice, by contrast it had significantly less effect on ERK1/2 activation than losartan (128). The authors reasoned that ongoing angiotensin II type 2 (AT2) receptor signaling is required for the attenuation of ERK phosphorylation and that enalapril's lack of effect on ERK is attributable to the loss of AT2 receptor signaling potential with this agent (128). We note that the mgR/mgR mouse is a fibrillin-1 underexpression mouse model which presents a more severe phenotype compared with the *Fbn1*$^{C1039G/+}$ mouse. This difference in the results could reflect the differences of underlying disease mechanism between these two mouse models, or different effects of the different treatment regimes on the cellular pathways involved in the pathogenesis of MFS.

4.4 Anti-inflammatory treatment and TAA in MFS

Macrophages have been considered as an early event in the pathogenesis of mgR/mgR mice and are known to play an important role in regulating the turnover of extracellular matrix in both normal and pathologic conditions via the secretion of proteases including MMPs, protease in-

hibitors, and cytokines. Recent studies have observed macrophage infiltration in aortic specimens from patients with MFS (85). In the current study, we examined whether the anti-inflammatory treatment could decrease the development of TAA in mgR/mgR mice. Indomethacin is known as a nonsteroidal anti-inflammatory drug and nonspecific cyclooxygenase (COX) inhibitor and its anti-inflammatory effects are mediated by inhibiting the activity of the COX-2 isoform (203). In this study, we choose 6 mg/L as the treatment dose, which has been confirmed successfully to reduce the extent of atherosclerosis by 55% with the same dosis of indomethacin in a low density lipoprotein receptor knockout mouse (204).

Indomethacin treatment significantly rescued elastin integrity and reduced the numbers of macrophages in the adventitia of aorta from mgR/mgR mice, which corresponded to the decreased MMP-2, MMP-9 and MMP-12 expression. COX-2 expression was found to be upregulated in the aorta of *Fbn1*$^{C1039G/+}$ mice (73). Consistent with theses findings, increased COX-2 expression was also observed in the aorta from mgR/mgR mice, and indomethacin decreased COX-2 expression nearly to that level of wild type. However, BA4 treatment has no effect on COX-2 expression, indicating that the rescue effect of BA4 maybe not associated with the decreased COX-2 expression. In contrast, similar studies have shown that indomethacin decreased MMP-9 expression and attenuated aneurysm growth via inhibition of the COX-2 isoform in a rat AAA model (203, 205). Another study with the same rat model demonstrated that indomethacin significantly decreased MMP-9 expression without decreasing aneurysm size (206). The importance of COX-2 in AAA can be further confirmed in COX-2 deficient mice, in which the incidence and severity of AAA was greatly reduced (207). It has been shown that COX-2 was expressed by macrophage-like cells within the inflammatory infiltrate of the AAA specimens but was not significantly expressed in the normal aorta, suggesting a possible functional relationship between macrophage COX-2 expression and AAA (203, 208). Marked increase of MMP-2 and MMP-9 expression could associate with increased macrophage migration, for instance, the induction of MMPs expression in macrophages is dependent in part on the production of prostaglandin E2 (PGE2) (209). PGE2 is synthesized from arachidonic acid via a pathway that is rate-limited by the enzyme cyclooxygenase synthase (COX) (203). Franklin et al. (210) showed that indomethacin reduces the production of PGE2 and inflammatory cytokines in an explant culture system for AAA tissue, suggesting that COX-2 inhibitors may control the inflammation in the aneurysm wall and potentially limit AAA growth by inhibiting MMP expression. COX-2 is known to regulate two endothelial relaxant (Thromboxane A2) and constricting (PGI2) prostanoids (73), which in turn influence the

vasomotor function of aorta. Studies have shown that contractility of the aorta from *Fbn1*$^{C1039G/+}$ mice at 6 and 9 months of age was significantly improved by pretreating with indomethacin, also the sensitivity to the relaxant effects of acetylcholine was increased 10 fold after pretreating the thoracic aortic segments from *Fbn1*$^{C1039/+}$ mouse with indomethacin (73). Although we did not test the aortic contractility in the current study, the benifical effects of indomethacin on the vasomotor function of the aorta from mgR/mgR mice could not be excluded. However, any beneficial effects that indomethacin may have on aneurysm expansion can't be attributed solely to inhibition of COX-2. Further studies will be needed to determine the therapeutic mechanism of indomethacin.

Similar to prior findings in mouse models treated with losartan there was decreased pSmad2 activity in the aorta of mgR/mgR mice after indomethacin treatment (Figure 3.13B). The study of muscle injury in wild type mice showed that TGF-β enhanced macrophage infiltration, which is thought to be mediated by the COX-2 pathway (211). Moreover, indomethacin is reported to completely blunt cell proliferation induced by TGF-β and markedly reduced activation of MAP kinases without influencing Smad2 phosphorylation in muscle regeneration (212). It can't be excluded that crosstalk and feedback loops between the COX-2 and TGF-β pathways may be responsible for the impact of indomethacin on pSmad2 activity. This will be the subject of further investigation. Collectively, our observations suggest that COX-2 mediated inflammatory infiltrate may contribute to the further destruction of aortic wall in mgR/mgR mice. Moreover, these results strongly suggest macrophages are participating in the pathogenesis of TAA via a synergistic combination of MMPs that degrade the matrix of the aorta. This observation is consistent with the premise that macrophages may play a role in the early stages of TAA in mgR/mgR mice.

4.5 Proposed vicious cycle of TAA in MFS

Since mutations of *FBN1* can make fibrillin-1 susceptible to proteolysis (46), we speculate that the production of low levels of proteolytic breakdown products could be an early event in the pathogenesis of aortic disease in MFS by inducing pathogenic events such as MMP up-regulation and macrophage infiltration, and in turn initiate a vicious cycle by promoting increased MMP expression and macrophage infiltration. This vicious cycle is schematically shown in Figure 4.1. We hypothesized following events. GxxPG containing fragments caused by fibrillin-1 proteolysis or elastolysis in the Marfan aorta could recruit macrophages into the media, the migrated

macrophages produce MMPs, which cause further elastin fragmentation in the aortic wall, and so on in a vicious cycle. Based on the results of this study we can conclude that antagonism of the GxxPG containing fragments or an anti-inflammatory treatment can break the vicious cycle, therefore slowing disease progression in mgR/mgR mice.

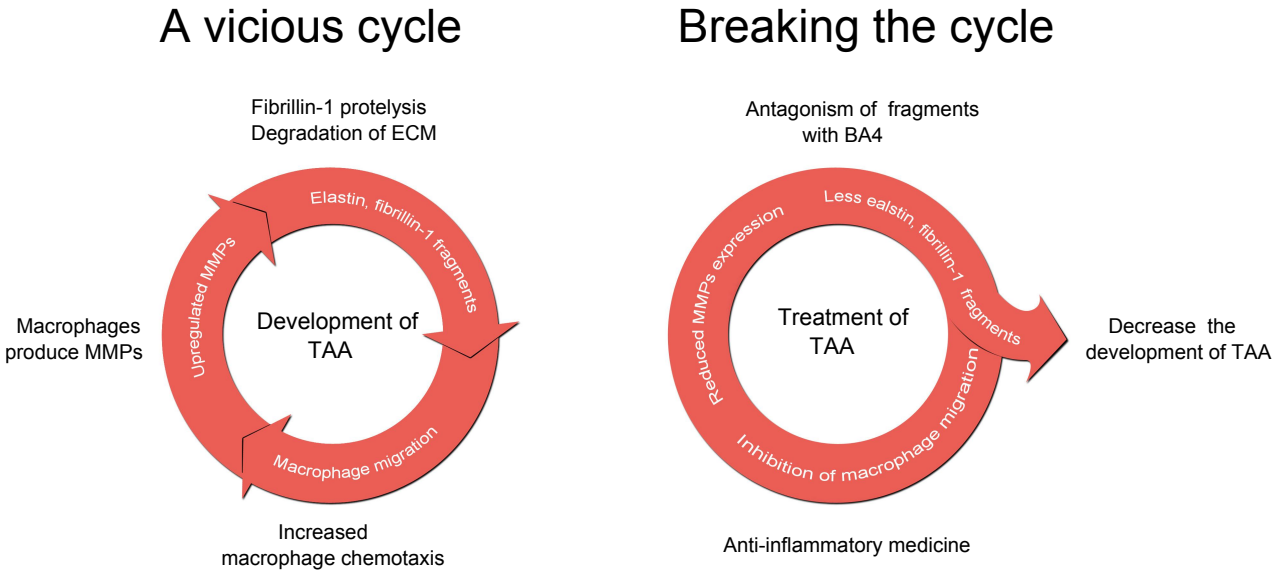

Figure 4.1: Schematic diagram showing the proposed vicious cycle. ECM, Extracellular matrix; MMP, Matrix Metalloproteinase; TAA, Thoracic aortic aneurysm

4.6 Future therapeutic perspectives

The understanding of the pathogenesis of MFS provides us a variety of therapeutic strategies. Blocking of the TGF-β via antibodies or losartan, an AT1 receptor blocker that reduces TGF-β activity, has been reported to be efficiently decrease aortic aneurysm in a Marfan mouse model (118, 119). A small clinical trial of losartan has been reported to reduce the diameter of aorta in Marfan children (124). Furthermore, doxycycline, which is known to inhibit MMP activity, has been reported to effectively decrease the development of aortic aneurysm in Marfan mouse (80, 99) and to have synergistic beneficial effects when given in combination with losartan (213). Our data about BA4 treatment in mgR/mgR mice suggest that targetting EBP signaling or its ligands may be exploited to prevent the development of aortic aneurysm. Monoclonal antibody therapy has been reported successfully in treating AAA patients and AAA mouse model. For instance, Ricci et al. (214) demonstrated that treatment with a monoclonal antibody directed against the CD-18 leukocyte adhesion molecule attenuated aneurysm growth of experimental AAA and was associated with a marked decrease in the number of infiltrating macrophages. An antibody with a

possible therapeutic application is usually evaluated based on its pharmacokinetic profile. Smaller antibodies in the form of IgGs are able to efficiently target. For instance, antibodies encompassing high affinity have been developed to efficiently bind cytokines and their receptors to reduce the inflammatory response. Patients with rheumatoid arthritis for example, can be treated with chimeric anti-tumor necrosis factor (TNF)-alpha antibodies which are also available for the treatment of Crohn's disease (215). Since antibodies are produced in cell lines or other expression systems, a possible contamination with viruses or other infectious agents can't be excluded. A further challenge is the appropriate therapeutical antibody concentration, which is crucial for a successful therapy. We recognize that these studies with BA4 antibody were conducted in mice and that clinical trials are needed to confirm its application to humans.

Although the role of inflammation in the pathogenesis of TAA remains unclear, cyclophilin A or Jun N-terminal kinase (JNK) inhibition have been shown efficiently to prevent aneurysm formation in animal models of abdominal aneurysms (161, 162). We believe that valuable data from the abdominal aneurysm should be considered in the therapeutic strategy for TAA. Considering the results of this study we hypothesize long-term treatment of indomethacin may also be efficient for preventing aortic aneurysm in Marfan patients. This intervention is attractive because nonsteroidal anti inflammatory drugs (NSAIDs) that inhibit both COX-1 and COX-2 activity are already in common use. Unfortunately, NSAIDs, and therefore indomethacin, have significant adverse effects, such as peptic ulceration, platelet inhibition, and nephrotoxicity. These adverse effects are mediated by inhibition of the COX-1 isoform of cyclooxygenase. The selection of appropriate COX-2 inhibitor for the prevention of aneurysm is crucial. If COX-2 inhibitors prove to be safe, it may be possible to pharmacologically treat MFS with minimal morbidity in the near future. A recent study performed in rats using NS-398, a selective COX-2 inhibitor, demonstrated that proinflammatory prostaglandin synthesis could be effectively blocked with this drug without the gastric ulcerogenic adverse effects that were seen with indomethacin in the same model (216). COX-2 inhibitors are currently in clinical trial in humans and have minimal adverse effects. Prospective clinical trials should be considered to determine if this treatment can delay progression of aortic disease in patients with MFS.

Collectively, the results of the current study suggest the above mentioned possible fruitful therapeutic strategy in Marfan syndrome. It is tempting to speculate that a similar therapeutic strategy might be successful for other vascular diseases characterized by tissue fragmentation and inflammation, such as abdominal aortic aneurysm.

5 Side project:Characterization of fibrillin-1 promoter

Published in: Guo G, Bauer S, Hecht J, Schulz MH, Busche A,Robinson PN: A Short Ultraconserved Sequence Drives Transcription from an Alternate *FBN1* Promoter *Int J Biochem Cell Biol.* 2008;40(4):638-50.

5.1 Introduction

FBN1 possesses three alternatively spliced 5' upstream exons initially termed exons B, A, and C, each of which can be spliced to the first coding exon (exon 1, previously termed exon M) (Figure 5.1A). Transcripts from several sources (placenta, neonatal fibroblasts, and osteosarcoma cells) showed a strong bias for the utilization of exon A. No clones containing more than one upstream exon was found, suggesting either initiation from alternative transcription initiation sites or mutually exclusive splicing from an as yet undetermined additional upstream exon. Elucidation of the mechanisms of genetic regulation of the fibrillins will be an essential step in understanding the different functional roles of the fibrillins and of the different splice forms of *FBN1*. However, to date, little is known about the molecular mechanisms governing the expression of *FBN1* and the other fibrillin genes.

In this work, we have investigated the sequences upstream of exon 1 and the three 5' alternatively spliced exons of *FBN1*. We show significant transcriptional activity for sequences of exon B, A and 1. Computional and biochemical analysis showed the presence of an ultraconserved sequence in the area of the core promoter exon A containing an initiator element (Inr), a downstream promoter element (DPE), and a transcriptionally active 10-nucleotide palindromic element.

5.2 Results and discussion

5.2.1 Upstream of exon A showed the highest promoter activity

Five constructs were designed to encompass regions of lying upstream of exon 1 and the three noncoding upstream exons (Figure 5.1A). The elements were cloned into pGL3-Basic and transiently transfected into HEK-293 and HT-1080 cells(Figure 5.1A). We show significant transcriptional activity in HEK-293 and HT-1080 cells for sequences upstream of exons B, A, and 1. Since the sequence upstream of exon A showed the highest activity in our assay system, we investigated it in further detail (Figure 5.1B).

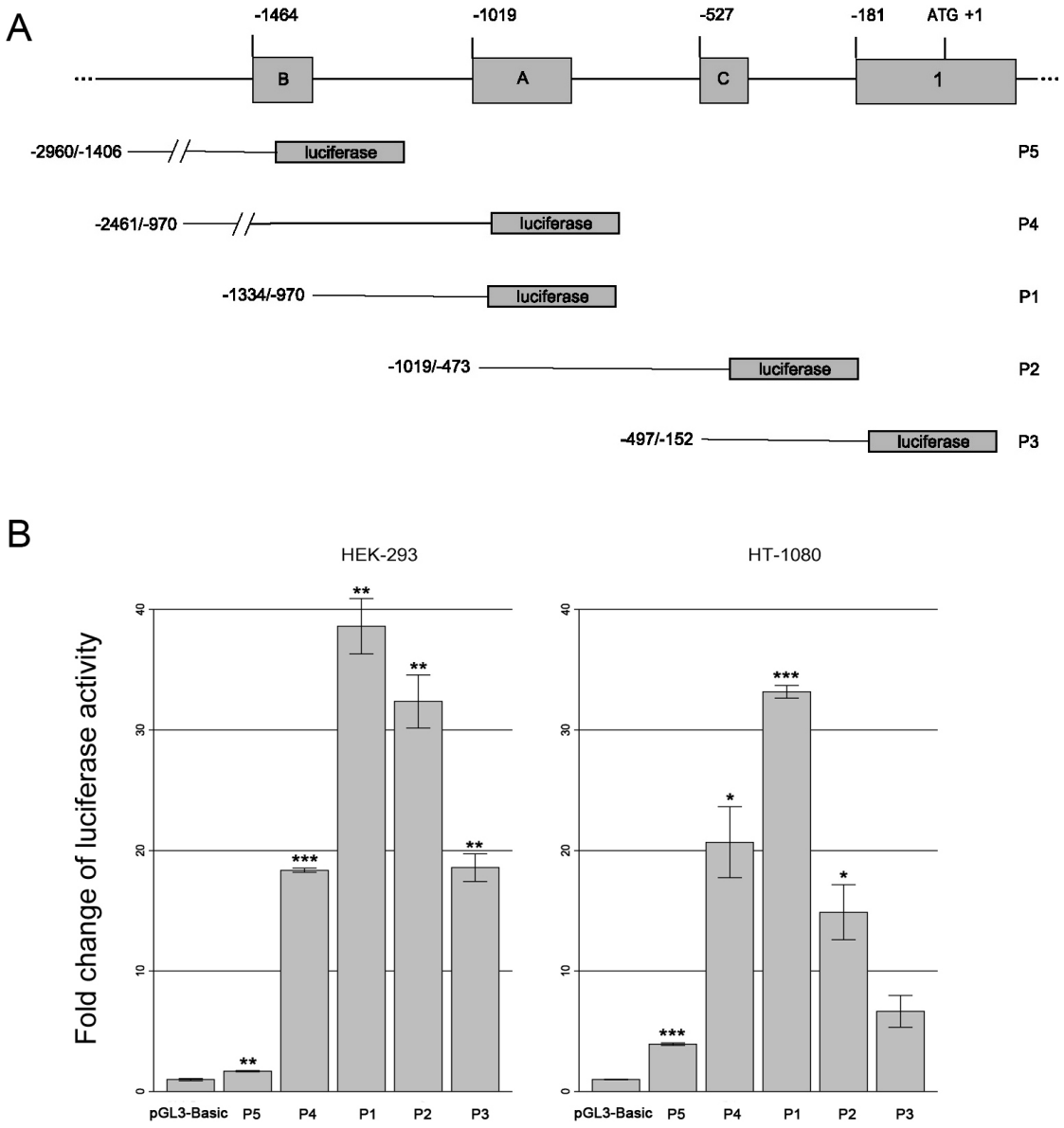

Figure 5.1: **(A)** A schematic diagram showing the three 5' upstream exons and exon 1 (previously referred to as exon M) of *FBN1*. The location of the *FBN1*-specific sequence that was cloned into the pGL3-Basic firefly luciferase vector is shown to the left of each construct. **(B)** Analysis of putative *FBN1* promoters in HEK-293 cells and HT-1080 cells. The mean and standard error for three replicates are shown. The experiment was repeated three times with similar results. $*P < 0.05$; $**P < 0.01$; $***P < 0.001$.

5.2.2 An ultraconserved sequence block in promoter A

In order to identify the sequence regions within promoter A that are most relevant for its transcriptional activity, we analyzed a series of deletion constructs in which 5' or 3' sequence regions were deleted from the main promoter A construct P1. As Figure 5.2A shown, removal of the entire upstream region (P1b construct) reduced activity to about 40% of that of the full length P1 construct. Computational and biochemical analysis showed the presence of an unusually high degree of se-

quence conservation centered around a 66 base-pair strech from -2 to +64 in P1b, which showed nearly 100% identity among the seven species (Figure 5.3). The 66 nucleotides stretching from position -2 to +64 with respect to the the transcriptional start site of exon A and comprising the initiator element (Inr), a downstream promoter element (DPE), and a 10-nucleotide palindromic element, TCTCGCGAGA, situated between the Inr and DPE motifs. It was recently demonstrated that the sequence motif TCTCGCGAGA is common not only in promoters of ribosomal genes, but also in cell cycle genes, chromatin structure modulators, and translation initiation factors (217).

5.2.3 Exon A contains Inr, a DPE and a transcriptionally active 10-nucleotide palindromic motif

To gain an initial understanding of whether the Inr or DPE motifs are important for transcriptional activity, additional deletion constructs were designed to remove either the Inr or the DPE sequences. Although our results suggest that the Inr and DPE sequences are important for the activity of the core promoter in *FBN1* exon, mutation of these elements did not completely abolish activity. Rather, mutation of both Inr and DPE reduced activity to somewhat under 20% in HEK 293 and 10% in HT 1080 cells (Figure 5.2A). Furthermore, two nucleotides were substituted in 10-nucleotide palindromic element (TCTCGCGAGA$\rightarrow$ TCTCaaGAGA) in the construct P1b. This muation reduced transcriptional activity to less than 10% in HEK-293 cells and completely abolished activity in HT-1080 cells (Figure 5.2A). Additionally, electrophoretic mobility shift assay (EMSA assay) of the 10-nucleotide palindromic element demonstrated that the wild type (TCTCGCGAGA), but not the mutant oligonucleotide (TCTCaaGAGA), displayed binding to a nuclear protein. To our knowledge, the results in the present work are the first to demonstrate the fact that a muation of the palindromic element can both abolish transcriptional activity in a luciferase assay and also abolish binding activity in EMSA.

Previous computational analysis had identified either TCTCGCGAGA or compatible positionally weighted sequence motifs in numerous other promoters of genes encoding ribosomal proteins or other types of protein (217–219). However, the protein or proteins binding to this sequence motif have not been identified to date. We suggest that a protein binding to the palindromic element may be able to interact with proteins of the core transcriptional complex that bind to Inr and DPE, or that different proteins can bind to the element in different sequence contexts.

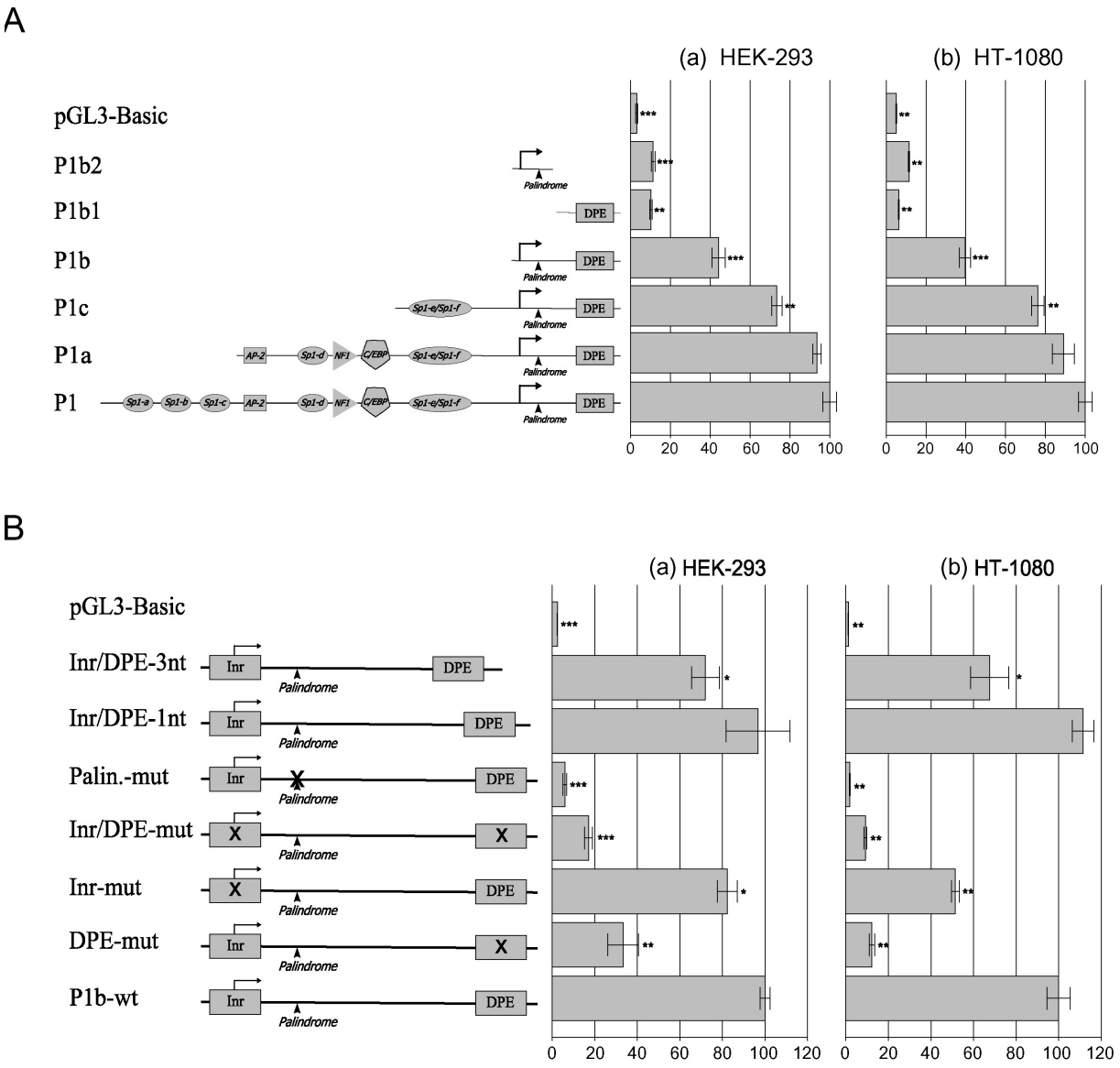

Figure 5.2: **(A)** Deletion analysis of human *FBN1* promoter A activity in HEK-293 (a) and HT-1080 (b) cells. A series of deletions from the 5' end of fragment P1 was performed to obtain fragments P1a, P1b, and P1c. Promoter activity is shown as percentage of the activity of the full length wild type construct (P1). **(B)** Mutational analysis of a putative Inr-DPE pair in *FBN1* promoter A. The construct P1b, which contains nucleotides -3 to +50 of *FBN1* exon A and encompasses a putative Inr and DPE site, was used as a template to carry out of series of mutations and deletions. Activities of the mutant constructs were normalized to that of the wild type P1b construct. The mean and standard error for three replicates are shown. The experiment was repeated three times with similar results. $*P < 0.05$; $**P < 0.01$; $***P < 0.001$.

Taken together, our analysis suggest that the 66 bp sequence in the P1b construct exhibits an unusually high degree of conservation even if compared to sequences presumed to be under selective pressure owing to the presence of regulatory elements such as transcription factor-binding sites. There is no exact definition of the term ultraconserved, and the length threshold and the number of species analyzed will determine the number of sequences identified as ultraconserved. Given the results of the analysis presented above, we propose that the core promoter region of

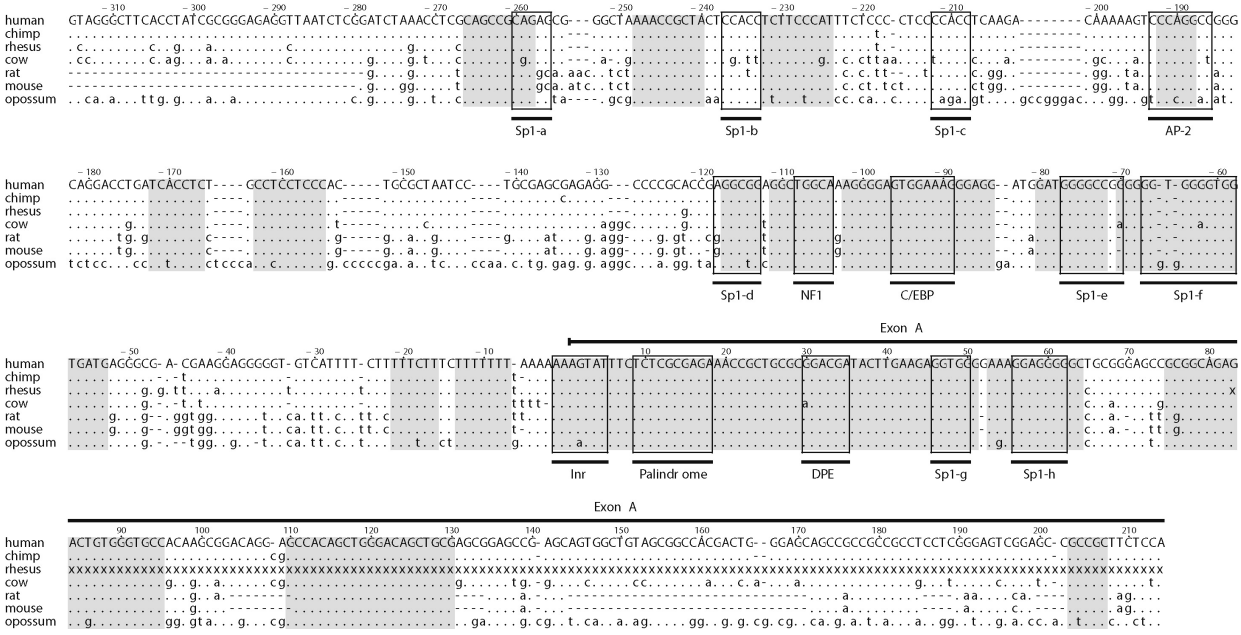

Figure 5.3: Sequence analysis of intron B and the 5' region of exon A. Homologous sequences from chimp, rhesus ape, cow, rat, mouse, and opossum were aligned to the human sequence. Identical nucleotides are shown as a dot (.) and gaps are shown as a dash (-). Consensus putative transcription factor-binding sites that displayed conservation among primates and at least one other species are boxed. Blocks of hyperconservation at least five nucleotides long with at most one deviation from the human sequence in the primate, cow, rodent or opossum sequences are shown in gray. The rhesus sequence was incomplete, extending only to position +82. The incomplete portion of the sequence is indicated by 'x'. Construct P1 extends from the start of the alignment (-315) to position +50.

the alternatively spliced exon A of *FBN1* is ultraconserved. We suggest that the ultraconservation may reflect the importance of finely tuned regulation of alternate transcription of *FBN1*and that the sequences involved have been under negative selective pressure for at least the last 180 million years of mammalian evolution. Additionally, this ultraconserved region may also be related to an absolute necessity for the usage of the alternate transcript regulated by this region at some point in development.

6 Abstract

Marfan syndrome (MFS) is an autosomal dominant connective tissue disorder that predominantly affects the skeletal, cardiovascular, and ocular systems. The primary cause of premature death in untreated patients is related to thoracic aortic aneurysms and dissections (TAA). MFS is caused by mutations in the gene for fibrillin-1, *FBN1*, and multiple factors such as halpoinsufficiency, fibrillin-1 proteolysis, abnormal TGF-β signaling, increased matrix metalloproteinase (MMP) expression, and changes in cell-matrix interaction contribute to the complex pathogeneisis of this disorder.

In the initial part of this study, we investigated whether recombinant fibrillin-1 polypeptides and aortic extracts from a fibrillin-1 underexpressing mouse model (mgR/mgR) and human Marfan patients can stimulate macrophage chemotaxis. Recombinant fibrillin-1 fragments containing a GxxPG motif and the corresponding synthetic peptides could induce macrophage migration mediated by elastin binding protein (EBP). Both aortic extrtacts from the mgR/mgR mice as well as aortic extracts from Marfan patients significantly increased macrophage chemotaxis compared with extracts from wild type mice and healthy controls. Because of the fact that the chemotaxis inductive effect of Marfan aortic extracts could be inhibited by pretreatment of the cells with lactose or pretreatment of the samples with monoclonal anti-elastin antibody (BA4), we infer that the induction of chemotaxis of Marfan aortic extracts is at least partially associated with EBP. Additionally, aortic extracts from patients with MFS showed a statistically significant increase in reactivity to BA4 in ELISA. BA4 recognizes GxxPG containing peptides or fragments which are ligands of EBP.

We additionally performed a therapeutic study on the mgR/mgR mice to test the effects of treatment with BA4 in an attempt to antagonize the secondary deleterious effects of elastin and fibrillin fragmentation. We investigated whether a monoclonal anti-elastin antibody (BA4) or treatment with the anti-inflammatory medication indomethacin could decrease the development of TAA in the mgR/mgR mice. Both treatments were started at 3 weeks of age and continued for 8 weeks. The mgR/mgR mice received BA4 through intraperitoneal injection once a week. In a separate group, indomethacin was added to drinking water continuously for 8 weeks. Here we show that both BA4 and indomethacin treatment significantly improves elastin integrity in the aortic wall of mgR/mgR mice. Treatment with BA4 significantly decreased MMP-2, MMP-9, MMP-12 expression and pSMAD2 activity. Compared to the untreated group, there were significantly less

macrophages in the aortic adventitia after BA4 treatment. Indomethacin treatment led to similar results.

The results of this study further confirm the hypothesis that abnormal secondary cellular events caused by GxxPG containing fragments contribute to the development of TAA in MFS. Chemotactic activity observed in Marfan aortic extracts and efficient anti-inflammatory treatment suggest an important role of matrix-fragment induced inflammatory activity in the aortic wall in the pathogenesis of TAA. Furthermore, this study might provide new impact on therapeutic approaches and could contribute to new strategies for the long-term management of aortic aneurysm in MFS.

7 Zusammenfassung

Das Marfan-Syndrom (MFS) ist eine relativ häufige autosomal dominant vererbte Störung des Bindegewebes mit zahlreichen Symptomen im Skelettsystem, am Auge, und im Herzkreislaufsystem. Die Haupttodesursache bei unbehandelten Patienten ist die akute Dissektion der aufsteigenden Aorta (TAA), das in der Regel nach einer jahrelangen, langsam fortschreitenden Erweiterung der aufsteigenden Aorta auftritt. Das MFS wird durch Mutationen im Gen für Fibrillin-1, *FBN1*, verursacht, und mehrere Faktoren wie Halpoinsuffizienz, Fibrillin-1 Proteolyse, abnormale TGF-β Aktivität, Erhöhung der Expression von Matrixmetalloproteinase (MMP) und Veränderungen in der Zell-Matrix-Interaktion können zur Pathogenese des MFS beitragen.

Im ersten Teil dieser Studie untersuchten wir, ob rekombinante Fibrillin-1-Polypeptide und Aortenextrakte aus einem Fibrillin-1-hypomorphen Mausmodell (mgR/mgR) und Marfan Patienten die Makrophagenchemotaxis stimulieren können. Rekombinante Fibrillin-1-Fragmente mit einem GxxPG (Glyzin-X-X-Prolin-Glyzin) Motiv und den entsprechenden synthetischen Peptiden konnten die Migration von Makrophagen durch Interaktion mit dem Elastin-bindendes-Protein (EBP) stimulieren. Sowohl die mgR/mgR-Aortenextrakte als auch die Aortenextrakte von MFS-Patienten erhöhten signifikant die Makrophagenchemotaxis im Vergleich zum Extrakten aus Wildtyp-Mäusen und gesunde Kontrollen. Aufgrund der Tatsache, dass die chemotaktische Aktivität von MFS-Aortenextrakten durch Vorbehandlung der Makrophagen mit Laktose (EBP-Hemmung) bzw. durch den monoklonalen Anti-Elastin-Antikörper (BA4) signifikant gehemmt werden, schliessen wir, dass die durch MFS-Aortenextrakte stimulierte Makrophagenchemotaxis zumindest teilweise durch das EBP vermittelt ist. Darüber hinaus zeigten Aortenextrakte von MFS-Patienten eine statistisch signifikante Zunahme der BA4-Reaktivität im ELISA. BA4 erkennt GxxPG Peptide oder Fragmente, die EBP-Liganden sind.

Zusätzlich führten wir eine Therapiestudie an mgR/mgR Mäusen durch, um die Wirkungen einer gezielten Blockade der sekundären schädlichen Auswirkung von Elastin und Fibrillin-1 Fragmente durch Behandlung mit BA4 zu prüfen. Wir untersuchten, ob Antikörper BA4 oder antiinflammatorische Therapie mit dem Medikament Indomethacin die Entstehung der Aortendissektion in dem Fibrillin-1-hypomorphen Mausmodell (mgR/mgR) reduzieren konnte. Beide Behandlungen begannen in der dritten Lebenswoche und dauerten 8 Wochen. Die mgR/mgR Mäuse erhielten BA4 durch intraperitoneale Injektion einmal pro Woche. In einer separaten Gruppe wurde Indomethacin im Trinkwasser kontinuierlich für 8 Wochen verabreicht. Wir könnten zeigen,

dass die Behandlung mit BA4 sowie durch Indomethacin die Elastinintegrität in Aortenwand in mgR/mgR Mäusen signifikant verbesserten. Die BA4 Behandlung verminderte signifikant die MMP-2, MMP-9, MMP-12 Expression und pSMAD2 Aktivität. Im Vergleich zu der unbehandelten Gruppe gab es signifikant weniger Makrophagen in der Aortenadventitia nach BA4 Behandlung. Indomethacin-Behandlung führte zu ähnlichen Ergebnissen.

Die Ergebnisse dieser Studie bestätigen die Hypothese, dass GxxPG-Fragmente abnormale sekundäre zelluläre Reaktionen hervorrufen und somit zur Entwicklung von TAA in MFS beitragen können. Die chemotaktische Aktivität bei Marfan Aortenextrakten und die Effizienz der Antiinflammatorische Therapie zeigen eine wichtige Rolle der durch Matrix-Fragment stimulierte entzündliche Aktivität in der Aortenwand bei der Pathogenese des TAA in MFS. Darüber hinaus zeigt diese Studie potentiell neue therapeutische Optionen auf.

8 References

1. H. C. Dietz, G. R. Cutting, R. E. Pyeritz, C. L. Maslen, L. Y. Sakai, G. M. Corson, E. G. Puffenberger, A. Hamosh, E. J. Nanthakumar, and S. M. Curristin. Marfan syndrome caused by a recurrent de novo missense mutation in the fibrillin gene. *Nature*, 352:337–339, Jul 1991.

2. J. R. Gray, A. B. Bridges, R. R. West, L. McLeish, A. G. Stuart, J. C. Dean, M. E. Porteous, M. Boxer, and S. J. Davies. Life expectancy in British Marfan syndrome populations. *Clin. Genet.*, 54:124–128, Aug 1998.

3. R. E. Pyeritz. The Marfan syndrome. *Annu. Rev. Med.*, 51:481–510, 2000.

4. J. L. Murdoch, B. A. Walker, B. L. Halpern, J. W. Kuzma, and V. A. McKusick. Life expectancy and causes of death in the Marfan syndrome. *N. Engl. J. Med.*, 286:804–808, Apr 1972.

5. A. De Paepe, R. B. Devereux, H. C. Dietz, R. C. Hennekam, and R. E. Pyeritz. Revised diagnostic criteria for the Marfan syndrome. *Am. J. Med. Genet.*, 62:417–426, Apr 1996.

6. B. L. Loeys, H. C. Dietz, A. C. Braverman, B. L. Callewaert, J. De Backer, R. B. Devereux, Y. Hilhorst-Hofstee, G. Jondeau, L. Faivre, D. M. Milewicz, R. E. Pyeritz, P. D. Sponseller, P. Wordsworth, and A. M. De Paepe. The revised Ghent nosology for the Marfan syndrome. *J. Med. Genet.*, 47:476–485, Jul 2010.

7. L. R. Scherer, P. H. Arn, D. A. Dressel, R. M. Pyeritz, and J. A. Haller. Surgical management of children and young adults with Marfan syndrome and pectus excavatum. *J. Pediatr. Surg.*, 23:1169–1172, Dec 1988.

8. P. D. Sponseller, W. Hobbs, L. H. Riley, and R. E. Pyeritz. The thoracolumbar spine in Marfan syndrome. *J Bone Joint Surg Am*, 77:867–876, Jun 1995.

9. J. M. Le Parc, S. Molcard, and F. Tubach. Bone mineral density in Marfan syndrome. *Rheumatology (Oxford)*, 40:358–359, Mar 2001.

10. G. Percheron, G. Fayet, T. Ningler, J. M. Le Parc, S. Denot-Ledunois, M. Leroy, B. Raffestin, and G. Jondeau. Muscle strength and body composition in adult women with Marfan syndrome. *Rheumatology (Oxford)*, 46:957–962, Jun 2007.

11. W. M. Behan, C. Longman, R. K. Petty, P. Comeglio, A. H. Child, M. Boxer, P. Foskett, and D. G. Harriman. Muscle fibrillin deficiency in Marfan's syndrome myopathy. *J. Neurol. Neurosurg. Psychiatr.*, 74:633–638, May 2003.

12. J. R. Gray and S. J. Davies. Marfan syndrome. *J. Med. Genet.*, 33:403–408, May 1996.

13. R. Finkbohner, D. Johnston, E. S. Crawford, J. Coselli, and D. M. Milewicz. Marfan syndrome. Long-term survival and complications after aortic aneurysm repair. *Circulation*, 91:728–733, Feb 1995.

14. P. N. Robinson and P. Booms. The molecular pathogenesis of the Marfan syndrome. *Cell. Mol. Life Sci.*, 58:1698–1707, Oct 2001.

15. Y. von Kodolitsch and P. N. Robinson. Marfan syndrome: an update of genetics, medical and surgical management. *Heart*, 93:755–760, Jun 2007.

16. W. C. Roberts and H. S. Honig. The spectrum of cardiovascular disease in the Marfan syndrome: a clinico-morphologic study of 18 necropsy patients and comparison to 151 previously reported necropsy patients. *Am. Heart J.*, 104:115–135, Jul 1982.

17. D. M. Milewicz, H. C. Dietz, and D. C. Miller. Treatment of aortic disease in patients with Marfan syndrome. *Circulation*, 111:e150–157, Mar 2005.

18. R. E. Pyeritz and M. A. Wappel. Mitral valve dysfunction in the Marfan syndrome. Clinical and echocardiographic study of prevalence and natural history. *Am. J. Med.*, 74:797–807, May 1983.

19. F. Alpendurada, J. Wong, A. Kiotsekoglou, W. Banya, A. Child, S. K. Prasad, D. J. Pennell, and R. H. Mohiaddin. Evidence for Marfan cardiomyopathy. *Eur. J. Heart Fail.*, 12:1085–1091, Oct 2010.

20. I. H. Maumenee. The eye in the Marfan syndrome. *Trans Am Ophthalmol Soc*, 79:684–733, 1981.

21. P. De Coster, G. De Pauw, L. Martens, and A. De Paepe. Craniofacial structure in Marfan syndrome: a cephalometric study. *Am. J. Med. Genet. A*, 131:240–248, Dec 2004.

22. J. R. Hall, R. E. Pyeritz, D. L. Dudgeon, and J. A. Haller. Pneumothorax in the Marfan syndrome: prevalence and therapy. *Ann. Thorac. Surg.*, 37:500–504, Jun 1984.

23. R. E. Pyeritz, E. K. Fishman, B. A. Bernhardt, and S. S. Siegelman. Dural ectasia is a common feature of the Marfan syndrome. *Am. J. Hum. Genet.*, 43:726–732, Nov 1988.

24. P. J. De Coster, L. C. Martens, and A. De Paepe. Orofacial manifestations of congenital fibrillin deficiency: pathogenesis and clinical diagnostics. *Pediatr Dent*, 26:535–537, 2004.

25. B. L. Loeys, J. Chen, E. R. Neptune, D. P. Judge, M. Podowski, T. Holm, J. Meyers, C. C. Leitch, N. Katsanis, N. Sharifi, F. L. Xu, L. A. Myers, P. J. Spevak, D. E. Cameron, J. De Backer, J. Hellemans, Y. Chen, E. C. Davis, C. L. Webb, W. Kress, P. Coucke, D. B. Rifkin, A. M. De Paepe, and H. C. Dietz. A syndrome of altered cardiovascular, craniofacial, neurocognitive and skeletal development caused by mutations in TGFBR1 or TGFBR2. *Nat. Genet.*, 37:275–281, Mar 2005.

26. P. N. Robinson, P. Booms, S. Katzke, M. Ladewig, L. Neumann, M. Palz, R. Pregla, F. Tiecke, and T. Rosenberg. Mutations of FBN1 and genotype-phenotype correlations in Marfan syndrome and related fibrillinopathies. *Hum. Mutat.*, 20:153–161, Sep 2002.

27. F. Tiecke, S. Katzke, P. Booms, P. N. Robinson, L. Neumann, M. Godfrey, K. R. Mathews, M. Scheuner, G. K. Hinkel, R. E. Brenner, H. H. Hovels-Gurich, C. Hagemeier, J. Fuchs, F. Skovby, and T. Rosenberg. Classic, atypically severe and neonatal Marfan syndrome: twelve mutations and genotype-phenotype correlations in FBN1 exons 24-40. *Eur. J. Hum. Genet.*, 9:13–21, Jan 2001.

28. P. N. Robinson, L. M. Neumann, S. Demuth, H. Enders, U. Jung, R. Konig, B. Mitulla, D. Muller, P. Muschke, L. Pfeiffer, B. Prager, M. Somer, and S. Tinschert. Shprintzen-Goldberg syndrome: fourteen new patients and a clinical analysis. *Am. J. Med. Genet. A*, 135:251–262, Jun 2005.

29. S. Sood, Z. A. Eldadah, W. L. Krause, I. McIntosh, and H. C. Dietz. Mutation in fibrillin-1 and the Marfanoid-craniosynostosis (Shprintzen-Goldberg) syndrome. *Nat. Genet.*, 12:209–211, Feb 1996.

30. C. L. Maslen, G. M. Corson, B. K. Maddox, R. W. Glanville, and L. Y. Sakai. Partial sequence of a candidate gene for the Marfan syndrome. *Nature*, 352:334–337, Jul 1991.

31. G. M. Corson, S. C. Chalberg, H. C. Dietz, N. L. Charbonneau, and L. Y. Sakai. Fibrillin binds calcium and is coded by cDNAs that reveal a multidomain structure and alternatively spliced exons at the 5' end. *Genomics*, 17:476–484, Aug 1993.

32. L. Pereira, M. D'Alessio, F. Ramirez, J. R. Lynch, B. Sykes, T. Pangilinan, and J. Bonadio. Genomic organization of the sequence coding for fibrillin, the defective gene product in Marfan syndrome. *Hum. Mol. Genet.*, 2:1762, Oct 1993.

33. N. J. Biery, Z. A. Eldadah, C. S. Moore, G. Stetten, F. Spencer, and H. C. Dietz. Revised genomic organization of FBN1 and significance for regulated gene expression. *Genomics*, 56:70–77, Feb 1999.

34. G. Guo, S. Bauer, J. Hecht, M. H. Schulz, A. Busche, and P. N. Robinson. A short ultra-conserved sequence drives transcription from an alternate FBN1 promoter. *Int. J. Biochem. Cell Biol.*, 40:638–650, 2008.

35. L. Y. Sakai, D. R. Keene, and E. Engvall. Fibrillin, a new 350-kD glycoprotein, is a component of extracellular microfibrils. *J. Cell Biol.*, 103:2499–2509, Dec 1986.

36. L. Y. Sakai, D. R. Keene, R. W. Glanville, and H. P. Bachinger. Purification and partial characterization of fibrillin, a cysteine-rich structural component of connective tissue microfibrils. *J. Biol. Chem.*, 266:14763–14770, Aug 1991.

37. C. M. Cardy and P. A. Handford. Metal ion dependency of microfibrils supports a rod-like conformation for fibrillin-1 calcium-binding epidermal growth factor-like domains. *J. Mol. Biol.*, 276:855–860, Mar 1998.

38. D. P. Reinhardt, D. E. Mechling, B. A. Boswell, D. R. Keene, L. Y. Sakai, and H. P. Bachinger. Calcium determines the shape of fibrillin. *J. Biol. Chem.*, 272:7368–7373, Mar 1997.

39. P. A. Handford. Fibrillin-1, a calcium binding protein of extracellular matrix. *Biochim. Biophys. Acta*, 1498:84–90, Dec 2000.

40. S. A. Jensen, A. R. Corbett, V. Knott, C. Redfield, and P. A. Handford. Ca2+-dependent interface formation in fibrillin-1. *J. Biol. Chem.*, 280:14076–14084, Apr 2005.

41. X. Yuan, A. K. Downing, V. Knott, and P. A. Handford. Solution structure of the transforming growth factor beta-binding protein-like module, a domain associated with matrix fibrils. *EMBO J.*, 16:6659–6666, Nov 1997.

42. D. P. Reinhardt, J. E. Gambee, R. N. Ono, H. P. Bachinger, and L. Y. Sakai. Initial steps in assembly of microfibrils. Formation of disulfide-cross-linked multimers containing fibrillin-1. *J. Biol. Chem.*, 275:2205–2210, Jan 2000.

43. L. Lonnqvist, L. Karttunen, T. Rantamaki, C. Kielty, M. Raghunath, and L. Peltonen. A point mutation creating an extra N-glycosylation site in fibrillin-1 results in neonatal Marfan syndrome. *Genomics*, 36:468–475, Sep 1996.

44. D. P. Reinhardt, D. R. Keene, G. M. Corson, E. Poschl, H. P. Bachinger, J. E. Gambee, and L. Y. Sakai. Fibrillin-1: organization in microfibrils and structural properties. *J. Mol. Biol.*, 258:104–116, Apr 1996.

45. D. M. Milewicz, R. E. Pyeritz, E. S. Crawford, and P. H. Byers. Marfan syndrome: defective synthesis, secretion, and extracellular matrix formation of fibrillin by cultured dermal fibroblasts. *J. Clin. Invest.*, 89:79–86, Jan 1992.

46. P. N. Robinson, E. Arteaga-Solis, C. Baldock, G. Collod-Beroud, P. Booms, A. De Paepe, H. C. Dietz, G. Guo, P. A. Handford, D. P. Judge, C. M. Kielty, B. Loeys, D. M. Milewicz, A. Ney, F. Ramirez, D. P. Reinhardt, K. Tiedemann, P. Whiteman, and M. Godfrey. The molecular genetics of Marfan syndrome and related disorders. *J. Med. Genet.*, 43:769–787, Oct 2006.

47. H. Zhang, S. D. Apfelroth, W. Hu, E. C. Davis, C. Sanguineti, J. Bonadio, R. P. Mecham, and F. Ramirez. Structure and expression of fibrillin-2, a novel microfibrillar component preferentially located in elastic matrices. *J. Cell Biol.*, 124:855–863, Mar 1994.

48. G. Lin, K. Tiedemann, T. Vollbrandt, H. Peters, B. Batge, J. Brinckmann, and D. P. Reinhardt. Homo- and heterotypic fibrillin-1 and -2 interactions constitute the basis for the assembly of microfibrils. *J. Biol. Chem.*, 277:50795–50804, Dec 2002.

49. G. M. Corson, N. L. Charbonneau, D. R. Keene, and L. Y. Sakai. Differential expression of fibrillin-3 adds to microfibril variety in human and avian, but not rodent, connective tissues. *Genomics*, 83:461–472, Mar 2004.

50. L Pereira, S Y Lee, B Gayraud, K Andrikopoulos, S D Shapiro, T Bunton, N J Biery, H C Dietz, L Y Sakai, and F Ramirez. Pathogenetic sequence for aneurysm revealed in mice underexpressing fibrillin-1. *Proc Natl Acad Sci U S A*, 96(7):3819–23, 1999.

51. B. L. Lima, E. J. Santos, G. R. Fernandes, C. Merkel, M. R. Mello, J. P. Gomes, M. Soukoyan, A. Kerkis, S. M. Massironi, J. A. Visintin, and L. V. Pereira. A new mouse model for marfan syndrome presents phenotypic variability associated with the genetic background and overall levels of Fbn1 expression. *PLoS ONE*, 5:e14136, 2010.

52. L. Carta, L. Pereira, E. Arteaga-Solis, S. Y. Lee-Arteaga, B. Lenart, B. Starcher, C. A. Merkel, M. Sukoyan, A. Kerkis, N. Hazeki, D. R. Keene, L. Y. Sakai, and F. Ramirez. Fibrillins 1 and 2 perform partially overlapping functions during aortic development. *J. Biol. Chem.*, 281:8016–8023, Mar 2006.

53. D. P. Judge, N. J. Biery, D. R. Keene, J. Geubtner, L. Myers, D. L. Huso, L. Y. Sakai, and H. C. Dietz. Evidence for a critical contribution of haploinsufficiency in the complex pathogenesis of Marfan syndrome. *J. Clin. Invest.*, 114:172–181, Jul 2004.

54. N. L. Charbonneau, E. J. Carlson, S. Tufa, G. Sengle, E. C. Manalo, V. M. Carlberg, F. Ramirez, D. R. Keene, and L. Y. Sakai. In vivo studies of mutant fibrillin-1 microfibrils. *J. Biol. Chem.*, 285:24943–24955, Aug 2010.

55. C. M. Kielty, M. Raghunath, L. D. Siracusa, M. J. Sherratt, R. Peters, C. A. Shuttleworth, and S. A. Jimenez. The Tight skin mouse: demonstration of mutant fibrillin-1 production and assembly into abnormal microfibrils. *J. Cell Biol.*, 140:1159–1166, Mar 1998.

56. H. C. Dietz, I. McIntosh, L. Y. Sakai, G. M. Corson, S. C. Chalberg, R. E. Pyeritz, and C. A. Francomano. Four novel FBN1 mutations: significance for mutant transcript level and EGF-like domain calcium binding in the pathogenesis of Marfan syndrome. *Genomics*, 17:468–475, Aug 1993.

57. Z. A. Eldadah, T. Brenn, H. Furthmayr, and H. C. Dietz. Expression of a mutant human fibrillin allele upon a normal human or murine genetic background recapitulates a Marfan cellular phenotype. *J. Clin. Invest.*, 95:874–880, Feb 1995.

58. D. W. Hollister, M. Godfrey, L. Y. Sakai, and R. E. Pyeritz. Immunohistologic abnormalities of the microfibrillar-fiber system in the Marfan syndrome. *N. Engl. J. Med.*, 323:152–159, Jul 1990.

59. M. Godfrey, S. Olson, R. G. Burgio, A. Martini, M. Valli, G. Cetta, H. Hori, and D. W. Hollister. Unilateral microfibrillar abnormalities in a case of asymmetric Marfan syndrome. *Am. J. Hum. Genet.*, 46:661–671, Apr 1990.

60. T. Aoyama, K. Tynan, H. C. Dietz, U. Francke, and H. Furthmayr. Missense mutations impair intracellular processing of fibrillin and microfibril assembly in Marfan syndrome. *Hum. Mol. Genet.*, 2:2135–2140, Dec 1993.

61. T. Aoyama, U. Francke, H. C. Dietz, and H. Furthmayr. Quantitative differences in biosynthesis and extracellular deposition of fibrillin in cultured fibroblasts distinguish five groups of Marfan syndrome patients and suggest distinct pathogenetic mechanisms. *J. Clin. Invest.*, 94:130–137, Jul 1994.

62. T. Brenn, T. Aoyama, U. Francke, and H. Furthmayr. Dermal fibroblast culture as a model system for studies of fibrillin assembly and pathogenetic mechanisms: defects in distinct groups of individuals with Marfan's syndrome. *Lab. Invest.*, 75:389–402, Sep 1996.

63. P. Whiteman and P. A. Handford. Defective secretion of recombinant fragments of fibrillin-1: implications of protein misfolding for the pathogenesis of Marfan syndrome and related disorders. *Hum. Mol. Genet.*, 12:727–737, Apr 2003.

64. E. C. Davis. Smooth muscle cell to elastic lamina connections in developing mouse aorta. Role in aortic medial organization. *Lab. Invest.*, 68:89–99, Jan 1993.

65. E. C. Davis. Immunolocalization of microfibril and microfibril-associated proteins in the subendothelial matrix of the developing mouse aorta. *J. Cell. Sci.*, 107 (Pt 3):727–736, Mar 1994.

66. D. G. Wilson, M. F. Bellamy, M. W. Ramsey, J. Goodfellow, M. Brownlee, S. Davies, J. F. Wilson, M. J. Lewis, and A. G. Stuart. Endothelial function in Marfan syndrome: selective impairment of flow-mediated vasodilation. *Circulation*, 99:909–915, Feb 1999.

67. S. S. Lee, V. Knott, J. Jovanovi, K. Harlos, J. M. Grimes, L. Choulier, H. J. Mardon, D. I. Stuart, and P. A. Handford. Structure of the integrin binding fragment from fibrillin-1 gives new insights into microfibril organization. *Structure*, 12:717–729, Apr 2004.

68. B. Mariko, Z. Ghandour, S. Raveaud, M. Quentin, Y. Usson, J. Verdetti, P. Huber, C. Kielty, and G. Faury. Microfibrils and fibrillin-1 induce integrin-mediated signaling, proliferation and migration in human endothelial cells. *Am J Physiol Cell Physiol*, Aug 2010.

69. D. Lorena, I. A. Darby, D. P. Reinhardt, V. Sapin, J. Rosenbaum, and A. Desmouliere. Fibrillin-1 expression in normal and fibrotic rat liver and in cultured hepatic fibroblastic cells: modulation by mechanical stress and role in cell adhesion. *Lab. Invest.*, 84:203–212, Feb 2004.

70. L. Pereira, K. Andrikopoulos, J. Tian, S. Y. Lee, D. R. Keene, R. Ono, D. P. Reinhardt, L. Y. Sakai, N. J. Biery, T. Bunton, H. C. Dietz, and F. Ramirez. Targetting of the gene encoding fibrillin-1 recapitulates the vascular aspect of Marfan syndrome. *Nat. Genet.*, 17:218–222, Oct 1997.

71. D. P. Judge and H. C. Dietz. Marfan's syndrome. *Lancet*, 366:1965–1976, Dec 2005.

72. G. Matyas, S. Alonso, A. Patrignani, M. Marti, E. Arnold, I. Magyar, C. Henggeler, T. Carrel, B. Steinmann, and W. Berger. Large genomic fibrillin-1 (FBN1) gene deletions provide evidence for true haploinsufficiency in Marfan syndrome. *Hum. Genet.*, 122:23–32, Aug 2007.

73. A. W. Chung, K. Au Yeung, G. G. Sandor, D. P. Judge, H. C. Dietz, and C. van Breemen. Loss of elastic fiber integrity and reduction of vascular smooth muscle contraction resulting from the upregulated activities of matrix metalloproteinase-2 and -9 in the thoracic aortic aneurysm in Marfan syndrome. *Circ. Res.*, 101:512–522, Aug 2007.

74. H. T. Syyong, A. W. Chung, H. H. Yang, and C. van Breemen. Dysfunction of endothelial and smooth muscle cells in small arteries of a mouse model of Marfan syndrome. *Br. J. Pharmacol.*, 158:1597–1608, Nov 2009.

75. H. H. Yang, C. van Breemen, and A. W. Chung. Vasomotor dysfunction in the thoracic aorta of Marfan syndrome is associated with accumulation of oxidative stress. *Vascul. Pharmacol.*, 52:37–45, 2010.

76. A. Vitarelli, Y. Conde, E. Cimino, I. D'Angeli, S. D'Orazio, S. Stellato, V. Padella, and F. Caranci. Aortic wall mechanics in the Marfan syndrome assessed by transesophageal tissue Doppler echocardiography. *Am. J. Cardiol.*, 97:571–577, Feb 2006.

77. R. D. Rudic, D. Brinster, Y. Cheng, S. Fries, W. L. Song, S. Austin, T. M. Coffman, and G. A. FitzGerald. COX-2-derived prostacyclin modulates vascular remodeling. *Circ. Res.*, 96:1240–1247, Jun 2005.

78. P. M. Vanhoutte. Endothelium-dependent hyperpolarizations: the history. *Pharmacol. Res.*, 49:503–508, Jun 2004.

79. I. B. Wilkinson, A. Qasem, C. M. McEniery, D. J. Webb, A. P. Avolio, and J. R. Cockcroft. Nitric oxide regulates local arterial distensibility in vivo. *Circulation*, 105:213–217, Jan 2002.

80. A. W. Chung, H. H. Yang, M. W. Radomski, and C. van Breemen. Long-term doxycycline is more effective than atenolol to prevent thoracic aortic aneurysm in marfan syndrome through the inhibition of matrix metalloproteinase-2 and -9. *Circ. Res.*, 102:73–85, Apr 2008.

81. M. Nataatmadja, M. West, J. West, K. Summers, P. Walker, M. Nagata, and T. Watanabe. Abnormal extracellular matrix protein transport associated with increased apoptosis of vascular smooth muscle cells in marfan syndrome and bicuspid aortic valve thoracic aortic aneurysm. *Circulation*, 108 Suppl 1:I329–334, Sep 2003.

82. A. M. Segura, R. E. Luna, K. Horiba, W. G. Stetler-Stevenson, H. A. McAllister, J. T. Willerson, and V. J. Ferrans. Immunohistochemistry of matrix metalloproteinases and their inhibitors in thoracic aortic aneurysms and aortic valves of patients with Marfan's syndrome. *Circulation*, 98:I331–337, Nov 1998.

83. R. He, D. C. Guo, A. L. Estrera, H. J. Safi, T. T. Huynh, Z. Yin, S. N. Cao, J. Lin, T. Kurian, L. M. Buja, Y. J. Geng, and D. M. Milewicz. Characterization of the inflammatory and apoptotic cells in the aortas of patients with ascending thoracic aortic aneurysms and dissections. *J. Thorac. Cardiovasc. Surg.*, 131:671–678, Mar 2006.

84. R. He, D. C. Guo, W. Sun, C. L. Papke, S. Duraisamy, A. L. Estrera, H. J. Safi, C. Ahn, L. M. Buja, F. C. Arnett, J. Zhang, Y. J. Geng, and D. M. Milewicz. Characterization of the inflammatory cells in ascending thoracic aortic aneurysms in patients with Marfan syndrome, familial thoracic aortic aneurysms, and sporadic aneurysms. *J. Thorac. Cardiovasc. Surg.*, 136:922–929, Oct 2008.

85. Gao Guo, Patrick Booms, Marc Halushka, Harry C Dietz, Andreas Ney, Sigmar Stricker, Jochen Hecht, Stefan Mundlos, and Peter N Robinson. Induction of macrophage chemotaxis by aortic extracts of the mgR Marfan mouse model and a GxxPG-containing fibrillin-1 fragment. *Circulation*, 114(17):1855–62, 2006.

86. N. Sakalihasan, R. Limet, and O. D. Defawe. Abdominal aortic aneurysm. *Lancet*, 365:1577–1589, 2005.

87. J. S. Lindholt and G. P. Shi. Chronic inflammation, immune response, and infection in abdominal aortic aneurysms. *Eur J Vasc Endovasc Surg*, 31:453–463, May 2006.

88. S. T. MacSweeney, J. T. Powell, and R. M. Greenhalgh. Pathogenesis of abdominal aortic aneurysm. *Br J Surg*, 81:935–941, Jul 1994.

89. T. Freestone, R. J. Turner, A. Coady, D. J. Higman, R. M. Greenhalgh, and J. T. Powell. Inflammation and matrix metalloproteinases in the enlarging abdominal aortic aneurysm. *Arterioscler. Thromb. Vasc. Biol.*, 15:1145–1151, Aug 1995.

90. F. A. Hellenthal, W. A. Buurman, W. K. Wodzig, and G. W. Schurink. Biomarkers of abdominal aortic aneurysm progression. Part 2: inflammation. *Nat Rev Cardiol*, 6:543–552, Aug 2009.

91. N. H. Sachdev, N. Di Girolamo, P. J. McCluskey, A. V. Jennings, R. McGuinness, D. Wakefield, and M. T. Coroneo. Lens dislocation in Marfan syndrome: potential role of matrix metalloproteinases in fibrillin degradation. *Arch. Ophthalmol.*, 120:833–835, Jun 2002.

92. R. W. Thompson, P. J. Geraghty, and J. K. Lee. Abdominal aortic aneurysms: basic mechanisms and clinical implications. *Curr Probl Surg*, 39:110–230, Feb 2002.

93. J. L. Ashworth, G. Murphy, M. J. Rock, M. J. Sherratt, S. D. Shapiro, C. A. Shuttleworth, and C. M. Kielty. Fibrillin degradation by matrix metalloproteinases: implications for connective tissue remodelling. *Biochem. J.*, 340 (Pt 1):171–181, May 1999.

94. R. P. Mecham, T. J. Broekelmann, C. J. Fliszar, S. D. Shapiro, H. G. Welgus, and R. M. Senior. Elastin degradation by matrix metalloproteinases. Cleavage site specificity and mechanisms of elastolysis. *J. Biol. Chem.*, 272:18071–18076, Jul 1997.

95. J. S. Ikonomidis, J. R. Barbour, Z. Amani, R. E. Stroud, A. R. Herron, D. M. McClister, S. E. Camens, M. L. Lindsey, R. Mukherjee, and F. G. Spinale. Effects of deletion of the matrix metalloproteinase 9 gene on development of murine thoracic aortic aneurysms. *Circulation*, 112:I242–248, Aug 2005.

96. J. M. Shipley, R. L. Wesselschmidt, D. K. Kobayashi, T. J. Ley, and S. D. Shapiro. Metalloelastase is required for macrophage-mediated proteolysis and matrix invasion in mice. *Proc. Natl. Acad. Sci. U.S.A.*, 93:3942–3946, Apr 1996.

97. J. A. Curci, S. Liao, M. D. Huffman, S. D. Shapiro, and R. W. Thompson. Expression and localization of macrophage elastase (matrix metalloproteinase-12) in abdominal aortic aneurysms. *J. Clin. Invest.*, 102:1900–1910, Dec 1998.

98. R. D. Hautamaki, D. K. Kobayashi, R. M. Senior, and S. D. Shapiro. Requirement for macrophage elastase for cigarette smoke-induced emphysema in mice. *Science*, 277:2002–2004, Sep 1997.

99. W. Xiong, R. A. Knispel, H. C. Dietz, F. Ramirez, and B. T. Baxter. Doxycycline delays aneurysm rupture in a mouse model of Marfan syndrome. *J. Vasc. Surg.*, 47:166–172, Jan 2008.

100. G. Collod-Beroud, C. Beroud, L. Ades, C. Black, M. Boxer, D. J. Brock, K. J. Holman, A. de Paepe, U. Francke, U. Grau, C. Hayward, H. G. Klein, W. Liu, L. Nuytinck, L. Peltonen, A. B. Alvarez Perez, T. Rantamaki, C. Junien, and C. Boileau. Marfan Database (third edition): new mutations and new routines for the software. *Nucleic Acids Res.*, 26:229–223, Jan 1998.

101. A. K. Downing, V. Knott, J. M. Werner, C. M. Cardy, I. D. Campbell, and P. A. Handford. Solution structure of a pair of calcium-binding epidermal growth factor-like domains: implications for the Marfan syndrome and other genetic disorders. *Cell*, 85:597–605, May 1996.

102. D. P. Reinhardt, R. N. Ono, H. Notbohm, P. K. Muller, H. P. Bachinger, and L. Y. Sakai. Mutations in calcium-binding epidermal growth factor modules render fibrillin-1 susceptible to proteolysis. A potential disease-causing mechanism in Marfan syndrome. *J. Biol. Chem.*, 275:12339–12345, Apr 2000.

103. J. Y. Suk, S. Jensen, A. McGettrick, A. C. Willis, P. Whiteman, C. Redfield, and P. A. Handford. Structural consequences of cysteine substitutions C1977Y and C1977R in calcium-binding epidermal growth factor-like domain 30 of human fibrillin-1. *J. Biol. Chem.*, 279:51258–51265, Dec 2004.

104. S. Kettle, X. Yuan, G. Grundy, V. Knott, A. K. Downing, and P. A. Handford. Defective calcium binding to fibrillin-1: consequence of an N2144S change for fibrillin-1 structure and function. *J. Mol. Biol.*, 285:1277–1287, Jan 1999.

105. P. Handford, A. K. Downing, Z. Rao, D. R. Hewett, B. C. Sykes, and C. M. Kielty. The calcium binding properties and molecular organization of epidermal growth factor-like domains in human fibrillin-1. *J. Biol. Chem.*, 270:6751–6756, Mar 1995.

106. P. Whiteman, A. K. Downing, and P. A. Handford. NMR analysis of cbEGF domains gives new insights into the structural consequences of a P1148A substitution in fibrillin-1. *Protein Eng.*, 11:957–959, Nov 1998.

107. P. Booms, F. Tiecke, T. Rosenberg, C. Hagemeier, and P. N. Robinson. Differential effect of FBN1 mutations on in vitro proteolysis of recombinant fibrillin-1 fragments. *Hum. Genet.*, 107:216–224, Sep 2000.

108. D. P. Reinhardt, R. N. Ono, and L. Y. Sakai. Calcium stabilizes fibrillin-1 against proteolytic degradation. *J. Biol. Chem.*, 272:1231–1236, Jan 1997.

109. M. E. Huff, L. J. Page, W. E. Balch, and J. W. Kelly. Gelsolin domain 2 Ca2+ affinity determines susceptibility to furin proteolysis and familial amyloidosis of finnish type. *J. Mol. Biol.*, 334:119–127, Nov 2003.

110. T. Vollbrandt, K. Tiedemann, E. El-Hallous, G. Lin, J. Brinckmann, H. John, B. Batge, H. Notbohm, and D. P. Reinhardt. Consequences of cysteine mutations in calcium-binding epidermal growth factor modules of fibrillin-1. *J. Biol. Chem.*, 279:32924–32931, Jul 2004.

111. A. J. McGettrick, V. Knott, A. Willis, and P. A. Handford. Molecular effects of calcium binding mutations in Marfan syndrome depend on domain context. *Hum. Mol. Genet.*, 9:1987–1994, Aug 2000.

112. A. Leask and D. J. Abraham. TGF-beta signaling and the fibrotic response. *FASEB J.*, 18:816–827, May 2004.

113. V. Kaartinen and D. Warburton. Fibrillin controls TGF-beta activation. *Nat. Genet.*, 33:331–332, Mar 2003.

114. Z. Isogai, R. N. Ono, S. Ushiro, D. R. Keene, Y. Chen, R. Mazzieri, N. L. Charbonneau, D. P. Reinhardt, D. B. Rifkin, and L. Y. Sakai. Latent transforming growth factor beta-binding protein 1 interacts with fibrillin and is a microfibril-associated protein. *J. Biol. Chem.*, 278:2750–2757, Jan 2003.

115. F. Drews, S. Knobel, M. Moser, K. G. Muhlack, S. Mohren, C. Stoll, A. Bosio, A. M. Gressner, and R. Weiskirchen. Disruption of the latent transforming growth factor-beta binding protein-1 gene causes alteration in facial structure and influences TGF-beta bioavailability. *Biochim. Biophys. Acta*, 1783:34–48, Jan 2008.

116. G. Ge and D. S. Greenspan. BMP1 controls TGFbeta1 activation via cleavage of latent TGFbeta-binding protein. *J. Cell Biol.*, 175:111–120, Oct 2006.

117. O. Tatti, P. Vehvilainen, K. Lehti, and J. Keski-Oja. MT1-MMP releases latent TGF-beta1 from endothelial cell extracellular matrix via proteolytic processing of LTBP-1. *Exp. Cell Res.*, 314:2501–2514, Aug 2008.

118. E. R. Neptune, P. A. Frischmeyer, D. E. Arking, L. Myers, T. E. Bunton, B. Gayraud, F. Ramirez, L. Y. Sakai, and H. C. Dietz. Dysregulation of TGF-beta activation contributes to pathogenesis in Marfan syndrome. *Nat. Genet.*, 33:407–411, Mar 2003.

119. J. P. Habashi, D. P. Judge, T. M. Holm, R. D. Cohn, B. L. Loeys, T. K. Cooper, L. Myers, E. C. Klein, G. Liu, C. Calvi, M. Podowski, E. R. Neptune, M. K. Halushka, D. Bedja, K. Gabrielson, D. B. Rifkin, L. Carta, F. Ramirez, D. L. Huso, and H. C. Dietz. Losartan, an AT1 antagonist, prevents aortic aneurysm in a mouse model of Marfan syndrome. *Science*, 312:117–121, Apr 2006.

120. M. Nataatmadja, J. West, and M. West. Overexpression of transforming growth factor-beta is associated with increased hyaluronan content and impairment of repair in Marfan syndrome aortic aneurysm. *Circulation*, 114:I371–377, Jul 2006.

121. P. Matt, F. Schoenhoff, J. Habashi, T. Holm, C. Van Erp, D. Loch, O. D. Carlson, B. F. Griswold, Q. Fu, J. De Backer, B. Loeys, D. L. Huso, N. B. McDonnell, J. E. Van Eyk, and H. C. Dietz. Circulating transforming growth factor-beta in Marfan syndrome. *Circulation*, 120:526–532, Aug 2009.

122. D. Gomez, A. Coyet, V. Ollivier, X. Jeunemaitre, G. Jondeau, J. B. Michel, and R. Vranckx. Epigenetic control of vascular Smooth Muscle Cells in Marfan and non-Marfan thoracic aortic aneurysms. *Cardiovasc Res*, Sep 2010.

123. I. M. van de Laar, R. A. Oldenburg, G. Pals, J. W. Roos-Hesselink, B. M. de Graaf, J. M. Verhagen, Y. M. Hoedemaekers, R. Willemsen, L. A. Severijnen, H. Venselaar, G. Vriend, P. M. Pattynama, M. Collee, D. Majoor-Krakauer, D. Poldermans, I. M. Frohn-Mulder, D. Micha, J. Timmermans, Y. Hilhorst-Hofstee, S. M. Bierma-Zeinstra, P. J. Willems, J. M. Kros, E. H. Oei, B. A. Oostra, M. W. Wessels, and A. M. Bertoli-Avella. Mutations in SMAD3 cause a syndromic form of aortic aneurysms and dissections with early-onset osteoarthritis. *Nat. Genet.*, 43:121–126, Feb 2011.

124. B. S. Brooke, J. P. Habashi, D. P. Judge, N. Patel, B. Loeys, and H. C. Dietz. Angiotensin II blockade and aortic-root dilation in Marfan's syndrome. *N. Engl. J. Med.*, 358:2787–2795, Jun 2008.

125. R. Derynck and Y. E. Zhang. Smad-dependent and Smad-independent pathways in TGF-beta family signalling. *Nature*, 425:577–584, Oct 2003.

126. L. Carta, S. Smaldone, L. Zilberberg, D. Loch, H. C. Dietz, D. B. Rifkin, and F. Ramirez. p38 MAPK is an early determinant of promiscuous Smad2/3 signaling in the aortas of fibrillin-1 (Fbn1)-null mice. *J. Biol. Chem.*, 284:5630–5636, Feb 2009.

127. T. M. Holm, J. P. Habashi, J. J. Doyle, D. Bedja, Y. Chen, C. van Erp, M. E. Lindsay, D. Kim, F. Schoenhoff, R. D. Cohn, B. L. Loeys, C. J. Thomas, S. Patnaik, J. J. Marugan, D. P. Judge, and H. C. Dietz. Noncanonical TGFÎš signaling contributes to aortic aneurysm progression in Marfan syndrome mice. *Science*, 332:358–361, Apr 2011.

128. J. P. Habashi, J. J. Doyle, T. M. Holm, H. Aziz, F. Schoenhoff, D. Bedja, Y. Chen, A. N. Modiri, D. P. Judge, and H. C. Dietz. Angiotensin II type 2 receptor signaling attenuates aortic aneurysm in mice through ERK antagonism. *Science*, 332:361–365, Apr 2011.

129. H. Pannu, V. T. Fadulu, J. Chang, A. Lafont, S. N. Hasham, E. Sparks, P. F. Giampietro, C. Zaleski, A. L. Estrera, H. J. Safi, S. Shete, M. C. Willing, C. S. Raman, and D. M. Milewicz. Mutations in transforming growth factor-beta receptor type II cause familial thoracic aortic aneurysms and dissections. *Circulation*, 112:513–520, Jul 2005.

130. T. Mizuguchi, G. Collod-Beroud, T. Akiyama, M. Abifadel, N. Harada, T. Morisaki, D. Allard, M. Varret, M. Claustres, H. Morisaki, M. Ihara, A. Kinoshita, K. Yoshiura, C. Junien, T. Kajii, G. Jondeau, T. Ohta, T. Kishino, Y. Furukawa, Y. Nakamura, N. Niikawa, C. Boileau, and N. Matsumoto. Heterozygous TGFBR2 mutations in Marfan syndrome. *Nat. Genet.*, 36:855–860, Aug 2004.

131. D. Horbelt, G. Guo, P. N. Robinson, and P. Knaus. Quantitative analysis of TGFBR2 mutations in Marfan-syndrome-related disorders suggests a correlation between phenotypic severity and Smad signaling activity. *J. Cell. Sci.*, 123:4340–4350, Dec 2010.

132. F. Ramirez and H. C. Dietz. Marfan syndrome: from molecular pathogenesis to clinical treatment. *Curr. Opin. Genet. Dev.*, 17:252–258, Jun 2007.

133. P. ten Dijke and H. M. Arthur. Extracellular control of TGFbeta signalling in vascular development and disease. *Nat. Rev. Mol. Cell Biol.*, 8:857–869, Nov 2007.

134. K. J. Fleischer, H. C. Nousari, G. J. Anhalt, C. D. Stone, and J. C. Laschinger. Immunohistochemical abnormalities of fibrillin in cardiovascular tissues in Marfan's syndrome. *Ann. Thorac. Surg.*, 63:1012–1017, Apr 1997.

135. T E Bunton, N J Biery, L Myers, B Gayraud, F Ramirez, and H C Dietz. Phenotypic alteration of vascular smooth muscle cells precedes elastolysis in a mouse model of Marfan syndrome. *Circ Res*, 88(1):37–43, 2001.

136. D. Recchia, A. M. Sharkey, M. S. Bosner, N. T. Kouchoukos, and S. A. Wickline. Sensitive detection of abnormal aortic architecture in Marfan syndrome with high-frequency ultrasonic tissue characterization. *Circulation*, 91:1036–1043, Feb 1995.

137. M. Godfrey. From fluorescence to the gene: the skin in the Marfan syndrome. *J. Invest. Dermatol.*, 103:58S–62S, Nov 1994.

138. G. A. Homandberg. Potential regulation of cartilage metabolism in osteoarthritis by fibronectin fragments. *Front. Biosci.*, 4:D713–730, Oct 1999.

139. S. Saito, N. Yamaji, K. Yasunaga, T. Saito, S. Matsumoto, M. Katoh, S. Kobayashi, and Y. Masuho. The fibronectin extra domain A activates matrix metalloproteinase gene expression by an interleukin-1-dependent mechanism. *J. Biol. Chem.*, 274:30756–30763, Oct 1999.

140. G. A. Homandberg, F. Hui, C. Wen, C. Purple, K. Bewsey, H. Koepp, K. Huch, and A. Harris. Fibronectin-fragment-induced cartilage chondrolysis is associated with release of catabolic cytokines. *Biochem. J.*, 321 (Pt 3):751–757, Feb 1997.

141. C. B. Forsyth, J. Pulai, and R. F. Loeser. Fibronectin fragments and blocking antibodies to alpha2beta1 and alpha5beta1 integrins stimulate mitogen-activated protein kinase signaling and increase collagenase 3 (matrix metalloproteinase 13) production by human articular chondrocytes. *Arthritis Rheum.*, 46:2368–2376, Sep 2002.

142. P. Booms, R. Pregla, A. Ney, F. Barthel, D. P. Reinhardt, A. Pletschacher, S. Mundlos, and P. N. Robinson. RGD-containing fibrillin-1 fragments upregulate matrix metalloproteinase expression in cell culture: a potential factor in the pathogenesis of the Marfan syndrome. *Hum. Genet.*, 116:51–61, Jan 2005.

143. S. S. Chaudhry, S. A. Cain, A. Morgan, S. L. Dallas, C. A. Shuttleworth, and C. M. Kielty. Fibrillin-1 regulates the bioavailability of TGFbeta1. *J. Cell Biol.*, 176:355–367, Jan 2007.

144. Patrick Booms, Andreas Ney, Frank Barthel, Gautier Moroy, Damian Counsell, Christoph Gille, Gao Guo, Reinhard Pregla, Stefan Mundlos, Alain J P Alix, and Peter N Robinson. A fibrillin-1-fragment containing the elastin-binding-protein GxxPG consensus sequence upregulates matrix metalloproteinase-1: biochemical and computational analysis. *J Mol Cell Cardiol*, 40(2):234–46, 2006.

145. S. Privitera, C. A. Prody, J. W. Callahan, and A. Hinek. The 67-kDa enzymatically inactive alternatively spliced variant of beta-galactosidase is identical to the elastin/laminin-binding protein. *J. Biol. Chem.*, 273:6319–6326, Mar 1998.

146. S. Mochizuki, B. Brassart, and A. Hinek. Signaling pathways transduced through the elastin receptor facilitate proliferation of arterial smooth muscle cells. *J. Biol. Chem.*, 277:44854–44863, Nov 2002.

147. L. Duca, N. Floquet, A. J. Alix, B. Haye, and L. Debelle. Elastin as a matrikine. *Crit. Rev. Oncol. Hematol.*, 49:235–244, Mar 2004.

148. A. Hinek, D. S. Wrenn, R. P. Mecham, and S. H. Barondes. The elastin receptor: a galactoside-binding protein. *Science*, 239:1539–1541, Mar 1988.

149. R. P. Mecham, A. Hinek, G. L. Griffin, R. M. Senior, and L. A. Liotta. The elastin receptor shows structural and functional similarities to the 67-kDa tumor cell laminin receptor. *J. Biol. Chem.*, 264:16652–16657, Oct 1989.

150. R. M. Senior, G. L. Griffin, R. P. Mecham, D. S. Wrenn, K. U. Prasad, and D. W. Urry. Val-Gly-Val-Ala-Pro-Gly, a repeating peptide in elastin, is chemotactic for fibroblasts and monocytes. *J. Cell Biol.*, 99:870–874, Sep 1984.

151. L. E. Grosso and M. Scott. PGAIPG, a repeated hexapeptide of bovine and human tropoelastin, is chemotactic for neutrophils and Lewis lung carcinoma cells. *Arch. Biochem. Biophys.*, 305:401–404, Sep 1993.

152. F. Bisaccia, M. A. Morelli, M. De Biasi, S. Traniello, S. Spisani, and A. M. Tamburro. Migration of monocytes in the presence of elastolytic fragments of elastin and in synthetic derivates. Structure-activity relationships. *Int. J. Pept. Protein Res.*, 44:332–341, Oct 1994.

153. A. Hinek. Nature and the multiple functions of the 67-kD elastin-/laminin binding protein. *Cell Adhes. Commun.*, 2:185–193, Jul 1994.

154. G. Moroy, A. J. Alix, and S. Hery-Huynh. Structural characterization of human elastin derived peptides containing the GXXP sequence. *Biopolymers*, 78:206–220, Jul 2005.

155. S. Kamisato, Y. Uemura, N. Takami, and K. Okamoto. Involvement of intracellular cyclic GMP and cyclic GMP-dependent protein kinase in alpha-elastin-induced macrophage chemotaxis. *J. Biochem.*, 121:862–867, May 1997.

156. B. Brassart, P. Fuchs, E. Huet, A. J. Alix, J. Wallach, A. M. Tamburro, F. Delacoux, B. Haye, H. Emonard, W. Hornebeck, and L. Debelle. Conformational dependence of collagenase (matrix metalloproteinase-1) up-regulation by elastin peptides in cultured fibroblasts. *J. Biol. Chem.*, 276:5222–5227, Feb 2001.

157. J. R. Cohen, I. Sarfati, D. Danna, and L. Wise. Smooth muscle cell elastase, atherosclerosis, and abdominal aortic aneurysms. *Ann. Surg.*, 216:327–330, Sep 1992.

158. A. Simionescu, K. Philips, and N. Vyavahare. Elastin-derived peptides and TGF-beta1 induce osteogenic responses in smooth muscle cells. *Biochem. Biophys. Res. Commun.*, 334:524–532, Aug 2005.

159. A. Hinek. Biological roles of the non-integrin elastin/laminin receptor. *Biol. Chem.*, 377:471–480, 1996.

160. L. E. Grosso and M. Scott. Peptide sequences selected by BA4, a tropoelastin-specific monoclonal antibody, are ligands for the 67-kilodalton bovine elastin receptor. *Biochemistry*, 32:13369–13374, Dec 1993.

161. K. Yoshimura, H. Aoki, Y. Ikeda, K. Fujii, N. Akiyama, A. Furutani, Y. Hoshii, N. Tanaka, R. Ricci, T. Ishihara, K. Esato, K. Hamano, and M. Matsuzaki. Regression of abdominal aortic aneurysm by inhibition of c-Jun N-terminal kinase. *Nat. Med.*, 11:1330–1338, Dec 2005.

162. K. Satoh, P. Nigro, T. Matoba, M. R. O'Dell, Z. Cui, X. Shi, A. Mohan, C. Yan, J. Abe, K. A. Illig, and B. C. Berk. Cyclophilin A enhances vascular oxidative stress and the development of angiotensin II-induced aortic aneurysms. *Nat. Med.*, 15:649–656, Jun 2009.

163. K. B. Mullis and F. A. Faloona. Specific synthesis of DNA in vitro via a polymerase-catalyzed chain reaction. *Meth. Enzymol.*, 155:335–350, 1987.

164. R. R. Aksamit, W. Falk, and E. J. Leonard. Chemotaxis by mouse macrophage cell lines. *J Immunol*, 126(6):2194–2199, Jun 1981.

165. S M Wei, J Erdei, T Jr Fulop, L Robert, and M P Jacob. Elastin peptide concentration in human serum: variation with antibodies and elastin peptides used for the enzyme-linked immunosorbent assay. *J Immunol Methods*, 164(2):175–87, 1993.

166. S. Turkmen, G. Guo, M. Garshasbi, K. Hoffmann, A. J. Alshalah, C. Mischung, A. Kuss, N. Humphrey, S. Mundlos, and P. N. Robinson. CA8 mutations cause a novel syndrome characterized by ataxia and mild mental retardation with predisposition to quadrupedal gait. *PLoS Genet.*, 5:e1000487, May 2009.

167. K. A. Hance, M. Tataria, S. J. Ziporin, J. K. Lee, and R. W. Thompson. Monocyte chemotactic activity in human abdominal aortic aneurysms: role of elastin degradation peptides and the 67-kD cell surface elastin receptor. *J. Vasc. Surg.*, 35:254–261, Feb 2002.

168. A. W. Chung, K. Au Yeung, S. F. Cortes, G. G. Sandor, D. P. Judge, H. C. Dietz, and C. van Breemen. Endothelial dysfunction and compromised eNOS/Akt signaling in the thoracic aorta during the progression of Marfan syndrome. *Br. J. Pharmacol.*, 150:1075–1083, Apr 2007.

169. J. S. Ikonomidis, J. A. Jones, J. R. Barbour, R. E. Stroud, L. L. Clark, B. S. Kaplan, A. Zeeshan, J. E. Bavaria, J. H. Gorman, F. G. Spinale, and R. C. Gorman. Expression of matrix metalloproteinases and endogenous inhibitors within ascending aortic aneurysms of patients with Marfan syndrome. *Circulation*, 114:I365–370, Jul 2006.

170. T. K. van den Berg and G. Kraal. A function for the macrophage F4/80 molecule in tolerance induction. *Trends Immunol.*, 26:506–509, Oct 2005.

171. M. Kretzschmar and J. Massagué. SMADs: mediators and regulators of TGF-beta signaling. *Curr Opin Genet Dev*, 8(1):103–111, Feb 1998.

172. C. M. Ng, A. Cheng, L. A. Myers, F. Martinez-Murillo, C. Jie, D. Bedja, K. L. Gabrielson, J. M. Hausladen, R. P. Mecham, D. P. Judge, and H. C. Dietz. TGF-beta-dependent pathogenesis of mitral valve prolapse in a mouse model of Marfan syndrome. *J. Clin. Invest.*, 114:1586–1592, Dec 2004.

173. D. Hubmacher, K. Tiedemann, R. Bartels, J. Brinckmann, T. Vollbrandt, B. Batge, H. Notbohm, and D. P. Reinhardt. Modification of the structure and function of fibrillin-1 by homocysteine suggests a potential pathogenetic mechanism in homocystinuria. *J. Biol. Chem.*, 280:34946–34955, Oct 2005.

174. G. W. Hunninghake, J. M. Davidson, S. Rennard, S. Szapiel, J. E. Gadek, and R. G. Crystal. Elastin fragments attract macrophage precursors to diseased sites in pulmonary emphysema. *Science*, 212:925–927, May 1981.

175. M. M. Long, V. J. King, K. U. Prasad, B. A. Freeman, and D. W. Urry. Elastin repeat peptides as chemoattractants for bovine aortic endothelial cells. *J. Cell. Physiol.*, 140:512–518, Sep 1989.

176. A. E. Postlethwaite and A. H. Kang. Collagen-and collagen peptide-induced chemotaxis of human blood monocytes. *J. Exp. Med.*, 143:1299–1307, Jun 1976.

177. N. Floquet, S. Hery-Huynh, M. Dauchez, P. Derreumaux, A. M. Tamburro, and A. J. Alix. Structural characterization of VGVAPG, an elastin-derived peptide. *Biopolymers*, 76:266–280, 2004.

178. P. Whiteman, R. S. Smallridge, V. Knott, J. J. Cordle, A. K. Downing, and P. A. Handford. A G1127S change in calcium-binding epidermal growth factor-like domain 13 of human fibrillin-1 causes short range conformational effects. *J. Biol. Chem.*, 276:17156–17162, May 2001.

179. A. M. Houghton, P. A. Quintero, D. L. Perkins, D. K. Kobayashi, D. G. Kelley, L. A. Marconcini, R. P. Mecham, R. M. Senior, and S. D. Shapiro. Elastin fragments drive disease progression in a murine model of emphysema. *J. Clin. Invest.*, 116:753–759, Mar 2006.

180. A. Heinz, M. C. Jung, L. Duca, W. Sippl, S. Taddese, C. Ihling, A. Rusciani, G. Jahreis, A. S. Weiss, R. H. Neubert, and C. E. Schmelzer. Degradation of tropoelastin by matrix metalloproteinases–cleavage site specificities and release of matrikines. *FEBS J.*, 277:1939–1956, Apr 2010.

181. D. J. Johnson, P. Robson, Y. Hew, and F. W. Keeley. Decreased elastin synthesis in normal development and in long-term aortic organ and cell cultures is related to rapid and selective destabilization of mRNA for elastin. *Circ. Res.*, 77:1107–1113, Dec 1995.

182. S. D. Shapiro, S. K. Endicott, M. A. Province, J. A. Pierce, and E. J. Campbell. Marked longevity of human lung parenchymal elastic fibers deduced from prevalence of D-aspartate and nuclear weapons-related radiocarbon. *J. Clin. Invest.*, 87:1828–1834, May 1991.

183. J. T. Powell, N. Vine, and M. Crossman. On the accumulation of D-aspartate in elastin and other proteins of the ageing aorta. *Atherosclerosis*, 97:201–208, Dec 1992.

184. S. Ritz-Timme, I. Laumeier, and M. J. Collins. Aspartic acid racemization: evidence for marked longevity of elastin in human skin. *Br. J. Dermatol.*, 149:951–959, Nov 2003.

185. T. J. Schlatmann and A. E. Becker. Histologic changes in the normal aging aorta: implications for dissecting aortic aneurysm. *Am. J. Cardiol.*, 39:13–20, Jan 1977.

186. T. Shinohara, K. Suzuki, M. Okada, M. Shiigai, M. Shimizu, T. Maehara, and F. Ohsuzu. Soluble elastin fragments in serum are elevated in acute aortic dissection. *Arterioscler. Thromb. Vasc. Biol.*, 23:1839–1844, Oct 2003.

187. T. J. Dillon, R. L. Walsh, R. Scicchitano, B. Eckert, E. G. Cleary, and G. McLennan. Plasma elastin-derived peptide levels in normal adults, children, and emphysematous subjects. Physiologic and computed tomographic scan correlates. *Am. Rev. Respir. Dis.*, 146:1143–1148, Nov 1992.

188. E. Petersen, F. Wagberg, and K. A. Angquist. Serum concentrations of elastin-derived peptides in patients with specific manifestations of atherosclerotic disease. *Eur J Vasc Endovasc Surg*, 24:440–444, Nov 2002.

189. J. Satta, A. Laurila, P. Paakko, K. Haukipuro, R. Sormunen, S. Parkkila, and T. Juvonen. Chronic inflammation and elastin degradation in abdominal aortic aneurysm disease: an immunohistochemical and electron microscopic study. *Eur J Vasc Endovasc Surg*, 15:313–319, Apr 1998.

190. Z. Varga, M. P. Jacob, L. Robert, J. Csongor, and T. Fulop. Age-dependent changes of K-elastin stimulated effector functions of human phagocytic cells: relevance for atherogenesis. *Exp. Gerontol.*, 32:653–662, 1997.

191. T. Fulop, A. Larbi, A. Fortun, L. Robert, and A. Khalil. Elastin peptides induced oxidation of LDL by phagocytic cells. *Pathol. Biol.*, 53:416–423, Sep 2005.

192. A. Krettek, G. K. Sukhova, and P. Libby. Elastogenesis in human arterial disease: a role for macrophages in disordered elastin synthesis. *Arterioscler. Thromb. Vasc. Biol.*, 23:582–587, Apr 2003.

193. S. D. Shapiro. Diverse roles of macrophage matrix metalloproteinases in tissue destruction and tumor growth. *Thromb. Haemost.*, 82:846–849, Aug 1999.

194. G. Ailawadi, J. L. Eliason, and G. R. Upchurch. Current concepts in the pathogenesis of abdominal aortic aneurysm. *J. Vasc. Surg.*, 38:584–588, Sep 2003.

195. C. Buckley, C. W. Wyble, M. Borhani, T. L. Ennis, D. K. Kobayashi, J. A. Curci, S. D. Shapiro, and R. W. Thompson. Accelerated enlargement of experimental abdominal aortic aneurysms in a mouse model of chronic cigarette smoke exposure. *J. Am. Coll. Surg.*, 199:896–903, Dec 2004.

196. D. M. Milewicz, D. C. Guo, V. Tran-Fadulu, A. L. Lafont, C. L. Papke, S. Inamoto, C. S. Kwartler, and H. Pannu. Genetic basis of thoracic aortic aneurysms and dissections: focus on smooth muscle cell contractile dysfunction. *Annu Rev Genomics Hum Genet*, 9:283–302, 2008.

197. V Marque, P Kieffer, B Gayraud, I Lartaud-Idjouadiene, F Ramirez, and J Atkinson. Aortic wall mechanics and composition in a transgenic mouse model of Marfan syndrome. *Arterioscler Thromb Vasc Biol*, 21(7):1184–9, 2001.

198. L. K. Harris, S. D. Smith, R. J. Keogh, R. L. Jones, P. N. Baker, M. Knofler, J. E. Cartwright, G. S. Whitley, and J. D. Aplin. Trophoblast- and vascular smooth muscle cell-derived MMP-12 mediates elastolysis during uterine spiral artery remodeling. *Am. J. Pathol.*, 177:2103–2115, Oct 2010.

199. A. Hinek and M. Rabinovitch. 67-kD elastin-binding protein is a protective "companion" of extracellular insoluble elastin and intracellular tropoelastin. *J. Cell Biol.*, 126:563–574, Jul 1994.

200. S. Taddese, A. S. Weiss, G. Jahreis, R. H. Neubert, and C. E. Schmelzer. In vitro degradation of human tropoelastin by MMP-12 and the generation of matrikines from domain 24. *Matrix Biol.*, 28:84–91, Mar 2009.

201. J. F. Santibanez, J. Guerrero, M. Quintanilla, A. Fabra, and J. Martinez. Transforming growth factor-beta1 modulates matrix metalloproteinase-9 production through the Ras/MAPK signaling pathway in transformed keratinocytes. *Biochem. Biophys. Res. Commun.*, 296:267–273, Aug 2002.

202. H. G. Munshi, Y. I. Wu, S. Mukhopadhyay, A. J. Ottaviano, A. Sassano, J. E. Koblinski, L. C. Platanias, and M. S. Stack. Differential regulation of membrane type 1-matrix metalloproteinase activity by ERK 1/2- and p38 MAPK-modulated tissue inhibitor of metalloproteinases 2 expression controls transforming growth factor-beta1-induced pericellular collagenolysis. *J. Biol. Chem.*, 279:39042–39050, Sep 2004.

203. M. Miralles, W. Wester, G. A. Sicard, R. Thompson, and J. M. Reilly. Indomethacin inhibits expansion of experimental aortic aneurysms via inhibition of the cox2 isoform of cyclooxygenase. *J. Vasc. Surg.*, 29:884–892, May 1999.

204. D. Pratico, C. Tillmann, Z. B. Zhang, H. Li, and G. A. FitzGerald. Acceleration of atherogenesis by COX-1-dependent prostanoid formation in low density lipoprotein receptor knockout mice. *Proc. Natl. Acad. Sci. U.S.A.*, 98:3358–3363, Mar 2001.

205. D. R. Holmes, D. Petrinec, W. Wester, R. W. Thompson, and J. M. Reilly. Indomethacin prevents elastase-induced abdominal aortic aneurysms in the rat. *J. Surg. Res.*, 63:305–309, Jun 1996.

206. P. J. Armstrong, D. P. Franklin, D. J. Carey, and J. R. Elmore. Suppression of experimental aortic aneurysms: comparison of inducible nitric oxide synthase and cyclooxygenase inhibitors. *Ann Vasc Surg*, 19:248–257, Mar 2005.

207. J. M. Gitlin, D. B. Trivedi, R. Langenbach, and C. D. Loftin. Genetic deficiency of cyclooxygenase-2 attenuates abdominal aortic aneurysm formation in mice. *Cardiovasc. Res.*, 73:227–236, Jan 2007.

208. D. R. Holmes, W. Wester, R. W. Thompson, and J. M. Reilly. Prostaglandin E2 synthesis and cyclooxygenase expression in abdominal aortic aneurysms. *J. Vasc. Surg.*, 25:810–815, May 1997.

209. A. P. Pentland, S. D. Shapiro, and H. G. Welgus. Agonist-induced expression of tissue inhibitor of metalloproteinases and metalloproteinases by human macrophages is regulated by endogenous prostaglandin E2 synthesis. *J. Invest. Dermatol.*, 104:52–57, Jan 1995.

210. I. J. Franklin, L. J. Walton, R. M. Greenhalgh, and J. T. Powell. The influence of indomethacin on the metabolism and cytokine secretion of human aneurysmal aorta. *Eur J Vasc Endovasc Surg*, 18:35–42, Jul 1999.

211. W. Shen, Y. Li, J. Zhu, R. Schwendener, and J. Huard. Interaction between macrophages, TGF-beta1, and the COX-2 pathway during the inflammatory phase of skeletal muscle healing after injury. *J. Cell. Physiol.*, 214:405–412, Feb 2008.

212. C. Ghayor, A. Rey, and J. Caverzasio. Prostaglandin-dependent activation of ERK mediates cell proliferation induced by transforming growth factor beta in mouse osteoblastic cells. *Bone*, 36:93–100, Jan 2005.

213. H. H. Yang, J. M. Kim, E. Chum, C. van Breemen, and A. W. Chung. Effectiveness of combination of losartan potassium and doxycycline versus single-drug treatments in the secondary prevention of thoracic aortic aneurysm in Marfan syndrome. *J. Thorac. Cardiovasc. Surg.*, 140:305–312, Aug 2010.

214. M. A. Ricci, G. Strindberg, J. M. Slaiby, R. Guibord, L. J. Bergersen, P. Nichols, E. D. Hendley, and D. B. Pilcher. Anti-CD 18 monoclonal antibody slows experimental aortic aneurysm expansion. *J. Vasc. Surg.*, 23:301–307, Feb 1996.

215. L. C. Silva, L. C. Ortigosa, and G. Benard. Anti-TNF-alpha agents in the treatment of immune-mediated inflammatory diseases: mechanisms of action and pitfalls. *Immunotherapy*, 2:817–833, Nov 2010.

216. C. Euchenhofer, C. Maihofner, K. Brune, I. Tegeder, and G. Geisslinger. Differential effect of selective cyclooxygenase-2 (COX-2) inhibitor NS 398 and diclofenac on formalin-induced nociception in the rat. *Neurosci. Lett.*, 248:25–28, May 1998.

217. S. Roepcke, D. Zhi, M. Vingron, and P. F. Arndt. Identification of highly specific localized sequence motifs in human ribosomal protein gene promoters. *Gene*, 365:48–56, Jan 2006.

218. L. S. Wyrwicz, P. Gaj, M. Hoffmann, L. Rychlewski, and J. Ostrowski. A common cis-element in promoters of protein synthesis and cell cycle genes. *Acta Biochim. Pol.*, 54:89–98, 2007.

219. R. P. Perry. The architecture of mammalian ribosomal protein promoters. *BMC Evol. Biol.*, 5:15, 2005.

9 Abbreviations

AAA	Abdominal aortic aneurysm
ACEi	Angiotensin converting enzyme inhibitor
APS	Ammonium persulfate
BCA	Bicinchoninic acid
BSA	Bovine Serum Albumin
CCA	Congenital Contractural Arachnodactyly
cbEGF	calcium-binding EGF module
CMD	Cystic medial degeneration
CF	Connecting Filament
CI	Chemotactic Index
COX-2	Cyclooxygenase 2
CV	Coefficient of variation
DAB	Diaminobenzidine tetrahydrochloride
DNA	Deoxyribonucleic acid
dNTP	Deoxynucleotide triphosphate
DMEM	Dulbecco's modified Eagle's medium
DPE	Downstream promoter element
DTT	1,4-dithiothreitol
EBP	Elastin-binding protein
ECL	Enhanced Chemiluminescence
ECM	Extracelluar matrix
EDP	Elastin derived peptide
EDTA	Ethylenediamine-tetraacetic acid
EGF	Epidermal growth factor
eGFP	Enhanced green fluorescent protein
EMSA	Electrophoretic mobility shift assay
ELISA	Enzyme Linked Immunoabsorbent Assay
ERK	Extracellular signal-regulated kinases
eNO	endothelial Nitric Oxide
et al.	et alia (and others)
FBN1	Fibrillin-1
FBS	Fetal bovine serum
GO	Gene Ontology
HEK 293	Human Embryonic Kidney cells
His	Histidine
Inr	Initiator element

i.p.	Intraperitoneal
JNK1	Jun N-terminal kinase-1
LAP	Latency-associated propeptide
LDS	Loeys-Dietz syndrome
LTBP	Latent TGF-β-binding protein
mAb	monoclonal antibody
MFS	Marfan syndrome
min	Minute
MMP	Matrix metalloproteinase
MVP	Mitral valve prolapse
NA	Not available
nMFS	neonatal MFS
NSAID	Nonsteroidal antiinflammatory drug
OD	Optical density
PAGE	Polyacrylamide gel electrophoresis
PBS	Phosphate buffered saline
PCR	Polymerase chain reaction
PFA	Paraformaldehyde
PMFS	Phenylmethylsulfonylfluoride
PNGase F	N-glycosidase F
PVDF	Polyvinylidene difluoride
RGD	Arginine-Glycine-Aspartic acid
RNA	Ribonucleic acid
SAP	Shrimp alkaline phosphatase
SDS	Sodium dodecyl sulfate
s.e.m.	Standard error
SGS	Sphrintzen-Goldberg syndrome
TBS	Tris buffered saline
TAA	Thoracic Aortic Aneurysm
TEMED	N,N,N',N'-Tetramethylethylendiamin
TGF-β	Transforming growth factor-β
TIMP	Tissue inhibitor of MMP
Tween 20	Polyoxyethylensorbitan mono laurate
VGVAPG	Val-Gly-Val-Ala-Pro-Gly
vSMC	vascular Smooth Muscle Cell
VVG	Verhoeff-Van Gieson stain
WT	Wild type

10 Map of the cloning vector pSec Tag A

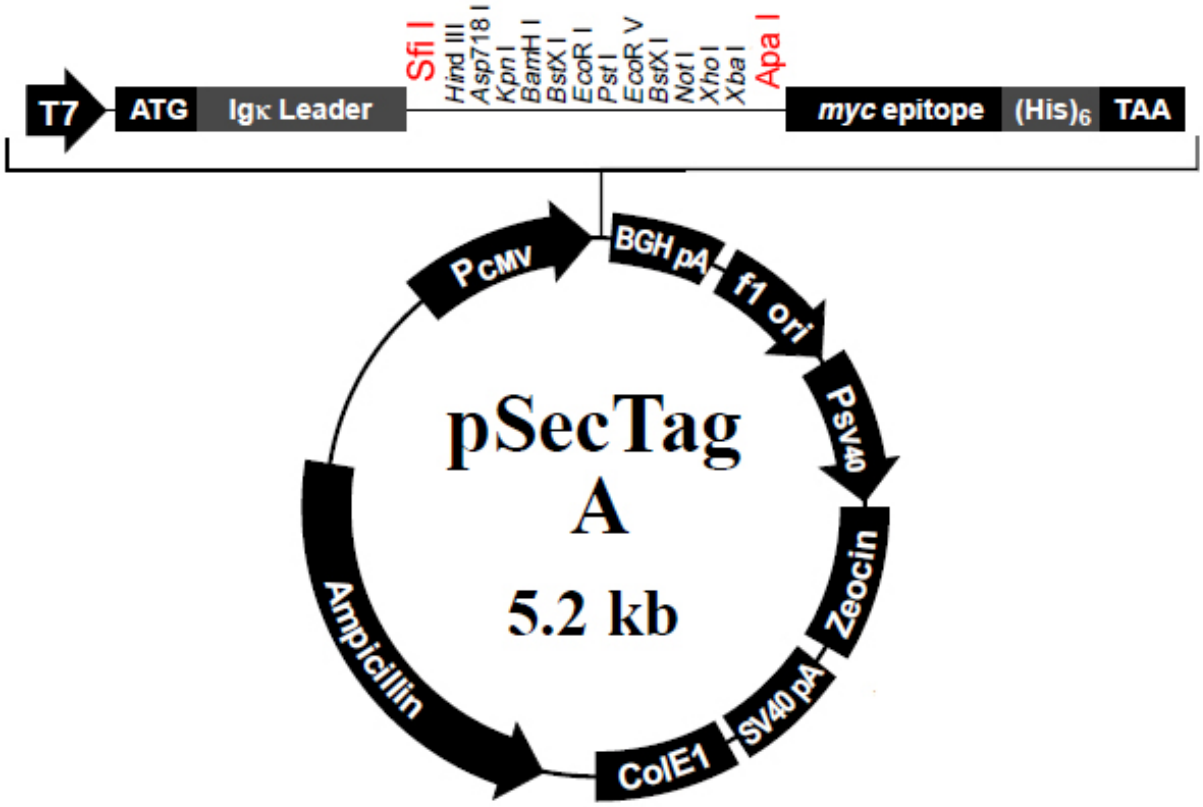

Figure 10.1: Physical map of pSec Tag A. pSec Tag A is a 5.2 kb expression designed for high-level stable and transient expression in mammalian hosts. Proteins expressed from pSec Tag A are fused at the N-terminus to the murine Igκ chain leader sequence for protein secretion and at the C-terminus to a peptide containing the c-myc epitope and six tandem histidine residues for detection and purification. Relevant restriction sites used to clone fibrillin-1 fragments are marked as red and indicated by name.

11 Curriculum Vitae

For reasons of data protection, the curriculum vitae is not published in the online version.

For reasons of data protection, the curriculum vitae is not published in the online version.

For reasons of data protection, the curriculum vitae is not published in the online version.

12 Erklärung

Hiermit erkläre ich, dass ich die Arbeit selbst verfasst habe sowie keine anderen als die angegebenen Quellen und Hilfsmittel in Anspruch genommen habe. Ich versichere, dass diese Arbeit in dieser oder anderer Form keiner anderen Prüfungsbehörde vorgelegt wurde.

Berlin, Juni 2011

Gao Guo